Aus dem Institut für Virologie und
Zellbiologie
Der Universität zu Lübeck
Direktor: Prof. Dr. Norbert Tautz

New Tools to Study Murine Norovirus-Host Interactions

Inauguraldissertation
Zur
Erlangung der Doktorwürde
der Universität zu Lübeck

Aus der Sektion der Naturwissenschaften

vorgelegt von
Marit Lingemann
aus Münster
Lübeck 2020

1. Berichterstatter: Prof. Dr. Stefan Taube

2. Berichterstatter: Prof. Dr. Lars Redecke

Tag der mündlichen Prüfung: 08.01.2021

Zum Druck genehmigt. Lübeck, den 20.01.2021

Erklärung:

Ich versichere, dass ich die Dissertation ohne fremde Hilfe angefertigt und keine anderen als die angegebenen Hilfsmittel verwendet habe. Weder vorher noch gleichzeitig habe ich andernorts einen Zulassungsantrag gestellt oder diese Dissertation vorgelegt. Ich habe mich bisher noch keinem Promotionsverfahren unterzogen.

Marit Lingemann

Parts of this thesis were presented:

Würzburg 2018, GfV

Henrik Wegener, **Marit Lingemann**, Álvaro Mallagaray, Alexander Domnick, Matthias Klinger, Holly Turula, Christiane E. Wobus, Thomas Peters and Stefan Taube

Murine norovirus binding to fucosylated blood group antigen enhances infection *in vitro* and *in vivo*

Düsseldorf 2019, GfV

Marit Lingemann, Antje Schoelzel, Stefan Taube

A Simple DNA-Based Reverse Genetics System and Novel Plaque Assay for Murine Noroviruses

Schöntal 2019, Glycovirology Meeting

Marit Lingemann, Henrik Wegener, Álvaro Mallagaray, Alexander Domnick, Holly Turula, Christiane E. Wobus, Thomas Peters and Stefan Taube

Common Roles for Sialylated and Fucosylated Glycans in Murine and Human Norovirus Infection

Für meine Familie

Summary:

Noroviruses are the main cause of non-bacterial acute gastroenteritis worldwide. Up to 685 million cases are reported each year worldwide. For human norovirus (HuNoV) research is limited by the availability of efficient cell culture systems. Different systems support HuNoV replication but only to a limited extend and propagation of the virus is limited and production of stocks for viral passaging.

For HuNoV the binding of different histo-blood group antigens present on cell surfaces or freely secreted in bodily fluids has been described by others. Especially the sialylated and fucosylated moieties of the glycans were shown to be of significant importance.

Due to the inability to efficiently cultivate HuNoVs, murine noroviruses (MNVs) have become a widely used model to study noroviruses biology. MNV has similar properties to other noroviruses, including genome organisation and replication in the cell. Binding to glycans and bile acid binding is shown for MNV, as well as different HuNoV strains. For MNV different tools are available including cell culture systems supporting efficient replication, a native animal model, as well as various reverse genetics systems.

The study presented here investigates host-virus interaction of MNV with different fucosylated and sialylated glycans. In addition, different functional assays were established to observe influences of glycan and bile acid binding on host-virus interaction. While an effect of glycans on infection could not be reproduced, binding to distinct bile acids such as glycochenodeoxycholic acid (GCDCA) showed an enhancing effect on MNV infection independent of the cell culture system used.

Furthermore, the *bona fide* receptor mCD300lf was recently described. The protruding domain of MNV is shown to bind to the *bona fide* mCD300lf receptor and neutralizing antibodies and was thus targeted in an alanine scan in order to study the interaction of the protruding domain with the different glycans and the bile acid GCDCA. Cell lines stably expressing the mCD300lf receptor become susceptible to MNV infection and different cell lines showed comparable results to the naturally susceptible cell lines included in the assay.

To identify regions involved in antibody binding and to study the mechanism of bile acid in infection, an alanine scan of surface exposed loops of the viral capsid was performed. To obtain recombinant viruses, a DNA-based reverse genetics system was used, showing only limited reproducibility and yield. To improve upon the ability to rescue viruses that are limited in their ability to infect or replicate, improved reverse genetics systems were established. For this, easily transfectable cell lines such as Huh7 and descendent cell lines were generated to stably express the mCD300lf entry receptor. These newly generated cell lines supported MNV reproducible rescue using DNA- and RNA-based reverse genetics systems and constitutes a highly useful tool studying MNV-host interactions. Functional analysis of the generated recombinant viruses was beyond the scope of this thesis. However, improved reverse genetics systems coupled with a reporter system to quantify infected cells was established. For this an eGFP reporter was stably introduced into susceptible cells that translocates into the nucleus upon MNV infection.

In summary, we were able to establish new tools to study murine norovirus host interactions and generated a number of recombinant murine noroviruses awaiting functional analysis.

Zusammenfassung:

Noroviren sind ein wichtiger Grund für akute, nicht-bakterielle Gastroenteritis und führen zu 685 Millionen Infektionen jedes Jahr Weltweit. Noroviren gehören zu der Familie der *Caliciviridae*, und sind einzelsträngige RNA Viren mit positiver Polarität. Humane Noroviren sind widerspenstige Organismen in der Forschung. Die Entwicklung von Zellkultursystemen für humane Noroviren erweist sich als äußerst schwierig und trotzdem sind Systeme zugänglich die eine geringe Virusreplikation unterstützen. Für humane Noroviren wurde auch eine Rolle von Histo-Blutgruppen Antigenen beschrieben, insbesondere der fucosylierten und sialylierten Einheiten.

Aufgrund der Problematik in der Entwicklung von Zellkultursystemen für humane Noroviren werden murine Noroviren oft als Modellorganismus eingesetzt. Hier gibt es ein Kleintiermodell, der natürliche Gast, die Maus sowie mehrere Zellkultursysteme, die eine effiziente Virusreplikation unterstützen. Des Weiteren sind unterschiedliche reverse Genetik Systeme publiziert.

In dieser Arbeit wird die Gast-Virus Interaktion von murinen Noroviren untersucht bezüglich der Bindung des *bona fide* Rezeptors mCD300lf und der Interaktion mit unterschiedlichen Kohlenhydraten, insbesondere fucosylierten und sialylierten Kohlenhydraten und Gallensäften. Mehrere funktionale Bindungsstudien konnten keinen Einfluss von unterschiedlichen Kohlenhydraten auf die Infektion zeigen. Des Weiteren wurde in mCD300lf Rezeptor exprimierenden Zellen mit signifikant reduzierter Sialinsäure an der Zelloberfläche kein Unterschied in der Infektion und Bindung von murinen Noroviren nachgewiesen. Allerdings konnte für den Gallensaft Glychochenodeoxycholinsäure ein fördernder Effekt der Infektion nachgewiesen werden. Dieser Effekt ist unabhängig von der Zelllinie und der Präsenz von Sialinsäure an der Zelloberfläche.

Um die Gast-Virus Interaktion noch ausführlicher zu erforschen wurden mehrere rekombinante murine Noroviren geplant. Hier sollte in dem hervorstehenden Oberflächenprotein (protruding domain) P Domäne ein Alanin Austausch an mehreren signifikanten Stellen, den sogenannten ‚loops' durchgeführt werden. Diese Stellen beruhen auf schon bekannten Bindedaten für den Rezeptor und Antikörpern sowie Kohlenhydratbindestellen in humanen Noroviren. Während der Erstellung der rekombinanten Viren mittels reverser Genetik wurden die limitierenden Faktoren der publizierten Systeme deutlich. Jedoch gelang es mit Hilfe von stabilen Zelllinien, die den mCD300lf Rezeptor exprimieren verbesserte DNS- und RNS-basierte reverse Genetik Systeme zu etablieren. Des Weiteren wurde ein Reportersystem etabliert, welches infizierte Zellen durch die Re-lokalisierung von eGFP sichtbar macht.

Die hier gezeigten Ergebnisse enthalten vor allem Methoden zur weiteren Charakterisierung von murinen Noroviren so wie Einsichten in die Gast-Virus Interaktion, die bei der Entwicklung von Systemen für die Erforschung von humanen Noroviren hilfreich sein wird.

Inhalt

List of figures

List of tables

Abbreviations

Abbreviation	Full name
ATP	Adenosine triphosphate
avSGs	Antiviral stress granules
Casp-3	Caspase 3
CPE	Cytopathic effect
CSP	Chemical shift perturbation
CTP	Cytidine triphosphate
DC	Dendritic cell
DENV	Dengue virus
DMEM	Dulbecco's modified eagle's medium
Dpi	Days post infection
Dpt	Days post transfection
dsRNA	Double-strand RNA
E.coli	*Escherichia coli*
EDTA	Ethylenediaminetetraacetic acid
EMCV IRES	Encephalomyocarditis virus internal ribosomal entry site
Epo	Electroporation
ER	Endoplasmic reticulum
F/S	Frameshift
FACS	Fluorescence-activated cell sorting
FCV	Feline calicivirus
FITC	Fluorescein isothiocyanate
FPV	Fowlpox virus
FUT	Fucosyltransferase
Gal	Galactose
GalNAc	N-acetylgalactosamine
GCDCA	Glycochenodeoxycholic acid
GI	Gastro-intestinal
GlcNAc	N-acteylglucosamine
GTP	Guanosine triphosphate
HBGA	Histo-blood group antigen
HCV	Hepatitis C virus
HIE	Human intestinal enteroid
HIV	Human immunodeficiency virus
Hpi	Hours post infection
HuNoV	Human norovirus
IEM	Immune electron microscopy
IFN	Interferon
kDa	Kilo Dalton
LB	Lysogeny broth
Lipo	Lipofectamine2000
LTR	Long terminal repeat
mAb	Monoclonal antibody
MAVS	Mitochondrial antiviral signal
mCD300lf	Murine CD300lf
MNV	Murine norovirus
Mϕ	Macrophage

NCWG	Norovirus Classification Working Group
NeoR	Neomycin resistance
Neu5Ac	N-acetylneuraminic acid (sialic acid)
NLS	Nuclear localisation marker
NMR	Nuclear magnetic resonance
NS	Non-structural
Nt	Nucleotide
NTP	nucleoside triphosphate
O/N	Over-night
ORF	Open reading frame
P domain	Protruding domain
PBS	Phosphate-buffered saline
Pei	Polyethylenimine MAX 4
PFU	Plaque forming unitsg
PPT	polypurine tract
PTS domain	Proline-threonine-serine domain
PuroR	Puromycin resistance
RBS	Receptor binding site
RC	Replication complex
Rcf	Relative centrifugal force
RdRp	RNA-dependent RNA polymerase
Rec.	recombinant
RF	Replicative form
RHDV	Rabbit haemorrhagic disease virus
RKI	Robert Koch Institute
RT	Room temperature
rtPCR	Reverse transcription polymerase chain reaction
S domain	Shell domain
SEAP	Secreted embryonic alkaline phosphatase
SEM	Standard error of the mean
SPR	Surface plasmon resonance
SRDC	Immortalized mouse spleen dendritic cells
ssRNA	Single-strand RNA
STD	Saturation transfer difference
T/E	Trypsin EDTA
TAR	TAT activation region
$TCID_{50}$	Tissue culture infectious $dose_{50}$
TTR	Translation termination reinitiation
TURBS	Translation upstream binding sites
UTP	Uridine triphosphate
v/v	Volume/volume
VCE	*Vaccinia* virus capping enzyme
VF	Virulence factor
VLP	Virus like particle
w/v	Weight/volume
WGA	Wheat germ agglutinin
Wt	Wild type

1. Introduction

1.1 The family of the *Caliciviridae*

The family of the *Caliciviridae* describes a group of non-enveloped viruses with a single-stranded RNA genome of positive polarity ranging from 7.4 - 8.3 kb [1]. The particles are between 27 - 40 nm in diameter and consist of 90 dimers generally leading to a T=3 icosahedral symmetry [2]. A unifying morphological feature of the *Caliciviridae* family are cup-shaped depressions on the capsid surface leading to the name (Latin *calyx* meaning cup) [3].

Caliciviridae are divided into 11 genera. There are seven genera that infect mammals, including *Lagovirus, Norovirus, Nebovirus, Recovirus [4], Sapovirus, Valovirus [5],* and *Vesivirus [6].* Viruses that infect and cause disease in humans are found in the Norovirus and Sapovirus genus. Additionally there are two genera that infect birds including *Bavovirus* [7] and *Nacovirus* [8] and two genera infecting fish including *Minovirus* [9] and *Salovirus* [10].

1.2 Disease

Noroviruses are a major agent of acute non-bacterial gastroenteritis. The disease caused by norovirus infection is also known as the 'two-bucket disease' or 'winter-vomiting disease'. Norovirus causes one out five cases of acute gastroenteritis worldwide [11]. Gastroenteritis is an inflammation of the stomach and intestines leading to vomiting and diarrhoea. Symptoms typically commence within 12 - 48 h post infection (hpi) [12] and last for 24-48 hours [13-15] but shedding of the virus can persist for weeks or even month in chronically infected patients [16-18].

Noroviruses produce significant morbidity leading to 685 million cases each year worldwide of which 200 million cases are in children under the age of 5 [12]. Of the infected children 70,000 deaths are counted each year mainly occurring in developing countries [11]. The disease burden leads to an estimated cost due to healthcare and lost productivity of $60 billion each year worldwide (CDC).

In Germany 77,583 cases of norovirus infections were reported in 2018 to the Robert-Koch Institute (RKI) leading to 25 reported death which accounts for 0.03% of the reported cases. In 2007 and 2008 a large outbreak was observed with reported cases reaching 201,227 cases (RKI). Until 2016 norovirus infections were the most reported disease in German. Since 2017 it has now become the second most reported disease in Germany after influenza infections [19].

Norovirus is a seasonal disease with most infections taking place during the winter months (December - February in the northern hemisphere; June - August in southern hemisphere) thus the name 'winter-vomiting disease' [20]. Noroviruses is an easily spread and transmitted by the faecal-oral route [17, 18]. Semi-closed environments like elderly homes, hospitals or cruise ships are often sources of infection and increased spreading [21-23].

1.3 Discovery of human and murine noroviruses

The first indication of a non-bacterial agent causing gastroenteritis was found already in the 1940s when brief studies were conducted showing that bacterial-free throat washings and faecal suspensions could lead to gastroenteritis transmission [24].

First tests to identify the causative agent of gastroenteritis aimed to show that human transmission is possible when using bacteria-free suspensions of stool-samples for oral administration [25]. One of the stool samples tested in this study was from a gastroenteritis outbreak in 1968 in Norwalk, Ohio in an elementary school. Here 50% of the students and teachers got infected within two days. However, cultivating an etiological Norwalk (NV)agent in cell and organ culture, as well as in different animals was not successful [26]. Thus, immune electron microscopy (IEM) was used to visualize the viruses [27]. Using stool samples from a volunteer infected with NV showed particles of 27 nm in diameter, which was further analysed and shown to be the causative agent of the gastroenteritis outbreak of Norwalk in 1968. Based on a 277-nucleotide (nt) region in the open reading frame two (ORF2) it was identified as a new cluster within the *Caliciviridae* family [28]. Additional Norwalk-like viruses were since identified and termed noroviruses [29].

Studying human pathogens often relies on animal models. In 2003, Karst et al. showed that in mice lacking both type 1 and type 2 interferon receptors (IFNαβγR$^{-/-}$) a pathogen surpassing a 0.2 µm filter led to lethal infection [30]. Intracerebral inoculation led to a lethal infection resulting in symptoms included encephalitis, vasculitis of the cerebral vessels, meningitis, hepatitis, and pneumonia. Histological analysis showed infection of the meninges, cerebral vessels, and brain. Yet, the diseased brain showed no signs of known human or murine pathogens. The brain homogenate from a diseased RAG/STAT$^{-/-}$ mouse was passed into 129 wild-type mice and sera were tested for different known pathogens after 35 days not showing any known pathogens. Analysis of the virus by representational difference analysis showed sequence homology to many calicivirus genomes. A consensus sequence showed the expected three ORFs of caliciviruses and phylogenetic analysis mapped it at the genus norovirus. Since it did not fit into any known genogroup a new genogroup V was proposed being murine norovirus 1 (MNV-1). MNV-1 infectivity was tested in different mice including Rag$^{-/-}$, IFNαßR$^{-/-}$ and IFNγR$^{-/-}$ mice. These observations showed an influence of the innate immunity on susceptibility to MNV-1 infection. It appears that the innate immunity is sufficient for resistance to MNV-1 infection and that the different interferon receptors can compensate for one another [30].

1.3.1 Human norovirus

For human noroviruses (HuNoVs) functional data is limited. Studies to cultivate HuNoV in different cells were not successful. So far, no cell culture system is available that allows productive passaging of the virus. Yet, a few systems allow limited passaging and infection which include a human enteroid system, a B cells system and a novel zebrafish system [31-34]. Establishing a robust cell culture system for HuNoV is still inhibited by the lack of knowledge concerning a *bona fide* entry receptor. So far Histo-blood group antigens (HBGAs) are considered to be an attachment factor for HuNoVs [35, 36]. HBGAs are found on red blood cells, gut and respiratory epithelium as well as different bodily secretions [37]. For different HuNoV genogroups the binding site of HBGAs varies and a few non-binding strains were also found [38-41]. This suggests that another receptor might be available for HuNoV. In addition, for certain strains a dependence on the fucosyltransferase 2 (FUT2) is known which was shown in the

enteroid system [33]. FUT2 determines the secretor status referring to the secretion of HBGAs. Non-secretors have no FUT2 leading to an absence of HBGAs which appears to influence susceptibility to HuNoV infection. Furthermore, the infection of B cells was improved when adding H-type HBGAs, either soluble or on HBGA expressing bacteria [34].

The dual tropism shown for MNV is also suspected for HuNoV. HuNoV infects different subsets of cells including intestinal epithelial cells and immune cells including macrophages, dendritic cells, T cells and B cells [42, 43].

1.3.2 Murine norovirus

MNV was first described in 2003 and is a great model system to study noroviruses since the natural host, the mouse, as well as different cell culture systems immediately became available. The small animal model was used to study the viral tropism of MNV *in vivo* and the different cell culture systems were used to study MNV *in vitro*. *In vivo* studies revealed a dual tropism for MNV opposed to the first believes after discovering noroviruses as a main cause of gastroenteritis [30]. The dual tropism refers to the phenomenon that MNV can infect epithelial as well as immune cells [44]. A tropism of MNV-1 for gut epithelial cells was shown upon discovery of MNV-1 in $STAT^{-/-}$ mice and a tropism for macrophage (Mϕ) as well as dendritic cells (DCs) was shown shortly after. This also led to the development of a cell culture system for MNV [30, 44]. Tissue and cell tropism of MNV depends on the *bona fide* receptor mCD300lf which is mandatory for an infection with MNV [45]. Knock-out of the receptor *in vitro* and *in vivo* led to a loss of susceptibility towards MNV infection. This receptor is present on different cells including Mϕ cells, DCs and tuft cells [43].

Furthermore, *in vivo* studies showed that different outcomes of an infection are possible, including an acute infection which typically clears within a week and a persistent infection that lasts for at least a month. Analysis of different MNV strains showed a high variability in nucleotide sequence between the laboratory strain MNV and the MNV found in wild mice. It is suggested that MNV laboratory strains cause acute infection and isolates from wild mice lead to persistent infection. Thus, acute infection might be an artificial effect in the laboratory [46, 47].

The acute infection is initiated in the distal part of the small intestine and continues to spread to the small and large intestine, the mesenteric lymph nodes and the spleen [48]. The virus replication in the first 24 h post infection (hpi) occurs in the gut lymphoid tissue like the Peyer's patches. Especially the macrophages, dendritic cells, B cells and T cells are a location of viral replication [48]. The shedding of the newly replicated virus happens in a limited time window at 12-24 hpi.

A persistent MNV infection is typically caused by the strains MNV-3, MNV-CR3, MNV-CR6 or MNV-CR10 [46]. Initial infection takes place in the cecum and then spreads to the small intestine, colon and mesenteric lymph nodes [48]. For MNV-CR6 it was shown that a specialized epithelial cell, the tuft cell, is a site of replication (Figure 1) [43]. The non-structural protein NS1 blocks the interferon-lambda response which leads to persistently infected tuft cells [49-52]. About 1.4% of the tuft cells which corresponds to about 100 cells per mouse are persistently infected upon infection with MNV-CR6 [43, 53].

For *in vitro* studies different cell culture systems are available. The cells susceptible to MNV infection which are commonly used in the laboratory include the macrophage cells Raw 264.7, the glial cells BV-2 and the immortalized mouse spleen dendritic cells (SRDC).

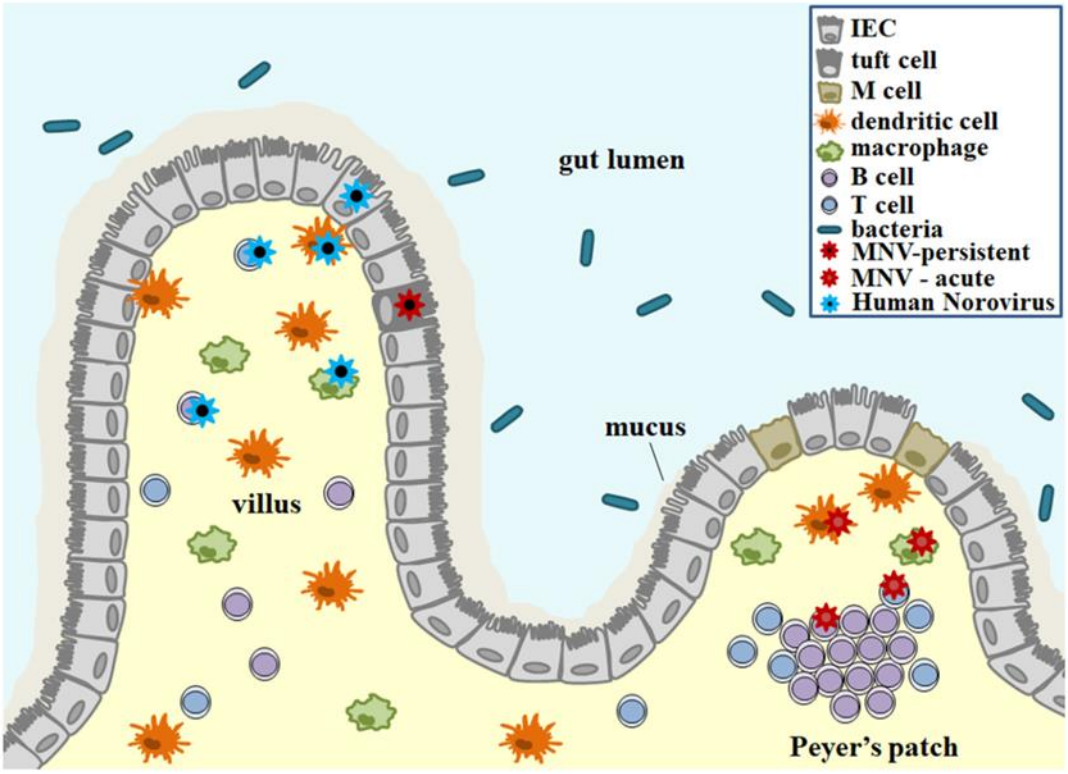

Figure 1 A section of the intestine showing the intestinal morphology. *The intestinal epithelial and immune cells are shown including the different cells present, the intestinal bacteria which were shown to influence norovirus infectivity and the site of infection for acute and persistent MNV as well as HuNoV. Figure taken from [54].*

1.4 Norovirus classification into genogroups

1990 the first classification of noroviruses into genogroups and genotypes based on a partial RNA-dependent RNA polymerase (RdRp) sequence was achieved [55-57]. With increasing sequences available the classification into genogroups and genotypes was shifted to the VP1 sequence where 20% (later adjusted to 15%) sequence difference was used as a threshold for a new genotype [58, 59]. The Norovirus Classification Working Group (NCWG) proposed a universal classification system in 2013 based on the VP1 sequence [60]. Nowadays, based on the VP1 sequence 10 genogroups (GI-GX) are known with two tentative genogroups. These 10 genogroups are further subdivided into 49 genotypes based on the VP1 sequence or 60 P-types which is based on the RdRp sequence [61]. Classification by VP1 sequence relies on the whole sequence whereas P-typing relies on a 762 nt sequence at the 3' end of the RdRp. Using both the VP1 and RdRp sequence recombination events are also taken into consideration. Especially, since it was found that most frequently recombination events occur at the ORF1-ORF2 junction [62-65].

The GI, GII and GIV genogroups are known to infect humans. Yet, the GII.11, GII.18 and GII.19 were also found in faecal samples of swine and the GIV.2 has so far only been detected in carnivores including cats and dogs. The genogroup GIII infects bovine, GV infects mouse and the GVI and GVII infects canine [62, 66, 67].

1.5 Genome structure

The genome of the caliciviruses consists of two to three major open reading frames (ORFs) flanked by short untranslated regions. HuNoVs contain three ORFs and murine noroviruses (MNVs) contain a fourth ORF overlapping with ORF2 (Figure 2). In addition, the caliciviruses depend on a VPg protein for translation, which is covalently linked to the 5' terminus of the genome [68]. A subgenomic RNA containing ORF2, ORF3 and ORF4 is produced mainly coding for the non-structural proteins [69].

The first ORF codes for the non-structural (NS) proteins, ORF2 codes for the major structural protein VP1, and ORF3 codes for the minor structural protein VP2. ORF4 is only found in murine noroviruses, it overlaps with ORF2 and codes for a virulence factor (VF1). The ORF1 is translated as a polyprotein and co- and post-translationally cleaved by the viral protease into six proteins.

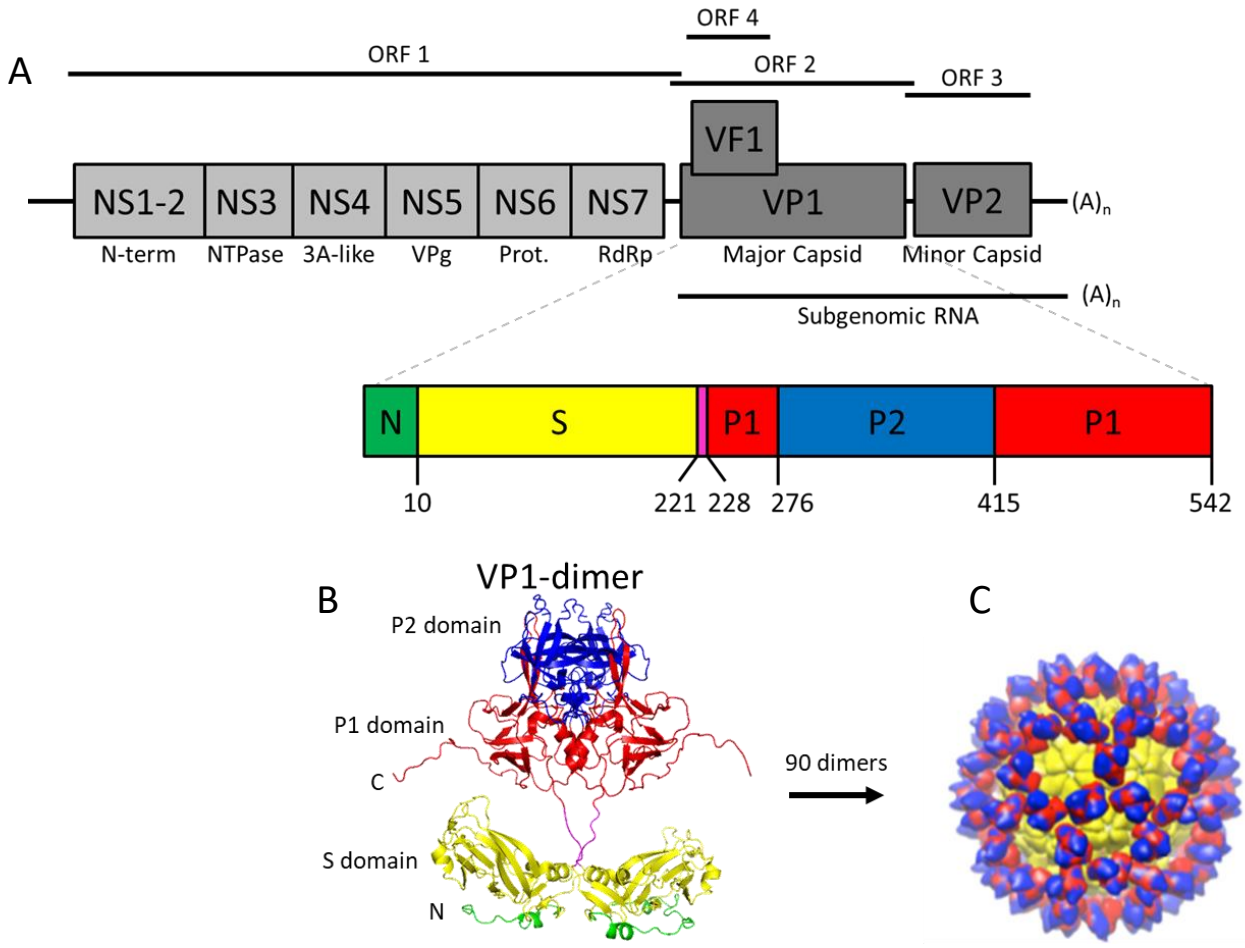

Figure 2 Genome organisation and capsid structure of noroviruses. *(A) The genome structure of norovirus is shown with the ORF4/VF being characteristic for MNV not HuNoV. The major structural protein VP1 is shown in more detail including the different domains. In green the N-terminus, in yellow the shell (S)-domain, in pink a linker, in red the protruding (P) 1-domain and in blue the P2-domain. The represented display the amino acid positions of the reference strain MNV-1.CW1. (B) The P dimer of MNV is shown with the same colour code as the amplification of the VP1 genome structure. (PDB 6CRJ). (C) A virion contains 90 VP1 dimers generally leading to a T=3 icosahedral symmetry.*

1.6 Virus structure and morphology

1.6.1 Non-structural proteins

1.6.1.1 NS1/2 N-term (p48)

The NS1/2 protein is also referred to as N-terminal protein or p48 and the sequence is highly variable among noroviruses. An additional proteolytic cleavage site was found in the GII Camberwell strain leading to two separate proteins with masses of 15 and 22 kDa [70]. For MNV-1 it is described that NS1/2 is cleaved by caspase-3 (Casp-3) to release NS1 and NS2 [71].

For NS1 a role in the IFN-λ resistance in mice is described. NS1 is secreted as a soluble monomer by an unconventional secretion pathway since it is driven by Casp-3 cleavage and without requiring a signal peptide [72]. It was further shown that secreted NS1 is necessary for the infection of specific intestinal epithelial cells called Tuft cells. In other cell types secreted NS1 was dispensable for the infection. Furthermore, NS1 is important for the IFN-λ resistance in mice and immunization with NS1 efficiently protects mice from infection. Still, since NS1 is highly variable it is thought that it is not a good vaccine candidate.

1.6.1.2 NS3 NTPase

NS3 is the nucleoside-triphosphatase of noroviruses and it localizes to replication clusters [30]. Furthermore, it was shown that NS3 induces vesicular structures that associate with microtubules [73, 74]. NS3 also localizes with double stranded (ds)RNA in the perinuclear region of infected cells [75]. Investigation of the vesicular structures showed that they depend on cholesterol and microtubule interaction which possibly achieves membrane curvature [76]. More recently, an enhancing effect of NS3 on the NS7/RdRp-mediated noroviral RNA synthesis was shown *in vitro*. It was shown that NS3 has NTP-dependent RNA helicase and NTP-independent RNA-chaperoning activities, which help to unwind RNA helices and destabilize and remodel structured RNA molecules. Thus, NS3 appears to play a critical role in replication [77].

1.6.1.3 NS4

About the function of the NS4 protein not a lot is known. So far it was shown that it localizes to the endosome [74] and the Golgi [73]. NS4 is the only ORF1 protein that is localized in the endosome which could suggest that it plays a role in the membrane recruitment for replication clusters. Furthermore, a dispersion of the Golgi was shown that is similar to the dispersion of the Golgi in cells infected with poliovirus. Here the dispersion was attributed to the picornavirus 3a protein [73].

1.6.1.4 NS5 VPg

The NS5 protein is the VPg protein, which replaces the 5’ cap and it is covalently linked to the 5’ end of the genomic and subgenomic RNA [78]. The VPg has a molecular mass of 16 kDa [71]. Capping of the RNA is important because it protects the viral RNA from host pathogen recognition receptor like

RIG-I and protein kinase R. Those receptors recognize uncapped 5' triphosphorylated RNA which activate the host antiviral mechanisms. In addition, the cap is important for viral replication. The hydroxyl group is recognized by NS7/RdRp which can be extended by the RdRp. For MNV it is known that upon infection of murine macrophages, a significant number of cells are in the G_0/G_1 phase which is caused by a cell cycle arrest at the G_1/S checkpoint. Expression of NS5 also led to a significant increase (24%) in the number of cells in the G_0/G_1 phase caused by a reduction of cyclin A [79].

1.6.1.5 NS6 viral protease

NS6 of noroviruses is the viral protease. In MNV-1 it ranges from amino acid 995 to 1177 and has a molecular weight of 19.2 kDa. It is a 3C-like protease which is based on its similarity to the 3C protease found in picornaviruses. The protease cleaves the polyprotein produced from ORF1 into six proteins. The five cleavage sites are ^{341}E/G^{342}, ^{705}Q/N^{706}, ^{870}E/G^{871}, ^{994}E/A^{995} and ^{1177}Q/G^{1178} [71]. The protease localizes to the mitochondria [74] and is highly conserved between different viruses. The sequence similarity is at 71 % [80, 81]. Structurally, the protease has a catalytic diade and the motif ^{1131}GDCG^{1134} is found in MNV-1 [82].

1.6.1.6 NS7 RNA-dependent RNA polymerase

The NS7 is the RNA-dependent RNA polymerase (RdRp) which has a molecular weight of 57.5 kDa. Comparing the structure of the norovirus RdRp with other positive-strand RNA viruses, revealed that they have a significant similarity [83-86]. Structures of the apoenzyme of HuNoV RdRp are available showing presence of divalent metals in the active site, presence of nucleoside triphosphates (NTPs), or are ternary complexes with template RNA and primer or nucleotide analogues. The structure of the RdRp can be described as a right hand that is partially closed containing the thumb and fingers as well as the palm. The thumb and the fingers form a channel, where the single-stranded RNA can thread into the polymerase. This channel is lined by highly conserved residues and at the convergence of the template channel and NTP channel the active site is located. The active site contains aspartate residues that coordinate divalent metals to promote nucleotide polymerization [83, 86].

1.6.2 Structural proteins

1.6.2.1 VP1

VP1 is the major structural protein of noroviruses and 90 VP1 dimer build a virus particle with T=3 icosahedral symmetry. The VP1 monomer is 530-555 amino acids long and has a molecular weight of 58-60 kDa. Looking at the structure of the VP1 it can be sub-divided into a shell domain (S domain) and a protruding domain (P domain). The latter one can again be sub-divided into a P1 and P2 domain. The P2 domain is flanked by the P1 domain (Figure 2). The P1 domain represents a hyper variable part of the P domain, which is involved in antibody and receptor binding [45, 87]. The P domain consists of different ß-strands (six antiparallel ß-strands in the P2 subdomain, two highly twisted antiparallel ß sheets in the P1 subdomain) [35], an α-helix and five different loops (A'B'-loop, C'D'-loop, D'E'-loop, E'F'-loop and P1 loop). The position 386 is part of the E'F'-loop and upon mutation the neutralizing effect of the antibody A6.2.1 is diminished showing the important role of the loops in antibody binding

[88]. Furthermore, the A'B'-loop and D'E'-loop are involved in the receptor binding of MNV to the cognate receptor CD300lf present on all cells known to be susceptible to MNV [89]. For HuNoV a binding of different fucosylated and sialylated glycans was shown with binding sites of fucose detected in the canyon of the P dimer [90-92]. The dimeric contact of the P domain increases stability and the P1 domain is the most distal part of the P dimer. Hydrogen bonds between the two P1 subdomains are found in the P dimer [35]. The S domain is present at the N terminal part of VP1 and is 225 amino acids long. The S domain forms an icosahedral shell building the basis of the of the virus particle and the P domain sits on top forming outwards facing protrusions.

1.6.2.2 VP2

VP2 is the minor structural protein of noroviruses. Its function is not yet fully understood. The protein consists of 208-268 amino acids and has a molecular weight of 22-29 kDa. The sequence variability between the strains is significant [70]. In an infectious particle 1-2 copies of VP2 are present which was first described for a related calicivirus, the rabbit haemorrhagic disease virus (RHDV) [93] and later also for norovirus and other members of the calicivirus family [94]. It has been shown that virus-like particles can assemble in the absence of VP2 but for the formation of infectious particles VP2 is essential [95]. The isoelectric point of VP2 is >10 meaning it is a basic protein, which is indicative for a role in RNA binding. The translation of VP2 is thought to be regulated by a translation termination-reinitiation strategy [96]. Translation upstream binding sites (TURBS) resembles a translation termination-reinitiation (TTR) signal, which is found in murine noroviruses at the ORF2/3 junction. TURBS require a stop and a start codon in close proximity to each other. For MNV the UAA stop codon of ORF2 overlaps with the AUG start codon of ORF3 and an efficient reinitiation is dependent of 43 nt RNA directly upstream of this UAAUG codon. [97].

1.6.2.3 VF1

The virulence factor 1 (VF1) encoded by the ORF4 is only found in MNV but no other noroviruses. The ORF4 overlaps with the ORF2 and is produced by frameshift +1 compared to ORF2 [47]. The function of the VF1 is the interference with the interferon mediated host response pathways and apoptosis [98].

1.6.3 Virus morphology

The virus particle is an icosahedral particle with a T=3 symmetry containing 180 VP1 monomers in the particle. The diameter is around 28-35 nm in diameter [99].

Since HuNoVs are recalcitrant in cell culture different means were taken to study the virus morphology including virus like particles (VLPs). For different viruses including noroviruses it is possible to obtain VLPs which are particles that resemble the virus morphology, but they do not carry genomic material. For HuNoV VLPs the synthesis of the capsid protein VP1 is sufficient to obtain VLPs [37, 100]. Often a baculovirus expression system is used for the synthesis of various HuNoV VLPs. Different HuNoV VLPs were found not containing the T=3 symmetry but a T=1 or T=4 icosahedral symmetry [101, 102].

1.7 Norovirus cultivation in cell culture

1.7.1 Enteroid system

The enteroid system is an established system used to study HuNoV. It is called a 'mini-gut' culture which describes its characteristics. It is a human intestinal enteroid (HIE) system which originates from patient samples of the human small intestine. The intestinal crypts are needed to grow such an HIE system in the laboratory. Various parts of the small intestine can be used and depending on the patient's phenotype different HBGAs are present in the enteroid. In addition, it was shown that the secretor status determined by the fucosyltransferase 2 plays a role in the performance of the enteroid system. Furthermore, different microbes need to be incorporated [103, 104].

The enteroid system can be used to study different mechanisms of HuNoVs which may lead to a better insight into viral replication as well as inactivation and inhibition.

In a 3D enteroid system the injection of viral samples is not easy without disrupting the system. Either a small needle or chemicals are used.

The enteroid system can be used to study different mechanisms of HuNoVs which may lead to a better insight into viral replication as well as inactivation and inhibition.

1.7.2 BJAB B cell system

The BJAB B cells are a cell line derived from the lymph node from a metastatic site (LGC ATCC) of the Burkitt-like lymphoma.

Since MNV showed replication in murine derived B cells the BJAB B cells appeared to be a promising target for HuNoV replication. The GII.4 Sydney strain is a prominent strain circulating worldwide [105-107] and was used to establish the BJAB B cell model. HuNoV positive stool samples were incubated with the BJAB B cells and analysis of the genome titres at 3 dpi and 5 dpi showed an increase of 10-fold and 25-fold in genome copy numbers compared to the input level. To control the experiments UV-inactivated stool samples were used for inoculation which showed no increase in genome copies. To further characterise the BJAB B cell system the stool samples used were filtered through a 0.2 µm filter before inoculation. A cofactor for infection appeared to be necessary since infection was decreased in the filtered stool samples. The H-type HBGA carrying bacteria *Enterobacter cloacae* restored the infectivity of filtered stool samples compared to unfiltered samples. In addition, synthetic H-type HBGAs had a similar effect [34].

1.8 Animal models to study noroviruses

Different models to study HuNoVs are available including animal models. One of the first model systems was the chimpanzee but due to the lack of disease and because of ethical concerns studies were no longer pursued.

1.8.1 Gnotobiotic pigs

One animal model to study HuNoVs the gnotobiotic pig. Gnõtos is Greek for 'known' and gnotobiotic animal is the description for a germ-free animal. Thus, a gnotobiotic pig is a pig born and raised in a germ-free environment. Those gnotobiotic animals are often used to study host-pathogen interaction in a controlled environment without interference of other microorganisms. The gnotobiotic pig is used for different studies on HuNoVs. It is an excellent model for gastrointestinal viruses because the gastrointestinal structure, physiology and immunology of the pig is similar to those of a human. In addition, a similarity in HBGAs is present. A and H type HBGAs can be found in the pig. It was shown that in gnotobiotic pig HuNoVs replicate in the enterocytes present on the top of the villi in the small intestine [108].

The different studies performed in gnotobiotic pigs include inactivation studies [109] that showed that heat inactivation under high pressure is efficient in norovirus sources like clamps, shellfish and oysters. Another study showed that the HBGAs (A/H type) found in the GI tract of pigs interact with HuNoV and sero-conversion takes place in pigs upon infection with HuNoVs. Yet, this study showed, that another factor might be present since A/H type HBGAs alone did not guarantee infection [108]. In a more recent study, the influence of bacteria on infection with HuNoVs was studied. For the B cell system supporting HuNoV replication it was shown that *Enterobacter cloacae* enhance infection [34]. *Enterobacter cloacae* express surface HBGAs and thus came up in a screen-testing for commensal enteric bacteria [110]. Surprisingly, it was shown that *Enterobacter cloacae* inhibited HuNoV infection in gnotobiotic pigs [111].

1.8.2 Mouse model for HuNoV

For the HuNoV strain GII.4 which is a prominent strain a mouse model is available [112]. The BALB/c $Rag^{-/-}$ $\gamma c^{-/-}$ mice show viral replication. This replication was observed in humanized and non-humanized mice yet, in immunocompetent BALB/c mice no infection was observed indicating that the immunodeficient status is more important than the human immune cells. The infection of the mice is dependent on intraperitoneal infection of the mice. Structural and non-structural proteins of HuNoV can be detected in cells with macrophage-like morphology present in the spleen and the liver. This first small animal model was successfully used in inhibitor studies [113].

1.8.3 Zebrafish system

Danio rerio also known as zebrafish is a widely used vertebrate model in research. The zebrafish is a tropical freshwater fish which is optical transparent. Its advantages in research is the similarity to the human. About 70% of its genes are shared with human and next to the remarkable genetic similarity is the similarity in physiology and pharmacology. Furthermore, its immune system is comparable to the human immune system as it contains B and T cells as well as macrophages, neutrophils and comparable signalling molecules and pathways [114].

For HuNoV a robust replication model was described in zebrafish [32]. They showed that different GI and GII virus strains could replicate in zebrafish larvae. At 3 days post fertilization (dpf) the HuNoV was injected into the yolk sac of the fish and replication was quantified by real-time PCR. Zebrafish larvae till 5 dpf are in better agreement with the EU law on experimental animal welfare and the 3R rule. Replication of the virus is dependent on the injection into the yolk sac of the larvae and on the amount of virus injected. An infectious dose 50 (ID_{50}) was determined for the GII.6 strain at ~10^3 viral RNA copies. This replication model is suitable to study inhibitors and replication of HuNoV.

1.9 Murine norovirus as a model system for HuNoV infections

Since HuNoVs are reluctant to be cultivated in the laboratory it is difficult to study the biology of HuNoV infections. Since MNV was discovered it has become a widespread model system for norovirus.

The advantages of MNV as a model system include the easy handling of MNV as it replicates efficiently in cell culture like Raw 264.7 and BV-2 cells [30, 44]. In addition, the natural host, the mouse is an animal model that is relatively inexpensive and versatile and often used to study viral pathogens. Using the mouse model MNV provides the first model for noroviruses to understand the mechanisms of replication in the natural host as well as in tissue culture. Furthermore, since the mouse model is an established model different mouse strains are available include knock-out mice, immunodeficient mice and humanized mice. In immunocompromised mice MNV pathogenic [30] whereas in wildtype (wt) mice MNV does not lead to overt signs of infection. The $Rag^{-/-}$ mice can be persistently infected with MNV-1 and shedding of the virus leads to virus transmission to littermates as well as via the bedding of the cage when naïve mice were introduced into the cage [115]. This shows that MNV can be transmitted via the faecal-oral route and possibly also via respiratory routes.

Looking at the structure of MNV particles compared to HuNoV significant similarities are found. The size of the viral particles varies between 28-35 nm in diameter for MNV and HuNoV, both have a T=3 icosahedral symmetry and the buoyant density is the same at 1.36± 0.04 g/cm^3 [1, 30]. Furthermore, MNV and HuNoV display a similar genome organisation involving three major ORFs. Since the molecular features are conserved it is suggested that studies of MNV may define mechanisms found in HuNoVs including replication and binding to attachment factors. Both, MNV and HuNoV rely on subgenomic RNA for the synthesis of structural proteins. This is suggested to be a regulatory mechanism which is also found in other RNA viruses [44, 116, 117]. Furthermore, MNV showed intracellular membrane reorganization in infected cells [44] which was also shown for HuNoV caused by non-structural proteins [118].

1.10 The norovirus replication cycle

Information on the norovirus replication cycle is mainly based on research on MNV (Figure 3).

Attachment of HuNoV depends on glycan binding, especially histo-blood group antigens (HBGAs) whereas MNV binds to the *bona fide* receptor mCD300lf (Step 2) which was recently discovered and shown to be essential for infection [45].

In addition, a role of sphingolipid biosynthesis during receptor binding was described. The *Sptlc1* and *Sptlc2* genes are genes which are essential members of the serine palmitoyltransferase complex which catalyses ceramide and sphingolipid biosynthesis [119, 120]. Those genes were shown to be important for MNV replication [45]. In a more recent study [121] it was shown that upon knock-out of *Sptlc2* the binding of MNV to BV-2 cells decreases. Furthermore, a conformation dependent antibody is no longer able to bind to mCD300lf. Thus, lipid composition of the host cells appears to be a critical determinant of MNV entry.

MNV is internalized by the cell by endocytosis depending on dynamin II and cholesterol (step 3) [122, 123]. Uptake is rapid (within 1 h) and in addition, it was shown that it is pH dependent [124]. The mechanism of MNV uptake by cholesterol- and dynamin II-dependent endocytosis is not well defined.

After the uncoating of the virus and the release of the viral RNA into the cytoplasm (step 4) the first round of viral translation takes place using the viral genome as a template (step 5). The VPg covalently linked to the 5' end of the RNA acts as a cap substitute and recruits the host cell translation initiation factors. This leads to the translation of the viral RNA into proteins by the cellular translation apparatus. It is known that the highly conserved C-terminus of VPg interacts with eIF4G [125]. This interaction is essential for the translation of the genome and as of today the function is unique to caliciviruses. After translation, the viral replicase components, originating from ORF1, are released into the cytoplasm. The ORF1 polyprotein is cleaved co- and post-translationally by the viral protease [126] into six proteins (step 6) [71]. The replicase complexes are needed in the cytoplasm to create subcellular compartments for the viral replication and synthesis of new viral genomes. In those membrane associated replication complexes the replication of the viral RNA via a double stranded RNA intermediate takes place. The double stranded RNA intermediate is called replicative form (step 7) (RF). Genomic and subgenomic RNA is synthesized via *de novo* mechanisms by the viral RdRp and VPg dependent mechanisms [78]. A localization of the RdRp, VPg and double stranded RNA in membrane complexes called replication complexes (RCs) was observed [127]. The synthesis of the VPg-linked genomic RNA occurs from the poly-A tail located at the 3' end of the negative sense RNA. The VPg-linked subgenomic RNA is primed at the subgenomic RNA promoter consisting of a stem loop that is six nucleotides downstream of the start site of the subgenomic RNA (step 8) [128]. With increasing amounts of genomic and subgenomic RNA the amount of viral proteins increases as well leading to the packaging of the genomic RNA into virions and their release (step 9) [129]. In FCV an interaction of the VPg and the major capsid protein VP1 is observed thus indicating a role of VPg during viral packaging [130]. How the virions are released from the cells still needs to be elucidated but it is known that MNV is cytopathic and an activation of caspases is involved (step 10). Furthermore, a downregulation of survivin, an apoptosis inhibitor, was observed [131]. Interestingly in B-cells a persistent infection was described [34].

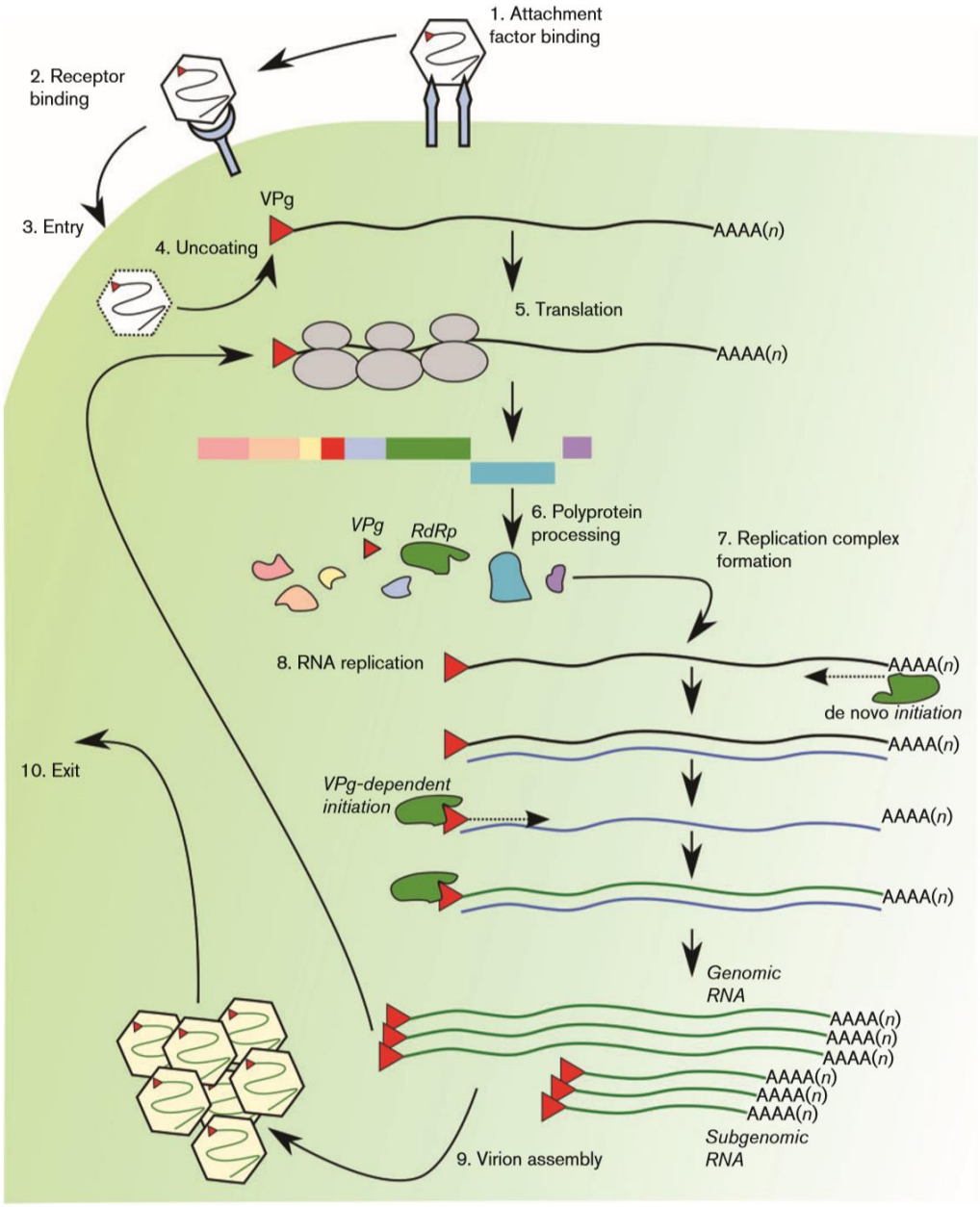

Figure 3 A schematic overview of the replication cycle proposed for noroviruses. *The lifecycle of noroviruses is depicted from results mainly obtained from MNV. The different steps of the viral replication taking place in the cytosol are numbered and further explained in the text [132].*

1.11 A *bona fide* receptor for murine noroviruses

For MNV, the entry receptor was identified as the murine CD300lf and CD300ld surface proteins [45]. To show that mCD300lf and mCD300ld are the *bona fide* receptors of MNV knock-out cells were created, the BV-2ΔmCD300lf and BV-2ΔmCD300ld cells. The BV-2ΔmCD300lf cells were resistant to infection with MNV whereas the BV-2ΔmCD300ld cells were still susceptible to MNV infection. Furthermore, expression of mCD300lf and mCD300ld in human, non-susceptible cell lines (HeLa cells) rendered them susceptible to MNV infection. The ectodomain of mCD300lf could also be used to neutralize MNV by incubating the virus with the ectodomain before infection.

The mCD300lf receptor belongs to the family of CD300 which are type-I transmembrane proteins in the immunoglobulin superfamily. The CD300 family contains eight proteins in mice which contain an IgV-like extracellular domain with two disulphide bonds and the transmembrane domain is a helix [133]. Sequence alignment of the CD300 family showed that the residues interacting with the P2 domain of mCD300lf were partially conserved in mCD300ld but varied in the other family members [89]. Next to mCD300lf also mCD300ld rendered HeLa cells susceptible to MNV infection. But compared to mCD300lf, mCD300ld knockouts in BV-2 cells showed no significant impact on infection with MNV. In addition, the ectodomain of mCD300ld was not able to neutralize MNV. The mCD300ld receptor seems to render eukaryotic cell lines susceptible to MNV infection yet it has no essential role in infection of BV-2 cells or mice. The other six molecules of the mCD300 family had no impact on infection with MNV [45].

Using X-ray crystallography, the binding of mCD300lf to the P domain was further investigated (Figure 4). The P domain of MNV-CR10 was crystallized with the soluble domain of mCD300lf. A network of hydrophobic and hydrophilic interactions binds the mCD300lf exodomain to the MNV-CR10 P domain. Crystallography showed that five hydrogen bonds are found in the interaction of the P domain with the mCD300lf receptor. Six interaction residues were found in the P domain of which five are highly conserved between the different strains. The CC' loop and CDR3 loop of the mCD300lf interact with the P domain. It was shown that the mutation of those loops diminishes or abolishes binding [45]. The binding site of the mCD300lf to the P domain overlaps with the contact area of two neutralizing antibodies (2D3 and A6.2) which might explain the neutralizing effect of those antibodies [89].

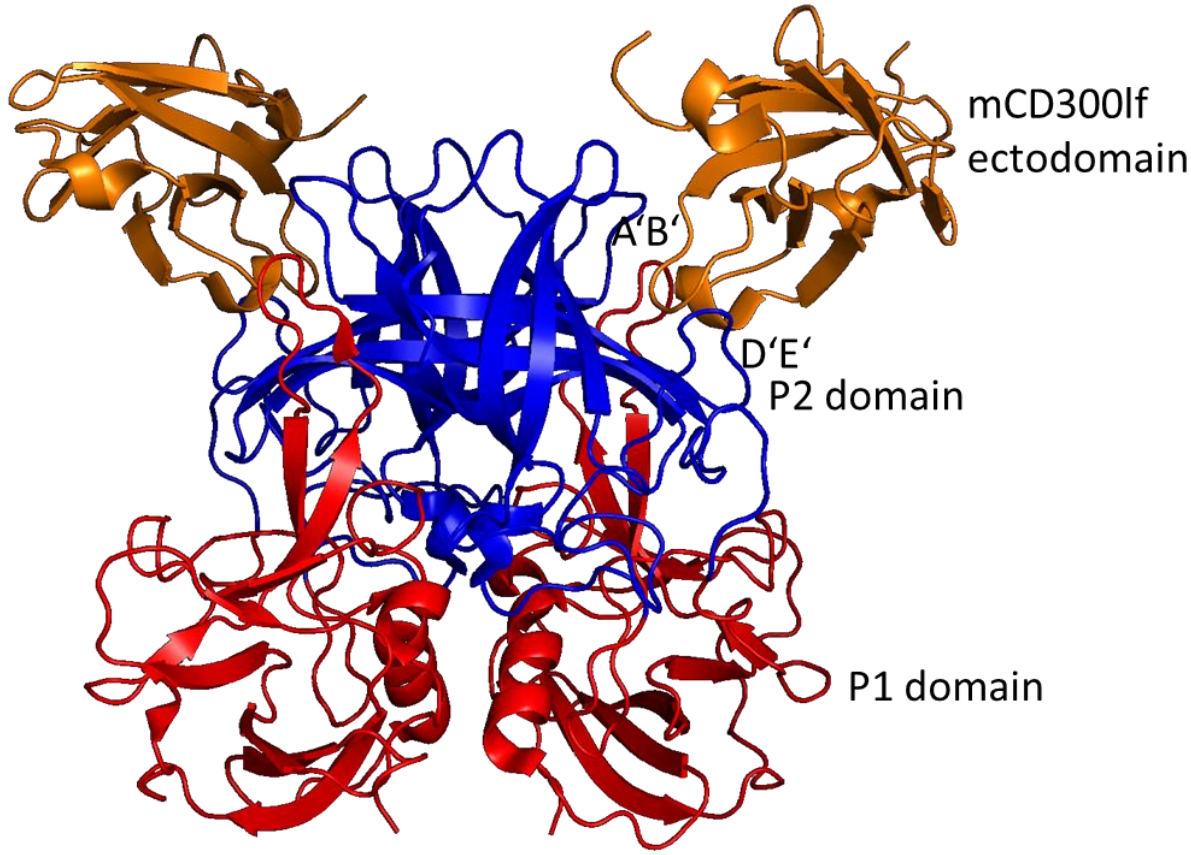

Figure 4 The murine CD300lf receptor binds to the P dimer of MNV.CR10. *The MNV.CR10 P dimer was co-crystallized with the soluble part of the murine CD300lf receptor showing the binding to the P2-subdomain (PDB 6C6Q) [87]. The colours refer to the P1 domain in red, the P2 domain in blue and the two receptors bound in orange. The A'B'-loop and D'E'-loop important for the receptor binding to the P2 domain are indicated.*

1.12 Host factors in norovirus infection

1.12.1 Histo-blood group antigens are binding factors for human noroviruses

Histo-blood group antigens (HBGAs) are carbohydrate-based antigens including the ABH and Lewis antigens. These HBGAs were identified as determinants for HuNoV infection almost 20 years ago [134-136]. The ABH antigens are the commonly known blood groups A, B and H (or O) found on red blood cells. The HBGAs are also present on epithelial and endothelial cells in the whole body and can be secreted and thus be found in body fluids including saliva and intestinal secretions [137]. One of these places of secretion is in the GI tract especially in the intestine where the mucus layer contains a rich display of HBGAs. A role of the HBGAs is the interaction with pathogens including viruses.

The HBGAs are synthesized from disaccharide precursor and different glycosyltransferases modify them

by adding monosaccharides (Figure 5) [137, 138]. The location of the addition of the monosaccharide determines the HBGA type. Fucosylation of the ABH and precursor antigens on the GlcNAc create the *Lewis* antigens. FUT 2 adds the so-called *Secretor* fucose. In Europe 20% lack the fucosyltransferase 2 leaving them with a non-secretor phenotype in which it is characteristic to not have secreted HBGAs in the body fluids or mucus [139]. In type 1 HBGAs the FUT2 adds monosaccharides to the Galß1-3GlcNAc precursor in an α-1,2 linkage leading to an H type 1 antigen. The Lewis enzyme FUT3 adds fucose in an α-1,3 linkage or α-1,4 linkage leading to the tetrasaccharide Le^B. In a similar fashion the A or B enzyme add N-acetygalactosamine or galactose in an α-1,3 linkage to the H type 1 antigen resulting in A type 1 or B type 1 antigens. Like the type 1 pathway in the type 2 pathway the Galß1-4GlcNAc precursor is modified by FUT1, FUT3, A and B enzyme resulting in H type 2, Le^x, Le^y, A type 2 and B type 2 antigens. The type 3 HBGAs are based on the precursor Galß1-3GalNAc and FUT2 addition of the monosaccharide leads to the H type 3 antigen. This can be further modified by A and B enzymes [137].

For noroviruses, especially HuNoVs it is known that they are capable of binding HBGAs and Lewis antigens which are important for infection [41, 136, 140]. Rockx et al. showed that at least nine different types of HBGAs are bound and they suggest that the expression of the H type leads to a higher chance of infection [141]. Multiple binding studies of HBGAs were performed with the prevalent GII HuNoV [38, 91, 142-144]. Furthermore, voluntary human challenge studies showed evidence for HBGA recognition by Norwalk virus. The infection rates observed in the volunteers match with the binding profile of Norwalk virus [145, 146]. However, between the different genogroups the binding sites vary significantly yet, they are located on the top of the arch-like P2 domain. The key residues for HBGA biding appear to be highly conserved [147].

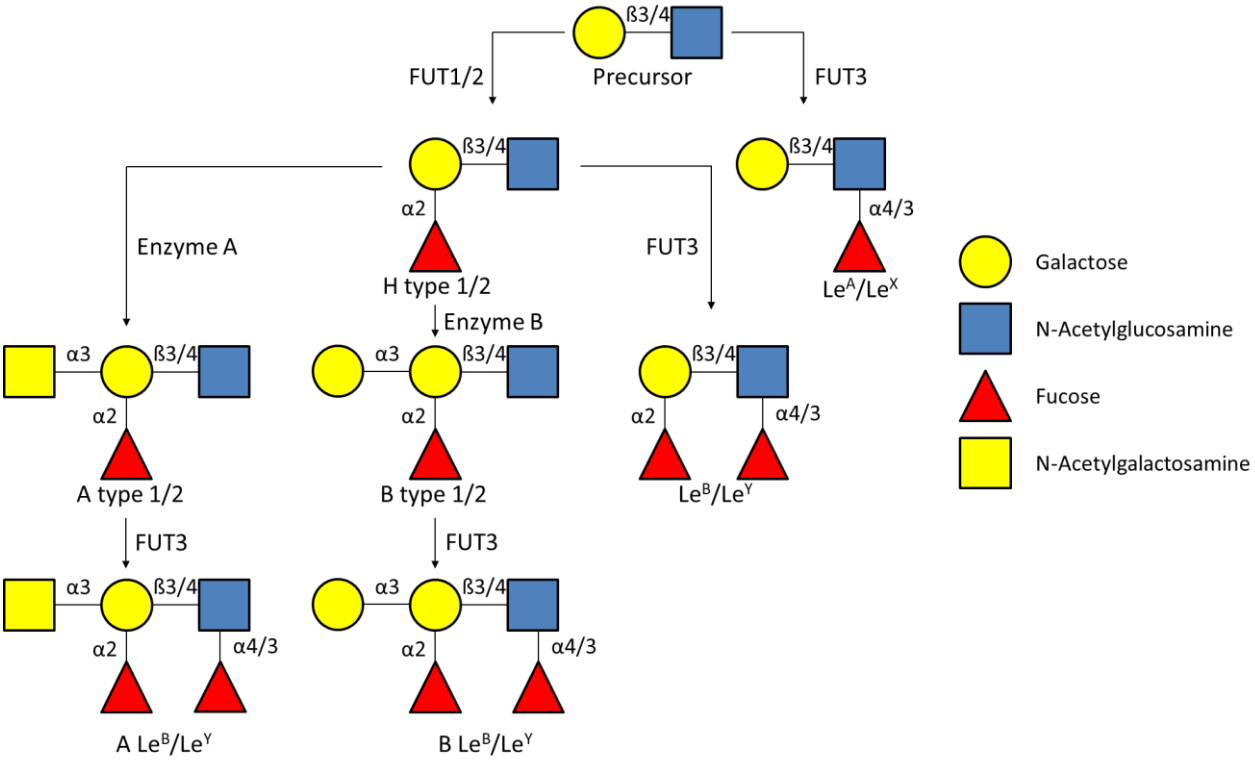

Figure 5 Schematic overview of the synthesis of the different HBGA and Lewis antigens*. The different steps of the synthesis of the different HBGAs and Lewis antigens is shown. Lewis = Le, fucosyltransferase = FUT. Adapted from [138, 148].*

1.12.2 Glycochenodeoxycholic acid (GCDCA)

Glycochenodeoxycholic acid (GCDCA) is a bile acid which is the glycine-conjugated form of the primary bile acid chenodeoxycholic acid [149, 150]. It is a surfactant that solubilizes lipids for absorption and is itself absorbed.

Orchard et al. already proposed in their paper describing the mCD300lf receptor that a possible co-factor exists that is below 5 kDa, heat stable up to 95 °C and is found in delipidated and proteinase K treated serum [45].

A co-factor was identified by Nelson et al. as being the bile acid GCDCA. The crystal structure of the P domain showed that a binding pocket for GCDCA is present at the interface of the two P monomers. More precisely the binding pocket is at the interface of the P1 and P2 subdomain leaving space for two GCDCA molecules. A K_D of ~5.76±1.26 µM was determined [87]. Next to MNV it was also observed that GCDCA binds to HuNoV VLPs. GCDCA binds to VLPs of the genogroup II (GII.1, GII.10 and GII.19) but not to GI.1, GII.4 or GII.17. When binding occurs the K_D was comparable to the K_D observed by Nelson et al. in the low µM range. Interestingly, the HuNoV is known to bind HBGA and need it as a factor for infection. Here binders and non-binders of HBGAs are known. GII.1 is known as a non-binder of HBGAs yet in the presence of GCDCA binding to HBGAs was observed. Furthermore, In GII.10 the binding of the P dimer to HBGAs was enhanced in the presence of GCDCA [89]. For MNV an enhancing effect in infection was also observed when GCDCA was present [87].

1.12.3 Mucus

The gastrointestinal tract, especially the intestine contains a mucus layer. This mucus layer varies in composition, organization, and thickness along the intestine [151]. In the intestine the mucus layer is

divided into an outer layer and an inner layer. The outer layer is a nutrient-rich habitat for microbiota and the inner layer is firmly attached to the surface of the epithelium and virtually free of bacteria [152, 153]. The mucus layer mainly consists of mucins which are either membrane bound or secreted [154, 155]. Structure-wise the mucin has an N-terminal signal peptide and a proline-threonine-serine (PTS) domain. The PTS domain is the side of *O-glycosylation* and the glycans account for 80% of the total mucin mass [156]. In other words, the mucins can be described as a filamentous protein backbone decorated outwardly protruding oligosaccharides which results in the typical 'bottle-brush'-like appearance [157]. The group of the membrane bound mucins are the essential contributor to the glycocalyx which places a role in cell-cell and cell-matrix interactions as well as cell signalling [158]. The secreted mucins are synthesized by the goblet cells in the small intestine and colon [159]. For the glycosylation of the mucins the glycosyltransferase of the host determines the structure and linkage. The structures mostly added are galactose (Gal), N-acetylglucosamine (GlcNAc), N-acetylgalactosamine (GalNAc), fucose or sialic acid (Neu5Ac) with the latter two frequently occupying terminal positions [160].

1.12.4 Microbiome

Norovirus is an enteric virus and it was shown that the gut microbiota plays a role in norovirus infection and norovirus infection also affects the gut microbiota.

In the gastrointestinal (GI) tract the taxa *Bacteroidetes* and *Firmicutes* are most predominant [30, 66]. For HuNoV it was shown that they interact with *Enterobacter cloacae* and *Clostridium difficile*. Both express HBGA-like carbohydrates on their surface and the viral capsid of HuNoV interacts with them [110, 161]. Since HuNoV and MNV were shown to interact with sialic acid residues it is expected that MNV is also able to interact with carbohydrates expressed on bacterial surfaces [31, 162]. The importance of the intestinal bacterial population was shown by depleting the intestinal bacteria with antibiotic treatment in mice. This antibiotic treatment reduced the severity of an acute infection and furthermore reduced or prevented persistent infections in the ileum and colon. An infection with MNV-CR6 which leads to a persistent infection can be rescued by a faecal transplant. Here, the faecal microbiota from a non-antibiotic-treated mouse is transferred to an antibiotic-treated mouse which shows signs of infection upon transplantation [163]. The tuft cells might play a role in the changes in infection observed. Tuft cells are regulated by the commensal bacteria which means that upon antibiotic treatment the bacteria are depleted and thus the number of tuft cells is reduced. Since tuft cells are susceptible to infection and MNV replicates in tuft cells a decrease in the number of tuft cells could lead to a decrease in viral titres [43].

Another effect of norovirus infection observed was the influence of norovirus on the bacterial composition of the GI tract. For HuNoVs it was shown that an infection significantly alters the human gut flora [164]. A dysbiosis is induced which leads to an enhanced ratio in *Firmicutes* to *Bacteroidetes*. This was observed for HuNoV as well as MNV, yet for MNV this was only observed in an early acute MNV-1 infection [165, 166]. In a different longitudinal study for acute and persistent MNV infection (MNV-1, MNV.CR6 and MNV-4) this change in ratio was not detected. This could be a hint that it is only a temporal effect, or it could be facility-based [167].

1.13 Tools to study norovirus biology

1.13.1 Virus like particles

VLPs are a a good model to study virus morphology and interaction with attachment factors. In VLPs the structural proteins form the viral capsid and thus represent a viral particle, yet no genetic material or non-structural proteins are present. For HuNoV the VLPs of different genogroups are available. Typically, the VP1 structural protein is enough to obtain VLPs. The VLPs self-assemble upon expression of VP1. Different expression systems are published including the protein synthesis in Hek 293T cells or a baculovirus expression system [129, 168]. Different T=1, T=3 and T=4 VLPs were found for HuNoV [101, 102].

1.13.2 HuNoV replicon

For the HuNoV establishing an efficient reverse genetics system is challenging since cell culture systems are still under development or were just recently published like the zebrafish model [32].

A replicon system can be used as a tool to study the non-structural proteins and their interaction with cellular proteins. In addition, inhibitor studies can be performed. A replicon system for HuNoV GI.1 (Norwalk virus) was established [169].

The described replicon system relies on the transfection of capped RNA into either Huh7 or BHK cells. By antibiotic selection using neomycin positive cells were selected. By Northern blot and reverse transcription (rt) PCR the presence of the viral RNA was determined. Unfortunately, the system works at a low efficiency which makes it unsuitable to study effects of mutations on viral replication. Still the wt RNA can be used to study replication and inhibitor effects on Norwalk virus.

1.13.3 Reverse genetics

Reverse genetics is a tool to study viruses. Compared to forwards genetics where a virus phenotype is observed and the genotype is determined, in reverse genetics the genotype of the virus is modified, and a resulting phenotype is analysed. Using this tool, a lot of knowledge was gained for different viruses.

Differing between the types of viruses are also the types of reverse genetics systems. For the DNA viruses' reverse genetics systems were developed as early as 1957 where a T2 bacteriophage was rescued [170]. For the rescue of the T2 bacteriophage the full-length DNA genome was transfected into viral replication supporting cell lines, thus the system is straightforward. The first reverse genetics system for an RNA virus was established in 1978 where the bacteriophage Qbeta was rescued from a cDNA-based system [171]. The first mammalian plus-strand RNA virus was rescued in 1981 being the poliovirus [172]. It was shown that the efficiency of virus rescue for plus-strand RNA viruses could be improved when using *in vitro* transcribed RNA [173]. At the same time, the first negative-sense RNA virus was rescued being the rabies virus [174]. Here the cDNA of the viral antigenome was used for transfection leading to the rescue of the recombinant virus.

Until today different reverse genetics systems are under development and are constantly being improved. Different bottlenecks need to be overcome to establish a robust system. For the family of the *Caliciviridae* the first reverse genetics system was established for the feline calicivirus (FCV) [175]. The *in vitro* transcribed and capped RNA from a full-length cDNA clone was transfected into permissive feline kidney cells leading to the rescue of the recombinant virus.

For noroviruses the MNV is a commonly used model to study host-virus interactions. Since the discovery of MNV in 2003 different reverse genetics systems were established including cDNA-based, RNA-based, helper virus-based, and baculovirus-based reverse genetics systems [176-178]. For HuNoVs reverse genetics systems are still at a starting point possibly due to the lack of a robust cell culture system that can easily be manipulated.

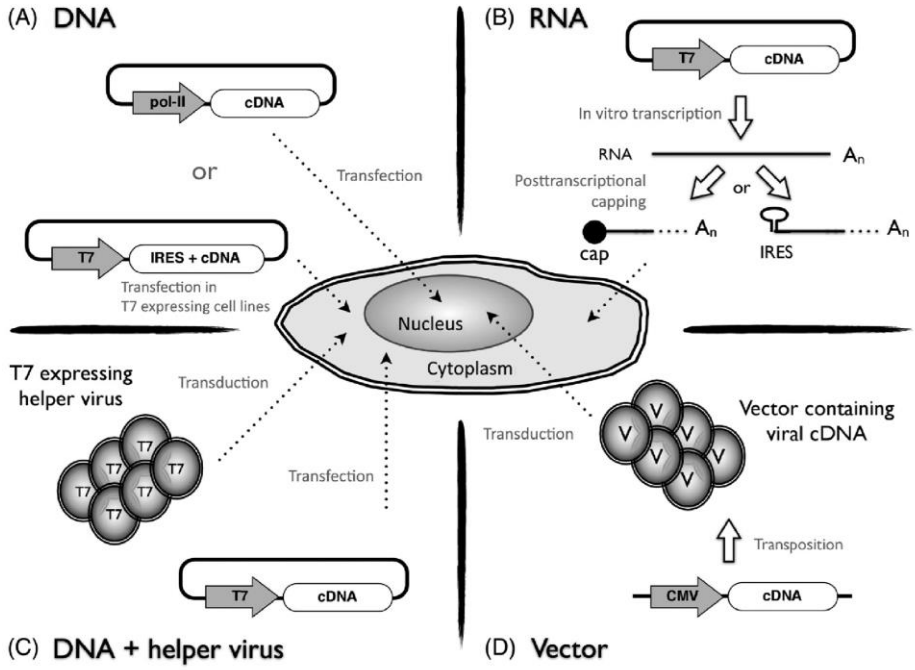

Figure 6 A summary of the different reverse genetics systems described for MNV. *For MNV different reverse genetics systems were described and are summed up with the basic steps and features including nucleotide source and mode of cell manipulation. Figure from [179].*

1.13.4 A cDNA-based reverse genetics system

A cDNA-based reverse genetics system was published in 2007 [176] where the full-length cDNA of MNV-1.CW1* was expressed by a polII promoter. This system is based on two different cell lines which are needed to obtain high viral titres. The cDNA containing construct was transfected into Hek 293T cells leading to viral titres of 10^3 PFU/mL. High titre viral stocks were then obtained by incubation of the rescued virus on naturally susceptible cell lines like Raw 264.7 cells. This reverse genetics system is easily reproducible and requires only a few steps. Yet, the low titres obtained from the transfection of the non-susceptible Hek 293T cells can become a problem when rescuing recombinant viruses with a growth defect.

A HuNoV reverse genetics system was established using the GII.3 U201F full length cDNA. A cDNA-based system was used in this approach. Different cell lines were tested for the replication of RNA by

reverse-transcription semiquantitative PCR. Four different cell lines were tested with different constructs. The best results were obtained for the GII.3 U201F in Cos7 (African green monkey kidney fibroblast-like cells) and Hek 293T cells with 10^4 genome copies per 10^6 cells. Next to the detection of the genome copies different non-structural and structural proteins were detected by Western blot and after purification by a caesium chloride gradient, viral particles were detected by electron microscopy. Next to the GII.3 U201F reverse genetics system a reporter system was described including a GFP tag between the NTP and 3A-like non-structural proteins. In cos7 and Hek 293T cells viral replication could be detected yet, the titres were significantly lower than for the GII.3 U201F clone. In addition, GFP signal was detected in the transfected cells [180].

However, the infectivity of the virions produced could not be tested in a cell culture system at the time of publication since they were still under development.

1.13.5 An RNA-based reverse genetics system

An RNA-based reverse genetics system was described by Yunus et al. [178] which is an efficient system to obtain recombinant MNV. The complete genome of MNV-1.CW1* with a T7 promoter was *in vitro* transcribed and capped before Raw 264.7 cells were electroporated with the RNA. The viral titres obtained were comparable to those obtained from an infection. Unfortunately, the manipulation of Raw 264.7 cells is difficult and depends on a special electroporator (Neon Transfection System, ThermoFisher Scientific) and is thus not available to a lot of research groups. Furthermore, the RNA-based system is more extensive then the DNA-based system. *In vitro* transcribed RNA needs to be prepared and capping is essential for the system to work.

1.13.6 A helper virus-based reverse genetics system

This helper virus-based reverse genetics system also relies on the transfection of a DNA plasmid containing the whole cDNA of MNV-1.CW1* into eukaryotic cells. The helper virus, in this case a fowlpox virus (FPV)-T7 delivers a T7 polymerase into the cells. The MNV cDNA has a truncated T7 promoter and is also inserted into the cells by lipid-mediated transfection. The co-infected and transfected cells can produce recombinant MNV. Different eukaryotic cells were tested including BHK, BSR-T7, Hek 293T and Huh7.5 cells. Viral titres obtained from a 35 mm petri dish vary between $6 \times 10^3 – 3.36 \times 10^4$ $TCID_{50}$ in total [181].

The baculovirus is a virus normally infecting different invertebrates like caterpillars yet it is known for its use in protein production in eukaryotic cells. In addition, it can be used to transduce different eukaryotic cells leading to the recovery of recombinant virus.

For MNV a baculovirus-based reverse genetics system is available for MNV-1.CW1*. The polII-driven construct contains the full-length genome of MNV-1.CW1*. A recombinant baculovirus containing the MNV genome was obtained by transfection of Sf9 cells. To obtain recombinant MNV the baculovirus was used to transduce HepG2 cells. Since HepG2 cells are not naturally susceptible to MNV infection the lysate of the transduced HepG2 cells was used to incubate Raw 264.7 cells to get a high titre stock of recombinant MNV [176].

2. Objectives:

2.1 Interaction with host factors

The first aim focusses on the interaction of the P domain with different host factors including glycans, bile acids or the entry receptor mCD300lf. Different functional assays are established to examine the influence of the different binding factors on MNV binding. This includes a binding assay to observe potential effects of glycans on binding, an enhancement assay determining the influence of bile acids on binding and different sialic acid deficient cell lines to examine the role of sialic acid during infection. To identify regions in the vial capsid linked to identified functional phenotype, an alanine scan of exposed surface loops of the P domain of the viral capsid was performed.

2.2 Novel reverse genetics system

Performing an alanine scan of exposed loops in the viral capsid, it became obvious that an improved reverse genetics approach is needed to efficiently rescue attenuated virions. Available reverse genetics systems are limited because naturally susceptible cell lines are hard to manipulate by transfection or electroporation. Thus, a DNA-based system relying on two different cell lines was used where non-susceptible cell lines were transfected and virus was passaged onto naturally susceptible cell lines for virus amplification. An RNA-based reverse genetics system describes the use of a special electroporator to manipulate Raw 264.7 cells which limits the access to the reverse genetics system by the lack of the electroporator [178]. Since the *bona fide* receptor mCD300lf was published for MNV [45] it is possible to render cells susceptible to MNV infection. Having susceptible stable cell lines that can easily be transfected gives the opportunity to explore DNA- and RNA-based reverse genetics systems in these cell lines.

Making use of the established reverse genetics system an alanine scan targeting the P domain of MNV-1.CW1* was performed. The P2 domain is the most exposed part of the P domain and contains the receptor as well as an antibody binding site. Targeting the loops and the canyon was an approach to investigate the binding of the P domain to the host and get more insight into their role in infection.

2.3 Novel reporter assay to quantify infected cells

For different virus's cell lines expressing a reporter exist. One example is a secreted embryonic alkaline phosphatase (SEAP) system established for HCV where SEAP activity can be measured upon infection to detect viral replication [182]. For norovirus so far, no reporter cell line has been described. Using the highly conserved cleavage sites of HuNoV different constructs were designed (Steeve Boulant, Heidelberg) including an eGFP followed by a cleavage site and a localization marker. Stable cell lines expressing the three different reporter constructs are created by lentiviral transduction. The three different reporter constructs are analysed by viral infection to observe the functionality as a reporter and whether the different designs of the reporter systems have an influence. In addition, the reporter expressing cell lines are tested in the RNA-based reverse genetics system. Here, we wanted to show how efficient the system is working and possibly get insight into how many successfully transfected cells are needed to produce recombinant virus and where a bottleneck of the system might be.

3. Materials and Methods

3.1 Materials

Table 1 *Chemicals and vendors*

Chemicals	**Vendor**
2-Propanol	Roth (Ger)
2x MEM	Gibco (USA)
3'-sialyllactose (GM3)	Elicityl-oligotech (France)
Acetic acid	Roth (Ger)
Acrylamide:Bisacrylamide 29:1	Roth (Ger)
Agarose	Invitrogen (USA)
Ammonium persulfate (APS	Merck (Ger)
Ammonium sulphate ((NH4)2SO4)	Merck (Ger)
Ampicillin	Sigma-Aldrich (USA)
ATP, lithium salt	Sigma-Aldrich (USA)
Avicel®	IMCD (NL)
Bacto Tryptone	BD (USA)
Bromophenol blue	Honeywell Fluka™, Thermo Fisher Scientific (USA)
BSA	PAA (UK)
Calcium chloride ($CaCl_2 \cdot H_2O$)	Merck (Ger)
Chloroform/Trichloroethane	Roth (Ger)
DAPI	Roche (CH)
D-Galactose	Merck (Ger)
Dipotassium phosphate/monopotassium phosphate (K_2HPO_4/KH_2PO_4)	Roth (Ger)
DNA 1 kb plus ladder GeneRuler	Thermo Fisher Scientific (USA)
Dulbecco`s modified essential medium	Gibco (USA)
EGTA	Sigma-Aldrich (USA)
ErythrosinB	Sigma-Aldrich (USA)
Ethanol p.a.	Roth (Ger)
Ethanol, spoilt	Roth (Ger)
Gel Code Blue Stain Reagent	Thermo Fisher Scientific (USA)
Glycerole	Roth (Ger)
Glycochenodeoxycholic acid (GCDCA)	Sigma-Aldrich (USA)
Glycine	Biomol (Ger)
Glyco blue	Ambion (USA)
H20, DNase/RNase free	Gibco (USA)
Hepes	Roth (Ger)
Hepes 1 M (cell culture)	C-C-Pro (Ger)
Hydrochloric acid p.a. (HCl)	Roth (Ger)
LB-Agar (Luria/Miller)	Roth (Ger)
LB-Meidum (Luria/Miller)	Roth (Ger)
L-Fucose	Sigma-Aldrich (USA)
L-Glutamine 200 mM	BIOZYM (Ger)
L-glutathione	Sigma-Aldrich (USA)
Lipofectamine2000	Thermo Fisher Scientific (USA)
Magnesium chloride ($MgCl_2 \cdot 6H_2O$)	Roth (Ger)

Methanol p.a.	Roth (Ger)
Midori Xtra	Nippon Genetics (Ger)
Milk powder	Roth (Ger)
n-octylglycopyranosid	Roth (Ger)
Non-essential amino acids	Capricorn Scientific (Ger)
PageRuler prestained protein ladder (10-180 kDa)	Thermo Fisher Scientific (USA)
Paraformaldehyde	Affymetrix (USA)
Peinicillin/Streptomycin	Lonza (CH)
Phenol chloroform isoamylalcohol	Roth (Ger)
Polyethylenimine HCl MAX, linear, MW 40,000 (PeiMAX)	Polysciences (USA)
Potassium chloride (KCl)	Roth (Ger)
Sodium chloride (NaCl)	Roth (Ger)
Sodium dihydrogen phosphate, dibasic (NaH2PO4)	Merck (Ger)
Sodium dodecyl sulphate (SDS)	Roth (Ger)
Sodium hydroxide (NaOH)	Roth (Ger)
ß-merCAptoethanol	Sigma-Aldrich (USA)
TAE buffer (50x)	Merck (Ger)
Tetramethylethylenediamide (TEMED)	Roth (Ger)
Trypan blue	Roth (Ger)
Trypsin EDTA	Sigma-Aldrich (USA)
Tween 20	Sigma-Aldrich (USA)
Yeast extract	Acros (BE)
αMEM	Gibco (USA)

Table 2 *Consumables and vendors*

Consumables	**Vendor**
Cell culture plate 6-well	TPP (CH)
Cell-culture plate 96-well	VWR (USA)
Cell culture flask	VWR (USA)
Cull culture dish	Greiner Bio-one (AT)
Cell scraper	Sarstedt (Ger)
Dialysis hose Type 20, 12-16 kDa MWCO	Biomol (Ger)
Disposable filter 0.45 µm	Kisker Biotech (Ger)
Disposable reagent reservoir	Roth (Ger)
Disposable syringe Omnifix 10/30 mL	B. Braun (Ger)
Filter paper Whatman GB500	GE HealthCAre (USA)
Microtubes 2 mL	Sarstedt (Ger)
Nitrocellulose blotting membrane 0.2 µm	Peqlab (Ger)
Parafilm	Bemis (USA)
Pipette tips	Sarstedt (Ger)
Reaction tubes 1.5/2mL	Sarstedt (Ger)
Tubes 15, 50 mL	Sarstedt (Ger)

Table 3 *Enzymes and vendors*

Enzymes	Vendor
DNase	Zymo research (Ger)
Pfu-polymerase	Jena Bioscience (Ger)
Recombinant RNasin® Ribonuclease Inhibitor	Promega (USA)
Restriction enzymes	NEB (USA)
T4-ligase	NEB (USA)
Taq-polymerase	Thermo Fisher Scientific (USA)

Table 4 *Kits and vendors*

Kits	Vendor
Direct-zol RNA MiniPrep Plus with TRI reagent and Zymo-Spin IIICG-Columns	Zymo Research (Ger)
Gelextraction Kit	Merck (Ger)
Gelextraction Kit QIAquick	QIAGEN (NL)
MAXIscript™ T7 Transcriptionkit	Invitrogen (USA)
NucleoBond PD100 (midiprep)	Macherey-Nagel (Ger)
pGemT kit	Promega (USA)
QIAGEN Plasmid Mega Kit	QIAGEN (NL)
Ribo m7G cap Analog	Promega (USA)
Riboprobe System-T7	Promega (USA)
ScriptCAp m7G CApping System	BIOZYM (Ger)
SuperScript II Reverse transcriptase	Thermo Fisher Scientific (USA)
Western Lightning PLUS-ECL	PerkinElmer (USA)

Table 5 *Machines and vendors*

Machine	Vendor
Abbe refractometer	Carl Zeiss (Ger)
Aspirator with trap flask	Grant Instruments (UK)
Aspirator FTA-1	Grant Instruments (UK)
Blue/green LED transilluminator	Nippon Genetics (JPN)
Centrifuge 5417R	Eppendorf, Hamburg (Ger)
Centrifuge 5804R	Eppendorf, Hamburg (Ger)
Centrifuge Avanti J-25	Beckmann Coulter (USA)
Centrifuge Sorvall RC6	Thermo Fisher Scientific (USA)
Digital CA (NL)mera AxioCA (NL)m	Carl Zeiss (Ger)
Diluphotometer OD600	Implen (Ger)
Electronic Pipette, Pipetboy Accu	Integra Biosciences (Ger)
Fluorescence microscope Axiovert 35 with AxioObserver Z.1	Carl Zeiss (Ger)
Fluorescene-activated cell sorting MoFlo Legacy Jet-in-Air Cell Sorter	Beckman Coulter (USA)
Gel electrophoresis system	MZI workshop, Justus-Liebig-University (Ger)
Glassware	Schott (Ger)
ImageQuant, LAS-4000mini	Fujifilm Europe (Ger)
Incubator for bacteria	Bachofen (Ger)
Incubator NuAire 5700	ibs tecnomara (Ger)

Inverted microscope Axiovert 25	Carl Zeiss (Ger)
ISFET Pocket pH Meter Model 24006	DeltaTRAK (USA)
Laminar-flow bench MSC Advantage	Thermo Fisher Scientific (USA)
Magnetic stirrer Rotilabo MH20	Roth (Ger)
Microfluidizer LM10	Microfluidics (CA)
Microscope cell culture	LeiCA (NL)
Mini-PROTEAN tetra cell	BioRad (USA)
Minishaker, Vibrax VXR	IKA (Ger)
Mr. Frosty freezing container	Thermo Fisher Scientific (USA)
Multipipette 12-Pette Costar	Corning, (USA)
NanoDrop 2000c UV/VIS spectrophotometer	Thermo Fisher Scientific (USA)
Neubauer counting chamber	Marienfeld-Superior (Ger)
Orbital platform shaker Polymax 2040	Heidolph (Ger)
pH Meter MP220	Mettler Toledo (Ger)
Pipettes 0.1-1000 µL	Eppendorf (Ger)
Pipettes 2-1000 µL	Gilson (USA)
Powerpac Basic/HC	Bio-Rad (USA)
Powerpac P25	Biometra (Ger)
Precision scale 1062 MP8	Satorius (Ger)
Rotator	NeoLab (Ger)
SCAle PBC 1000-2	Kern & Sohn (Ger)
Shaker Typ 3005	GFL (Ger)
Spinner flasks (0.25/0.5 L)	Integra (Ger)
Thermalcycler Piko	Finnzymes (USA)
Thermomix	Eppendorf (Ger)
Thermostat 5320	Eppendorf (Ger)
Thermostatic cabinet Lovibond TC 255 S	Tintometer (Ger)
Ultracentrifuge XPN-80	Beckmann Coulter (USA)
UV Transilluminator 302 nm	UVP (USA)
UV Transiluminator 302 nm with Foculus IEEE1394 digital camera	Bachhofer (Ger) NET (Ger)
Vortex mixer 7-2020	neoLab (Ger)
Vortex mixer REAX 2000	Heidolph (Ger)
Waterbath 37 °C	Memmert (Ger)

Table 6 *Primers and their function and sequence that were used for cloning and sequencing. Capital letters are binding regions to DNA template and small letters are non-binding regions.*

Primers	**Function**	**Sequence 5'-3'**
Cite100 ase	Sequencing pWPI construct	CAACAGACCTTGCATTCCTTTG
EF1α	Sequencing pWPI construct	TTGGAATTTGCCCTTTTTGAG
ML-190	Mutation SG299-230AA	GAGGCTGCCTATGAGTTCCAAgcggctACCGGTGAGGTGGCGAC
ML-191	Mutation SG299-230AA	GTCGCCACCTCACCGGTagccgcTTGGAACTCATAGGCAGCCTC
ML-192	Mutation SGT299-231AAA	GAGGCTGCCTATGAGTTCCAAgctgctgccGGTGAGGTGGCGACATTCAC
ML-193	Mutation SGT299-231AAA	GTGAATGTCGCCACCTCACCggcagcagcTTGGAACTCATAGGCAGCCTC
ML-194	Mutation ETTK342-345AAAA dT346-350	CTGGAGATCGAGGTCCAGACtgctgctgccgcgAAGGTCACCACTTTTGAGATGATTC
ML-195	Mutation ETTK342-345AAAA dT346-350	GAATCATCTCAAAAGTGGTGACCTTCGCggcagcagcaGTCTGGACCTCGATCTCCAG
ML-196	Mutation ETTK342-345AAAA dT346-350	CTGGAGATCGAGGTCCAGACtgcagctgcGgcggctGTCACCACTTTTGAGATGATTC
ML-197	Mutation ETTKT342-346AAAAA dT347-351	GAATCATCTCAAAAGTGGTGACagccgcggcagctgcaGTCTGGACCTCGATCTCCAG
ML-198	Mutation dL359-363 NDQ364-367AAA	CACTTTTGAGATGATTGCtgctgccgccGCCCCCTACCAGGGCAG
ML-199	Mutation dL359-363 NDQ364-367AAA	CTGCCCTGGTAGGGGGCggcggcagcaGCAATCATCTCAAAAGTGGTGACCTTG
ML-200	Mutation dL359-365 DQPYQG366-372AAAAAA	AAGGTCACCACTTTTGAGATGATTGCagcagctgccgcagcggccAGGGTGTTCGCCAGCGTC

ML-201	Mutation dL359-365 DQPYQG366-372AAAAAA	GACGCTGGCGAACACCCTggccgctgcggcagctgctGCAATCATCTCAAAA GTGGTGACCTTG
ML-202	Mutation VT-378-379AA-dS383-388	GCAGGGTGTTCGCCAGCgctgctGCTGCGGCCGGCAGG
ML203	Mutation VT-378-379AA-dS383-388	CCTGCCGGCCGCAGCagcagcGCTGGCGAACACCCTGC
ML-204	Mutation TS379-383AA dL384-388	CAGGGTGTTCGCCAGCGTCgctGCTGCtGCtgcaGGCAGGGTTCGTGCG GTC
ML-205	Mutation TS379-383AA dL384-388	GACCGCACGAACCCTGCCtgcaGCaGCAGCagcGACGCTGGCGAACAC CCTG
ML-212	Colony PCR control VT-378-379AA-dS383-388	GTGTTCGCCAGCGCTGC
ML-219	Colony PCR control SG299-230AA	TGCCTATGAGTTCCAAGCGGC
ML-220	Colony PCR control SGT299-231AAA	CCTATGAGTTCCAAGCTGCTGC
ML-221	Sequencing P domain 3'-end	TGCAACGCAAATTCAAGCCC
ML-222	Sequencing pRevGen position 8402	CCTTCTTTCTAAGCCGGCGG
ML-223	Sequencig P domain	CTGCTGCGGCCTCTCTTGAC
ML-237	Amplification mCD300lf for lentivirus insert	gatccctgcaggATGCATTTGTCATTGCTGGTCC
ML-238	Amplification mCD300lf for lentivirus insert	gatcacgcgtttaAGGCATGGCTGCAGGCAAGG
ML240	MNV ORF2 position 9221	GCCCAGTCAGGGTGTTCCTG
MR-106	Rv primer rtPCR	TTGTTTGAGCATTCGGCCTGT

MST-112	MNV ORF2 position 6829	TCTCTGGGGCTCTGACCTTGGC
MST-144	Mutation T441A	CATGCGTCAGATCGACgCCGCTGACGCCGCAGCAGAG
MST-145	Mutation T441A	CTCTGCTGCGGCGTCAGCGGCGTCGATCTGACGCATG
MST-146	Mutation E338A	GGCAACTGGAGATCGcGGTCCAGACCGAGACC
MST-147	Mutation E338A	GGTCTCGGTCTGGACCGCGATCTCCAGTTGCC
MST-148	Mutation V352A	GGAGACAAGCTCAAGGcCACCACTTTTGAGATG
MST-149	Mutation V352A	CATCTCAAAAGTGGTGGCCTTGAGCTTGTCTCC
MST-150	Mutation R396A	GGTTCGTGCGGTCCCAgcATCCATCTACGGTTTTC
MST-151	Mutation R396A	GAAAACCGTAGATGGATGCTGGGACCGCACGAACC
MST-152	Mutation R437A	GTTCCGGACCTACATGgcTCAGATCGACACCGCTG
MST-153	Mutation R437A	CAGCGGTGTCGATCTGAGCCATGTAGGTCCGGAAC
ST-13	Sequencing M13 Fw	GTTTTCCCAGTCACGAC
ST-14	Sequencing M13 Rv	GGAAACAGCTATGACCATG

Table 7 *Plasmids and their function*

Plasmids	**Function**
pCMV.gag/pol #252	Plasmid for lentivirus production
pGEM-T-MNV-PD #177	Cloning vector for DNA-based reverse genetics system
pMD.G_vsv-g #253	Plasmid for lentivirus production
pRevGen-MNV-1* #27	DNA-based reverse genetics system
pT7 MNV #245	RNA-based reverse genetics system
pT7 MNV F/S #246	Frameshift control RNA-based reverse genetics system
pWPI_eGFP_NLS_noro cleavage 1_MAVS #289	Plasmid for reporter construct for lentivirus production
pWPI_eGFP_NLS_noro cleavage 2_MAVS #290	Plasmid for reporter construct for lentivirus production
pWPI_eGFP_NLS_noro cleavage 2_sec61b #291	Plasmid for reporter construct for lentivirus production
pWPI_mcs GUN_mCD300lf #221	Plasmid with mCD300lf gene for lentivirus production

Table 8 *Buffer composition and the function of the buffer*

Purpose	**Buffer**	**Chemicals**
Cell culture	1 x PBS	1.5 mM KH2PO4, 4.3 mM Na2HPO4, 137 mM NaCl, 2.7 mM KCl, pH 7.4
	DAPI solution	2 mg/mL DAPI in H_2O
Competent bacteria	LB Medium	25 % (w/v) LB-Medium (Luria/Miller), autoclaved
	LB^{++} medium	20 mM MgSO4 and 10 mM KCl in LB Medium, autoclaved
	LB + agar	40 % (w/v) LB-Agar (Luria/Miller)
	TfBI	30 mM KCH3COO, 100 mM RbCl, 10 mM CaCl2, 50 mM MnCl2, 15 % (v/v) Glycerol, pH 5.8 adjusted with CH3COOH, sterile filtered
	TfBII	10 mM MOPS, 75 mM CaCl2, 10 mM RbCl, 15 % (v/v) Glycerol, pH 6,5 adjusted with KOH, sterile filtered
	LB-Amp medium	100 mg/l amp in LB
DNA gel electrophoresis	1 x TAE gel electrophoresis buffer	40 mM Tris-Acetate, 0.1 mM Na2EDTA, pH 8.0 (Merck (Ger)-Millipore)
	6 x DNA- loading dye	0.1 % (w/v) Orange G, 30 % (v/v) Glycerol
DNA-preparation	P1/S1	50 mM Tris-HCl pH 8, 10 mM EDTA, 100 µg/mL RNase A
	P2/S2	200 mM NaOH, 1 % (w/v) SDS
	P3	2.3 M KCH3COO, pH 5,1
	S3 (Macherey-Nagel)	2 M KCH3COO, pH 5.1
	P3 (Invitrogen)	3 M KCH3COO, pH 5.5
	N2 (Macherey-Nagel)	100 mM Tris pH 6.3, 15 % Ethanol, 900 mM KCl, 0.15 % (v/v) Triton X-100
	N3 (Macherey-Nagel)	100 mM Tris pH 6.3, 15 % Ethanol, 1.15 M KCl, 0,15 % (v/v) Triton X-100
	N5 (Macherey-Nagel)	100 mM Tris pH 8.5, 15 % Ethanol, 1 M KCl, 0.15 % (v/v) Triton X-100
	QBT (equilibration buffer)	750 mM NaCl, 50 mM MOPS (pH 7) 15 % isopropanol (v/v), 0.15 % Triton® X-100 (v/v)
	QC (wash buffer)	1.0 M NaCl, 50 mM MOPS (pH 7), 15 % isopropanol (v/v)
	QF (elution buffer)	1.6 M NaCl, 50 mM Tris-Cl (pH 8.5), 15 % isopropanol (v/v)
Electroporation	Electroporation buffer Cytomix	120 mM KCl, 0.15 mM $CaCl_2$, 10 mM K_2HPO_4/KH_2PO_4 (pH 7.6), 25 mM HEPES, 2 mM EGTA, 5 mM $MgCl_2$, pH 7.6 (adjust with KOH)

pH assay	NaAc	25 mM NaAc in H_2O, pH 3
	NaP	25 mM NaP in H_2O, pH 7.4
SDS-gel	Anode buffer	0.2 M Tris-HCl, pH 8.9
	Cathode buffer	0.1 M Tris-HCl, 0.1 M Tricin, 0.1 % SDS, pH 8,25
	SDS-gel/Western blot transfer buffer	25 mM Tris, 192 mM Glycine, 20 % (v/v) Methanol
	Stacking gel	10 % Acrylamide, 25 % Jagow Gelbuffer, 64 % H2O, 0.1 % (w/v) APS, 0.2 % (v/v) TEMED
	Running gel	25 % Acrylamide, 33 % Jagow Gelbuffer, 36 % H2O, 0,05 % (w/v) APS, 5 % Glycerol, 0,1 % (v/v) TEMED
	SDS-sample buffer	62.5 mM Tris, 2 % (w/v) SDS, 10 % (v/v) Glycerol, 5 % (v/v) ß-mercaptoethanol, 0.1 % (v/v) Bromophenol blue, pH 6.8
	1 x Jagow-buffer	0.3 M Tris, 0.3 % (v/v) SDS, pH 8.45 adjusted with HCl
WB/ Plaque assay	1 x PBS-T	1 x PBS, 0.05 % (v/v) Tween20

Table 9 Cell culture medium for eukaryotic cells

Cell Culture Medium	Chemicals
DMEM0	DMEM 50,000 U penicillin/streptomycin 2 mM L-glutamine 0.1 mM NEAA
DMEM5	DMEM 5% FCS 50,000 U penicillin/streptomycin 2 mM L-glutamine 0.1 mM NEAA
DMEM10	DMEM 10% FCS 50,000 U penicillin/streptomycin 2 mM L-glutamine 0.1 mM NEAA 1 mM Hepes
DMEM10 for plaque assays	DMEM 10% FCS 50,000 U penicillin/streptomycin 2 mM L-glutamine 0.1 mM NEAA
αMEM5	αMEM 5% FCS 50,000 U penicillin/streptomycin 2 mM L-glutamine 0.1 mM NEAA 1 mM Hepes
+G418	+ 0.2 mg/mL
+Puromycine	+ 1 µg/mL

Table 10 Antibodies, their binding target and the vendor

Antibody	Target	Vendor
TV19, α-VP1	Binds to norovirus VP1 at the S-domain at the IDPWI amino acid sequence, raised in mouse	R-Biopharm Darmstadt, Germany
Monoclonal anti Flag M2	Flag epitope DYKDDDDK, raised in mouse	Sigma-Aldrich (USA)
Anti-mouse HRP	Polyclonal antibody targeting murine IgG, HRP conjugated, raised in goat	Dianova, Hamburg, Germany
Cy3-conjugated anti-mouse IgG	Monoclonal antibody targeting murine IgG, conjugated with Cy3, raised in goat	Dianova, Hamburg, Germany
Lectin from Triticum vulgaris FITC conjugated/wheat germ agglutinin lectin	Sialic acid residues	Merck (Ger), Darmstadt, Germany

3.2 Important cell lines and bacteria

3.2.1 BV-2

BV-2 cells are macrophage-like cells called microglia. Microglial cells play a role in the brain's innate immunity and in inflammatory neuropathologies [183]. They were derived from far/myc-immortalized murine neonatal microglia. Immortalization was obtained by a retrovirus [184]. The cells are used for *in vitro* studies of microglia [185] and are susceptible to MNV infection.

3.2.2 Raw 264.7

The Raw 264.7 cells are macrophage cells that originate from a tumour found in mice. The tumour is caused by the Abelson leukaemia virus that was used to infect BALB/c mice [186]. The cell line is often used to study cellular responses to microbes and is also known to be susceptible to MNV infection [44].

3.2.3 Hek 293T

Hek 293T cells [187] are human embryonic kidney cells derived from the Hek 293 cells. Compared to the Hek 293 cells the Hek 293T cells contain the SV40 large T antigen. SV40 is the simian virus 40 a polyomavirus and the large T antigen can bind to SV40 enhancers which leads to an increase protein production from expression vectors.

3.2.4 Huh7 and descendent cell lines

Huh7 cells are human hepatocyte derived carcinoma cells which are commonly used for HCV and DENV studies. They were established in 1982 from a well differentiated hepatocyte derived carcinoma cell line [188]. The Huh7 cell line is the parental cell line to the Huh7.5 and Huh7lunet cell lines. Both, the Huh7.5 as well as the Huh7lunet cells were infected with an HCV replicon and cured from the infection by inhibitor treatment. Both cell lines support HCV RNA replication and particle production yet virus spread was impaired in the Huh7lunet. The expression of the CD81 receptor was decreased in the Huh7lunet cells [189]. Due to the IFN-α treatment of the Huh7.5 cells to cure them from HCV [190] they became RIG-I deficient [191]. RIG-I is a pattern recognition receptor responsible for the type-I interferon response and thus an essential molecule in the cells own innate immune system.

3.2.5 Pro5 and descendent cell lines

Pro5 cells are Chinese hamster ovarian epithelial (CHO) cells which are commonly used in Adenovirus research [192]. In addition, they are the parental cell line to the Lec2 cells which are deficient in sialic acid. The Lec2 cells were obtained by selection to lectin resistance. The selection caused a defective in the CMP-sialic acid transporter leading to a decrease of sialic acid [193].

3.2.6 Bacterial strains

Two different bacterial strains belonging to the *Escherichia coli* were used for standard cloning. Both strains contained a different set of mutations enabling optimal plasmid uptake and multiplication. The HB101 (K12) were used for all standard cloning and amplification experiments and the DH5α were especially used for cloning strategies where the pGemT® cloning kit was used for a ligation reaction. The list of mutations present in the two strains are listed below:

HB101 (K12): F-, mcrB, mrr, hsdS20(rB-, mB-), reCA13, leuB6, ara-14, proA2, lacY1, galK2, xyl-5, mtl-1, rpsL20(SmR), glnV44, λ-

DH5α: F-, endA1, glnV44, thi-1, reCA1, relA1, gyrA96, deoR, nupG, purB20, φ80dlacZΔM15, Δ(lacZYA-argF)U169, hsdR17(rK-mK+), λ-

3.3 Viruses

Different viruses were used in the experiments performed. This included the murine noroviruses MNV-1CW1* and MNV-1.CW3 as well as different lentiviruses.

MNV-1 is the first strain to be isolated from mice [30]. MNV-1.CW3 is a virus isolated further referred to as MNV-1 and MNV-1.CW1* is the strain obtained by reverse genetics and further referred to as MNV-1* [176] containing an extra silent mutation leading to an EcoRV restriction site in the NS1/2 encoding part of the genome.

The different lentiviruses used were obtained from transfected Hek 293T cells for the lentiviral packaging system of the second generation. Different lentiviruses were generated carrying the genome of either the mCD300lf receptor or the different reporter constructs tested.

3.4. Methods

3.4.1 DNA/RNA work

3.4.1.1 Preparation of chemically competent *Escherichia coli*

The chemically competent *E. coli* (HB101, DH5α) were produced using the method of Hanahan [194].

A starting culture of 10 mL was prepared in LB medium without antibiotics incubating over-night (O/N) at 37 °C while shaking. The O/N culture was used to start a 100 mL culture in 100 mL LB^{++} using 1 mL of the starting culture. Again, the culture was incubated at 37 °C while shaking and the OD_{600nm} was measured until a density of 0.4-0.55 OD_{600nm} was reached. Once the density was reached the culture was cooled on ice for 10 min followed by the pelleting of the *E.coli* at 3000 x g for 10 min at 4 °C. The cell pellet was resuspended in 30 mL ice cold TfBI buffer, again incubated on ice for 10 min and centrifuged for 20 min at 3000 x g at 4 °C. The pellet was then resuspended in 4 mL ice cold TfBII and aliquoted in 20 µL aliquots. The aliquots were stored at -20 °C and once tested for quality moved to -80 °C.

3.4.1.2 Transformation of chemically competent *Escherichia* coli

Different strains of *E.coli* were used for transformation in order to amplify DNA plasmids. The protocol of how the chemically competent cells were transformed was the same for all *E.coli* strains.

The chemically competent *E.coli* were stored at -80 °C and thawed on ice for the transformation. The plasmid DNA (up to 100 ng) was added to the *E.coli* followed by an incubation on ice for 20 min. Then a heat-shock was performed at 42 °C for 2 min and another 2 min on ice. To the *E.coli* suspension of 50 µL 200 µL of fresh LB without antibiotics was added and the cells were allowed to recover at 37 °C while shaking vigorously for 30 min. Then the cells were plated on LB + agar plates with according antibiotics and incubated O/N at 37 °C.

3.4.1.3 Plasmid preparation performed by alkaline extraction

3.4.1.3.1 Minipreparation of plasmid DNA

For the purification of plasmid DNA by minipreparation the method of Bimboim and Doly was used. By alkaline extraction, the plasmid DNA is extracted whereas the chromosomal DNA is removed from the sample. The degree of purity is enough to analyse the plasmid samples by restriction, gel electrophoresis and sequencing [195].

For the minipreparation an O/N culture of *E.coli* carrying the plasmid of interest was prepared in 3 mL liquid LB + antibiotics. The liquid culture of *E.coli* was centrifuged down at 15,700 x g for 1 min after which the supernatant was discarded and the pellet was resuspended in 200 µL P1 buffer. The resuspended bacteria were lysed by adding 200 µL P2 buffer and incubating it on the shaker for max 5 min at RT. The lysis was then neutralized by adding 200 µL P3 buffer. The sample was inverted and then centrifuged for 10 min at 15,700 x g at 4 °C. The supernatant containing the plasmid DNA was

transferred to a new Eppendorf tube already containing 500 µL isopropanol. The DNA was precipitated by centrifugation for at least 20 min at 15,700 x g and 4 °C. The isopropanol was removed, and the DNA pellet was washed once with 70 % EtOH. The EtOH was removed and the pellet was dried at max 60 °C after which it was resuspended in 50 µL H_2O by incubating it on a shaker for 5 min.

3.4.1.3.2 Midipreparation of plasmid DNA

The midipreparation compared to the minipreparation is also a preparation of plasmid DNA but higher quantities of plasmid DNA is isolated. Furthermore, due to the use of a column for purification the grade of purity is higher. For the midipreparation the NucleoBond Kit from Macherey-Nagel was used.

The protocol was adapted from the manufacturer's guidelines. An *E.coli* culture of 100 mL was prepared in LB + antibiotics by growing it O/N at 37 °C. The O/N culture was centrifuged for 15 min at 4,500 x g and 4 °C to spin down the *E.coli* and remove the supernatant. The bacteria pellet was resuspended in 5 ml S1 buffer and then the bacteria were lysed in 5 mL S2 buffer during an incubation of 2-3 min at RT. The lysis was stopped by adding 5 mL S3 buffer, inverting the tube and incubating the sample for 5 min on ice. In the meantime, the column was prepared by equilibrating it with 3 mL N2 buffer. To the column a funnel with a filter was added. The lysed bacteria were applied through the filter holding back the cell debris onto the column. The DNA was bound to the column and washed once with 10 mL N3 buffer. After the washing step the DNA was eluted into a separated tube already containing 3 mL isopropanol by adding 3 mL of N5 buffer onto the column. The DNA was precipitated by centrifugation at 15,700 x g for at least 40 min at 4 °C. The supernatant was removed, and the DNA pellet was washed once with 200 µL 70% EtOH followed by a 5 min centrifugation step at 15,700 x g and 4 °C. Again, the supernatant was removed, and the DNA pellet was dried at max 60 °C. The DNA was then resuspended in a total of 150 µL RNase free H_20 by shaking it for 5 min at RT.

3.4.1.3.3 Megapreparation of plasmid DNA

To purify large amounts of a DNA plasmid a megapreparation was performed using the EndoFree® Plasmid Mega Kit from QIAGEN

Megapreparation was done according to the manufacturer's protocol. The starting volume of the liquid *E.coli* O/N culture was 500 mL in LB + antibiotics. The bacteria were spun down at 6,000 x g for 15 min at 4 °C. The pellet was resuspended in 50 mL P1 buffer. Then the bacteria were lysed by adding 50 mL P2 and incubating it for 5 min at RT. The lysis was stopped by adding 50 mL P3 buffer and inverting the tube 4-6 times. The lysate was cleared by pouring it onto The QIAfilter cartridge attached to a vacuum pump and a 45 mm neck-glass bottle. After an incubation of 10 min on the filter the liquid was pulled through by vacuum. Then 50 mL FWB2 buffer was added, the cell debris was stirred with a spatula and the liquid was pulled through the filter. The cleared lysate was mixed with 12.5 mL ER buffer and incubated on ice for 30 min. In the meantime, the QIAGEN-tip 2,500 column for DNA binding and washing was equilibrated by applying 35 mL QN buffer to the column. Then the cleared lysate was applied to the column and allowed to enter the resin by gravity flow. The bound DNA was washed with 200 mL QC buffer and eluted with 35 mL QN buffer. After elution, the DNA was precipitated by adding 24.5 mL RT isopropanol and centrifuging the mix at ≥15,000 x g for 30 min at 4 °C. The pellet was washed once with 7 mL 70% EtOH followed by a 10 min centrifugation step at ≥15,000 x g. The EtOH was removed, the pellet was air-dried and re-dissolved in 500 µL H_20.

3.4.1.4 Agarose gel electrophoresis

3.4.1.4.1 Visualization of DNA by gel electrophoresis

For the visualization of DNA prepared either by a plasmid isolation and restriction or by PCR a 1% agarose gel was run. Due to the negative charge of DNA it can be separated by size using current.

For a 1% agarose gel 1% of agarose powder (w/v) (Invitrogen) was heated in 1x modified TAE (Qiagen) until it was dissolved. The DNA was visualized by adding Midori Xtra (Nippon Genetics) to the agarose before pouring the gel (Table 11).

Table 11 *Midori Xtra concentrations used for agarose gels.*

Agarose	**Midori Xtra**
25 mL	0.5 µL
40 mL	1 µL
60 mL	1.5 µL

The agarose gel was run in 1x modified TAE with 10 µL (0.00001% (v/v)) Midori Xtra per L. The DNA sample was mixed with a 6x loading dye before being loaded into the gel slots. As a size reference 5 µL of a DNA ladder (GeneRuler 1 kb Plus, Thermo Fisher Scientific) were loaded onto the gel. At 120 V the gel had to run for 25-30 min. The DNA was visualized on a blue/green light table.

3.4.1.4.2 Visualization of RNA by gel electrophoresis

Like the DNA agarose gel RNA was also separated by size on a 1% agarose gel. The gel tray and the comb were cleaned by an incubation in a 1:10 diluted P2 buffer for 10 min. They were then rinsed with water followed 70 % EtOH. The RNA that was prepared in an *in vitro* transcription was mixed with formamide buffer (Ambion) before applied to the gel. 2 µL of *in vitro* transcribed RNA was mixed with 5 µL RNase/DNase free water and 2 µL formamide buffer. Since RNA degrades quickly the time the gel ran was only 10 min. As a reference again the GeneRuler 1 kb Plus DNA ladder was applied but since RNA is single stranded it runs faster on the gel and the DNA ladder cannot be used to estimate the size of the RNA product.

3.4.1.4.3 DNA extraction from an agarose gel

To purify DNA fragments separated by gel electrophoresis the Montage Gel Extraction Kit from Merck was used.

In short, the DNA fragment was cut out from the gel including as little as possible from the agarose. The DNA fragment was then transferred to a filter device and centrifuged for 10 min at 5,000 x g. The flow through contained the DNA fragment in modified TAE buffer and was ready to be used for ligation reactions.

3.4.1.5 Enzymatic restriction of DNA

3.4.1.5.1 Analytical and preparative restriction of DNA

Digestion reactions of DNA were used either in an analytical or preparative way. For an analytical restriction 400-800 ng DNA (mini or midipreparation) and for a preparative 1 µg DNA (midipreparation) were used. For the restriction of PCR products (preparative) the whole 50 µL PCR reaction was used. Depending on the enzyme (NEB) 5-20 U were used and 10% (v/v) of the 10x reaction buffer (NEB) were used. The incubation time varied between 30 min (analytical) and 1 h (preparative) and took place at 37 °C.

For a preparative restriction to prevent self-ligation of the vector fragments a phosphatase treatment was included if only a single restriction enzyme was used. In this case 1 U of calf-intestinal alkaline phosphatase (NEB) was added to the reaction for another 30 min at 37 °C.

3.4.1.5.2 Linearization of DNA for *in vitro* transcription

As a preparation for *in vitro* transcription of DNA into RNA the plasmid DNA had to be linearized. Therefore 10 µg DNA, 10% (v/v) of a 10x buffer and 5U of enzyme were used in a 200 µL restriction reaction. Incubation took place for 2 h at 37 °C. The linearization was checked on an analytical 1% agarose gel and purified using a phenol-chloroform extraction (Chapter 3.4.1.8).

3.4.1.6 Ligation of DNA fragments

To link different DNA fragments together at juxtaposed 5’ phosphate and 3’ hydroxyl ends a ligation with the T4 ligase from enterobacteriophages-T4 was used.

A ligation was performed either of DNA fragments obtained by restriction (Chapter 3.4.1.5) or a PCR fragment was inserted into the pGemT®-vector system I (Promega).

The ligation of DNA fragments was done with an excess of insert compared to the vector of roughly 3-10x. Of the T4 DNA ligase (NEB) 200 U were used and 10% (v/v) of the T4 buffer containing ATP. The ligation reaction took place either 10 min at RT or O/N at 4°C and was subsequently used for the transformation into *E. coli* K12.

For insertion of a PCR fragment into the pGemT®-vector it is important that the PCR fragment is obtained by PCR with Taq polymerase. The Taq polymerase generates a 3’ adenine overhang which is of importance for the ligation since the pGemT®-vector contains a 3’ thymine overhang. For the ligation of a PCR fragment into a pGemT® vector 3 µL of the purified PCR product, 1 µL (50 ng) vector, 50% (v/v) 2x buffer and 1 µL T4 ligase (3 U). The ligation was subsequently incubated for 1 h at 16 °C before transformation into *E. coli* Dh5α. The pGemT®-vector includes a ß-galactosidase gene allowing a blue-white screening. Thus, to the LB-medium after transformation 10% (v/v) of a 4% (w/v) X-gal solution were added. Upon successful insertion of the PCR product white colonies were obtained and re-ligation of the vector led to blue colonies.

3.4.1.7 Polymerase chain reaction

3.4.1.7.1 Polymerase chain reaction with a proofreading polymerase

For the amplification of DNA fragments, a standard PCR reaction using the PfuX polymerase (Jena Bioscience) was performed. This polymerase contains a proofreading mechanism and has an error rate 0.25×10^{-6}.

In table 12 the reagents needed for a 50 µL reaction are shown and in table 13 the standard PCR protocol is displayed. The amplified PCR product was checked on a 1% agarose gel (Chapter 3.4.1.4) and used for further cloning or sequencing.

3.4.1.7.2 Site-directed mutagenesis by Quikchange polymerase chain reaction

The Quikchange protocol was adapted to the protocol of Liu et al., [196] using a PfuX polymerase.

The reaction mix was as listed in table 12 and the program used is displayed in table 13.

Table 12 *Composition of the polymerase chain reaction (PCR) composition using PfuX.*

Reagent	**Amount in µL** (total 50µL)
RNase/DNase free H_2O (Gibco)	40.4-x
10x reaction buffer (Jena Bioscience)	5
dNTPs (10 mM)	2
Fw primer (25 µM)	0.8
Rv primer (25 µM)	0.8
DNA (x)	2-10 ng
Pfu	1

Table 13 *Protocol used for the PCR amplification by PfuX.*

Temperature in °C	**Time**	**Cycles**
94	2 min	1
94	30s	25
45	45s	25
72	25 min	25
72	15 min	1
16	∞	1

Following the Quikchange PCR a DpnI (NEB) digest was performed. DpnI recognizes methylated DNA leading to a degradation of the template DNA leaving the PCR product that should contain the inserted mutation. For the digest 1 µL DpnI (20 U) was directly added to the PCR reaction and incubated for 30 min at 37 °C.

3.4.1.7.3 Reverse-transcription polymerase chain reaction

For the cDNA synthesis of RNA isolated from virus the SuperScript II Reverse Transcriptase (Thermo Fisher Scientific) was used. The RNA used was isolated as described in chapter 3.4.1.8.

For the cDNA synthesis (Table 14) about 130 ng of isolated RNA was mixed with 2.5 x 10^{-5} µM reverse primer specific for the to be amplified RNA segment and 2 mM dNTP-Mix [197]. The mix was incubated at 65 °C for 5 min and then chilled on ice. The First-strand-buffer, DTT and RNaseOUT™ (Thermo Fisher Scientific) was added to the mix and incubated at 42 °C for 2 min. Then the SuperScript II Reverse Transcriptase was added and the reaction mix was transferred to a PCR tube. For the cDNA synthesis the mix was incubated at 42 °C for 50 min followed by a reverse-transcriptase inactivation step of 15 min at 70 °C. For the amplification of the cDNA 2.5 µL of the reaction was used in a PCR reaction using the PfuX polymerase.

Table 14 *Reaction mix of the reverse transcription of RNA into cDNA.*

Reagent	**Concentration**
Isolated RNA	~130 ng
Reverse primer	2.5 x 10^{-5} µM
dNTP-Mix	2 mM
First strand buffer (5x)	4 µL
DTT	20 mM
RNaseOUT™	20 U
SuperScript II Reverse Transcriptase	200 U
	Final: 20 µL

3.4.1.7.4 Purification of PCR products by QIAquick gel extraction kit

To be able to sequence the cDNA obtained from reverse-transcription PCR and amplification it was purified to remove nucleotides and primers. For the purification, the QIAquick gel extraction kit (Qiagen) was used.

The protocol was performed according to manufacturer's guidelines. Briefly, the PCR product was mixed with 3 times QG-buffer (v/v) and 1 times isopropanol. The mix was applied to the QIAquick spin column, flow-through was collected by spinning the column at 17,900 x g for 1 min. The bound DNA was washed with 700 µL PE-buffer by applying the buffer, incubating it for 3 min at RT and removing it by spinning the column at 17,900 x g for 1 min. For the elution of the DNA the column was placed in a clean Eppendorf tube, 30 µL RNase-free H_2O was applied (to increase DNA elution pre-heat the water to 37 °C) and spun at max. speed for 1 min. The eluted DNA could then be sent to sequencing.

3.4.1.7.5 Analysis of genetically transformed *Escherichia coli* by colony polymerase chain reaction

A colony PCR is a way to control whether the plasmid of interest is present in the transformed *E.coli* and whether a deletion, insertion or mutation is present in plasmid obtained by Quikchange PCR.

For the colony PCR the Taq polymerase (Thermo Fisher Scientific) was used and primers that have a Tm around 55 °C. The reaction mix is shown in table 15 and the PCR program is shown in table 16.

Table 15 *PCR reaction mix of a Tag-based PCR amplification.*

Taq buffer	2.5 µl
dNTPS (10 mM)	1 mM
Fw (25 µM)	2.5 µM
Rv (25 µM)	2.5 µM
Bacteria	Resuspend
MQ	20.875 µl
Taq	5 U
Total volume	25 µl

Table 16 *Amplification cycle used for a Taq-based PCR reaction.*

Step	**Temperature**	**Time**
Initial Denaturation	95 °C	30 s
25-30 cycles	95 °C 45-68 °C 68 °C	30 s 45 s 1 min/kb
Final Extension	68 °C	5 min
Hold	16 °C	∞

The primers used for the colony PCR are designed in different ways. If the primer is supposed to control a ligation reaction normally one primer lies in the insert region of the plasmid and one primer lies in the vector region of the plasmid. To check whether a mutation is present after a Quikchange reaction the primer is designed in such a way that Forward primer binds with the 3’ end on the mutation. If the mutation is not present the primer will not bind with the 3’ end and is not functional. The bacteria used for the colony PCR are also used for the inoculation of a miniprep and plated on an archive LB + agar plate

3.4.1.7.6 Design of oligonucleotides

For the design of oligonucleotides the tools offered by Benchling as well as oligoCalc [198] were used. In general, the GC content should be 40-60% and the 3’ end of an oligonucleotide should be a G or C.

Oligonucleotides for amplification polymerase chain reaction and sequencing

For a DNA fragment amplification not including a site directed mutagenesis or nucleotide addition at either end of the PCR product the optimal length of the oligonucleotide was 18-22 nt and the desired Tm was 55 °C.

Oligonucleotides to control the insertion of a mutation by polymerase chain reaction

Oligonucleotides used to control a Quikchange PCR are a normal reverse oligonucleotide and a forward oligonucleotide that binds at the site of mutation. For a deletion, the oligonucleotide has to span the deletion and bind for 2-3 nt on the 3' site of the deletion. For an insertion and a mutation, the 3' end of the oligonucleotide was located at the changed nucleotide. In this way if the Quikchange did not work the 3' end of the oligonucleotide is not able to bind, and the oligonucleotide is not functional.

Oligonucleotides for Quikchange polymerase chain reaction

For the site-directed mutagenesis using a Quikchange PCR the possibility is either a deletion, an insertion or a mutation. The oligonucleotides for the three options look different but have some similarities. The oligonucleotide consists of two regions the overlapping (o) and non-overlapping (no) region. The T_m of the of the non-overlapping region is generally 5-10 °C higher than the $T_{m\,o}$. Figure 7 shows the location of the mutation in the oligonucleotide depending on whether you want a mutation, an insertion or a deletion [196].

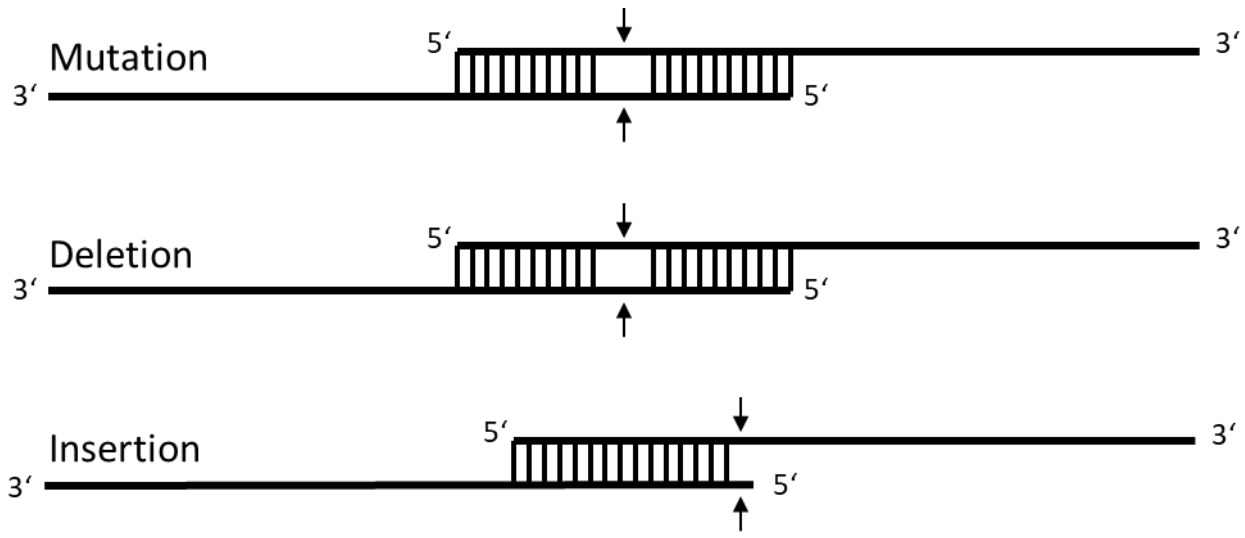

Figure 7 Primer design for Quikchange PCR reaction. *The primers for the Quikchange PCR consist of a non-overlapping and overlapping region. In the overlapping region or in close proximity to the overlapping region the desired mutation is present in the primer. The location is indicated with an arrow for the mutation, deletion, and insertion.*

3.4.1.8 Preparation of RNA by *in vitro* transcription

3.4.1.8.1 Phenol-chloroform extraction of the DNA template

The previously linearized DNA (Chapter 3.4.1.5) was extracted using phenol-chloroform-isoamylalcohol (25:24:1) (Roth) and precipitated with 3M Sodium acetate (NaOAc pH 5.2).

For the linearization using NheI a 200 µL reaction was performed using 10 µg of DNA. The linearized DNA was mixed in a 1:1 ration with phenol-chloroform-isoamylalcohol (25:24:1), vortexed thoroughly for 30 s and then centrifuged for 5 min at 15,700 x g. The upper aqueous phase was then transferred into a new Eppendorf tube already containing 200 µL chloroform. Since the aqueous phase should also be 200 µL it again is a 1:1 ratio. The sample was vortexed again for 30 s and centrifuged for 5 min at 15,700 x g. The aqueous (upper) phase was again taken and mixed with 579 µL EtOH, 20 µL 3 M NaOAc (pH 5.2) and 1 µL glycogen blue (Ambion). The sample was mixed and stored at -80 °C for at least 1 h but preferably O/N. The DNA was precipitated by centrifugation at 15,700 x g for 30 min at 4 °C. The supernatant was removed, and the pellet was washed once with 70% EtOH followed by a 5 min centrifugation step at 15,700 x g and 4 °C. The EtOH was removed, the pellet was air dried and then resuspended in 55 µL RNase free H_20.

3.4.1.8.2 *In vitro* transcription of linearized DNA

For the *in vitro* transcription of linearized DNA two different methods were compared. The one method includes post-transcriptional capping of the RNA whereas the other method has co-transcriptional capping. For both methods, the plasmid DNA was linearized the same way and purified by phenol-chloroform extraction.

3.4.1.8.3 Post-transcriptional Capping of the *in vitro* transcribed RNA

For the post-transcriptional capping approach two different kits were used. For the *in vitro* transcription, the Ambion MEGAscript T7 transcription kit was used and additionally the ScriptCap m7G capping system from BIOZYM was used for the post-transcriptional capping [199]. Between the different transcription and capping steps test agarose gels (Chapter 3.4.1.4) were run and the RNA was purified by TRIzol extraction (Chapter 3.4.1.8).

For the *in vitro* transcription, a double reaction was performed. The final reaction volume was 40 µL consisting of 10% (v/v) 10x transcription buffer, 2.5 µM CTP, ATP, UTP, GTP, 40 U T7 RNA polymerase, 5µg linearized DNA template and 20 U RNase inhibitor. The linearized DNA was added at last and the whole mix was incubated for 1.5 h at 37 °C. The DNA template was removed by adding 1 U DNaseI per µg DNA template for another 30 min at 37°C.

Before capping, the RNA was purified as explained in chapter 3.4.1.8. The RNA was eluted in 69 µL of RNase free water. To maximize the RNA eluted the water was pre-heated to 50 °C.

For the post-transcriptional first the RNA was denatured by heating it to 65 °C for 5-10 min after which the RNA was chilled on ice. The capping mix contained 10% (v/v) 10x capping buffer, 1 mM GTP, 0.1 mM S-adenosyl methionine (SAM) and 100 U RNase inhibitor. To the mix the chilled RNA was added and 40 U capping enzyme leading to a final volume of 100 µL. The capping took place for 30 min at 37 °C. The capped RNA was either used directly or stored at -80 °C until further used.

3.4.1.8.4 Co-transcriptional capping of the *in vitro* transcribed RNA

For the co-transcriptional capping 2 different kits from Promega were used being the transcription kit (P1440) and the capping kit (P1711) [200]. The RNA was controlled on an agarose gel after transcription and purified using the TRIzol column purification (Chapter 3.4.1.8).

For the in-vitro transcription following reagents were mixed and filled up to 50 µL with RNase and DNase free water: 20% (v/v) transcription optimized buffer, 10 mM DTT, 50 U RNasin, 0.5 mM rATP, rCTP and rUTP and 0.05 mM rGTP, 0.5 mM Ribo m7 Cap Analog, 5 µg of the previously linearized DNA template and 40 U T7 RNA polymerase. The mix was prepared at RT since the spermidine in the transcription optimized buffer leads to the precipitation of nucleotides at low temperatures. The transcription reaction took place for 1.5 h at 37 °C followed by a DNase treatment with 5 U/µg DNA template of DNase for 15 min at 37 °C.

After the integrity of the RNA product was checked on a 1% agarose gel the RNA was purified by TRIzol column purification and stored at -80 °C until further usage.

3.4.1.8.5 Purification of RNA by TRIzol column purification

For the purification of the *in vitro* transcribed RNA a TRIzol RNA extraction kit (Zymoresearch) was used. TRIzol is a reagent containing phenol, ammonium rhodanide and guanidinthiocyanat and thus safety-precautions including working under the fume hood are required.

The protocol was adapted from manufacturer's guidelines. To the *in vitro* transcribed RNA 100 µL of TRIzol (1:1 v/v) reagent was added and mixed. Then an equal volume 100% EtOH was added and mixed. Next, the sample was transferred onto a column and centrifuged at 15,700 x g for 30 s. The flow through was discarded and the column was washed with 400 µl PreWash buffer, centrifuged for 15,700 x g for 30s. This was followed by a washing step with 700 µL Wash buffer and a centrifugation step of 2 min at 15,700 x g. The RNA was eluted using RNase free water pre-heated to 37 °C. An elution volume of 69 µL was used. The column was placed on a fresh Eppendorf tube and centrifuged for 2 min at 15,700 x g to collect the eluted RNA. The RNA was directly used for the post-transcriptional capping. The RNA produced in co-transcriptional capping was stored at -80 °C until further usage.

3.4.2 Cell culture

Different eukaryotic cells were used and generally kept in a 37 °C incubator with 5% CO_2 and maximum humidity. The cell lines were passaged up to a passage number of 40-50.

3.4.2.1 Scraping of BV-2 and Raw264.7 cells

BV-2 cells (murine microglial cells) and RAW264.7 cells (murine macrophage cells) are cell lines that are naturally susceptible to MNV infection. Those cell lines were used for virus propagation and titration as well as functional assays.

Both cell lines are adherent and were cultured when a confluency of 90-100% was reached (every 2-4 days). BV-2 cells were grown in DMEM5 whereas Raw264.7 were grown in DMEM10. For the passaging, the old medium was removed by aspiration. For a T-75 flask 5 mL and for a T-150 10 mL of fresh medium was added. Using a scraper, the cells were detached from the culture flask and resuspended in medium. The cells were split 1:2-1:40 and grown in 15 mL medium for a T-75 flask and 25 mL medium for a T-150 flask.

3.4.2.2 Flushing of Hek293T cells

Hek 293T cells (human embryonic kidney cells) are great producers of protein and are also used for a MNV reverse genetics system [176].

The passaging of Hek 293T cells was done every 2-4 days by first aspirating the old medium and replacing it with DMEM10, 5 mL for a T-75 flask and 10 mL for a T-150 flask. Next, the cells were detached from the flask surface by flushing them loose with the medium. After detachment of the cells they were carefully resuspended by pipetting them up and down and by pushing the glass-pipette against the bottom of the flask and move the cell suspension out of the pipette by pressure. Hek 293T cells were split in a dilution of 1:5-1:20 in DMEM10.

3.4.2.3 Trypsinizing of Huh7 and descendent cells as well as Lec2 and Pro5 cells

Huh7 cells are human hepatoma cells and are known from HCV research and their ability to support the replication of HCV replicons [201]. Pro5 and Lec2 cells are ovarian epithelial cells from the *Cricetulus griseus* hamster [202, 203]. The Pro5 cells are the parental cells whereas the Lec2 cells show a decrease in sialic acid.

Huh7 cells and their descendants (Huh7.5 and Huh7lunet) were passaged every 2-4 days in DMEM10 medium and Pro5 and Lec2 cells were passaged in αMEM5 medium. To detach them from the flask they were treated with trypsin/EDTA (T/E). To do so the medium was aspirated, the cells were washed once with PBS and T/E was added to the cells. The cells were washed with the T/E and it was aspirated afterwards. Then, the cells were incubated at 37 °C until detached. The T/E was inactivated by adding medium to the cells. The detached cells were then diluted 1:5 to 1:40 (Huh7 only up to 1:10) in fresh medium and incubated at 37 °C, 5% CO_2.

3.4.3. Transfection of eukaryotic cells

For the transfections in general the cells were seeded the day prior to transfection to allow them to attach to the plate. A confluency of 80-90% is desired. All transfection reactions were carried out in optiMEM (Gibco).

3.4.3.1 Using polyethyleneimine

Transfection protocols using polyethyleneimine MAX (PeiMAX) (Polyscience) were adopted from Boussif et al. [204].

Transfection of DNA

For the transfection of DNA using PeiMAX a 1:3 ratio of DNA (in µg) to Pei (in µL) was used. In a 6-well plate a 200 µL transfection mix was used. This transfection mix consisted of 100 µL optiMEM (Gibco) containing the DNA and 100 µL optiMEM containing the diluted Pei. The PeiMAX was always pipette directly into the optiMEM. The diluted DNA and diluted Pei was then mixed and incubated for 10 min at RT. During the incubation time the medium of the cells was replaced with 800 µL optiMEM and right after the incubation time the transfection mix was carefully added to the cells in a drop-wise manner to spread it evenly reaching a final volume of 1 mL. The cells with the transfection mix were incubated for 3-5 h at 37 °C and 5% CO_2 after which the transfection mix was replaced with complete medium. The transfected cells were then incubated at 37 °C and 5% CO_2.

Transfection of RNA

For the transfection of RNA with PeiMAX the procedure was similar to the transfection with DNA using PeiMAX. Only the amounts of RNA needed, and the incubation times are different. In general, a 1:1 (v/v) ratio of RNA and Pei was used. This was about 750 ng RNA (equals around 3 µL). In addition, the incubation time of 10 min at RT was prolonged to 30 min at RT. The rest of the protocol was the same as during the transfection of DNA using PeiMAX.

3.4.3.2 By lipofectamine 2000/transfection of RNA

For different transfection experiments lipofectamine2000 (Thermos Fisher Scientific) was used. The liposomes formed by lipofectamine2000 contain the RNA and thus transfect the cell.

The cells used for the transfection were seeded the day prior to the transfection and should reach a confluency of 80-90% at the day of transfection. For the transfection itself the medium used was optiMEM (Gibco) which was pre-heated to 37 °C and the lipofectamine was adjusted to RT before transfection. In a 6-well plate 100 µL optiMEM were used to dilute the lipofectamine2000 and 100 µL optiMEM were used to dilute the RNA. A 1:1 ratio (v/v) RNA to lipofectamine was used for the transfection commonly being about 750 ng RNA and 3 µL lipofectamine2000. The diluted RNA and lipofectamine2000 was incubated for 5 min at RT after which the two dilutions were pipetted together and incubated for another 30 min at RT. In the meantime, the medium of the cells was replaced with optiMEM so that a final volume of 1 mL was achieved after adding the transfection mix. Once incubated

for 30 min the transfection mix was added to the cells in a dropwise manner. The cells were incubated for 4 h at 37 °C and 5% CO_2 after which the transfection mix was removed and replaced with normal medium. Again, the cells were incubated at 37 °C and 5% CO_2 until further used.

3.4.3.3 Electroporation of Huh7 cells

The electroporation next to the transfection is a way to make the cell membrane permeable for ribonucleotides for a short time. An electrostatic field is applied to the cell solution using a BioRad Gene-pulser.

The cells were prepared by splitting them the day prior to the transfection 1:2 to have them in an optimal growth face. At the day of the electroporation the cells are trypsinized to get a single-cell suspension. The medium was removed by centrifugation and the cells were washed twice with 50 mL 1x PBS to remove any remaining FCS. Per electroporation 400 µL of cell suspension in Cytomix2 (freschly mix 372 µL cytomix, 20 µL 100 mM L-glutathione (Sigma-Aldrich), 8 µL 100 mM ATP(Sigma-Aldirch)) were prepared the ribonucleotides were added and the mix was transferred to an electroporation cuvette with a 0.4 cm gap. The cells were immediately pulsed at 975 µF and 270 V leading to an expected time constant of 20-25 ms. Directly after pulsing the cells 600 µL DMEM10 was added and the cells were plated in a cell culture dish. Incubation of the cells took place in the incubator at 37 °C, 5% CO_2 and max humidity.

3.4.3.4 Transduction of eukaryotic cells to stably express proteins

Transduction is a process where a gene of interest is inserted into the cells' genome by recombination. Different viruses, including the human immune deficiency virus (HIV), make use of this and are called retroviruses. Based on HIV-1 a system called the lentiviral packaging system was designed and established. Using this system allows the transduction of a broad range of eukaryotic cells which leads to the stable expression of a gene of interest in the transduced cell.

HIV-1 belongs to the genus lentivirus and contains nine ORFs encoding 15 proteins which are involved in the infectious cycle. A lot of the cis-acting elements are required at various stages of the life cycle which include the long terminal repeats (LTRs), TAT activation region (TAR), splice donor and acceptor sites, packaging and dimerization signal, Rev-response element and the central and terminal polypurine tracts (PPT) [205, 206]. The earliest lentiviral packaging system used was replication competent which was a safety issue. Thus, the development of the lentiviral packaging system of the first generation included the division of the genes onto 3 separate plasmids being a packaging plasmid, an Env plasmid containing a viral glycoprotein and a transfer vector genome plasmid containing the gene of interest flanked by the LTRs. Here, the packaging and enveloping plasmids have been constructed without either a packaging signal or LTRs to reduce the chance of replication competent particles. A second-generation lentiviral packaging system contains the same set-up of 3 plasmids but to increase the safety of the system it has modified accessory genes (Vif, Vpu, Vpr or Nef). To further increase safety the following measures were taken [207]:

- The genes needed for packaging were reduced to the three essential genes being gag, pol, and rev
- The 3' LTR contains a U3 region which was deleted to ensure self-inactivation of the lentivirus after transduction and integration of the DNA into the genome
- The U3 region from the 5' LTR was replaced with a strong CMV promoter which makes the transcription Tat-independent

The lentiviral packaging system of the second generation was used in this study to transduce different cell lines delivering the mCD300lf gene and obtain stable cell lines expressing the mCD300lf receptor.

Transduction is used to insert a gene into a cell to create stable cell lines that stably express that gene of interest. A lentiviral packaging system of the second generation was used for the transduction [207].

The lentivirus was generated by co-transfecting Hek 293T cells (3 x 10^6 cells in 10 cm dish) using PeiMAX with 6 µg of the pWPI plasmid, 3 µg pCMV.gag/pol #252 and 1.5 µg pMD.G vsv-g #253 (Chapter 3.4.3.1) and harvesting the virus progeny at 3 dpt. The virus was sterile filtered over a 0.45 µm filter and stored at -80 °C until further usage. For the transduction of different eukaryotic cells, the cells were seeded in a 6-well plate the day prior to the transduction. Since the lentiviral stocks were not titrated 1 mL of virus was mixed with 5 µg/mL polybrene. The lentivirus was applied to the cells, incubated for 6-8 h after which the virus was removed and replaced with fresh medium. At 24-48 h post transduction the selection of the cells with antibiotics was started. Depending on cell death observed during selection three rounds of selection are done.

3.4.4 Infection with MNV

BV-2 cells and Raw264.7 cells are naturally susceptible to MNV infections whereas the cell lines transduced with the murine CD300lf receptor were made susceptible to MNV infection.

For an infection with MNV the cells were passaged the day before to ensure that they were in an optimal growth phase and 80-90% confluent. For the infection the cells were incubated with a defined MOI for 1h at 37 °C. The infection took place in complete medium. After 1h the medium was replaced with fresh medium. When the growth kinetics of recombinant MNV was checked complete medium was used whereas for a MNV stock DMEM0 was used. The infection was stopped by freezing the cells at -80 °C.

3.4.4.1 MNV purification by ammonium sulphate precipitation and rate-zonal centrifugation in a sucrose gradient

To obtain a pure, high-titre MNV stock, the lysate obtained by an infection of BV-2 cells was precipitated via ammonium sulphate precipitation and purified by rate-zonal centrifugation on a sucrose gradient (60-10%).

The process to obtain a high titre stock started by clearing the lysate by centrifugation at 4,500 x g for 15 min and 4 °C to remove cell debris. The cleared lysate was used for the precipitation of the virus by ammonium sulphate using a 40 % saturated ammonium sulphate solution (at 25 °C). The precipitation

took place O/N at 4°C while shaking. The virus was harvested by centrifugation at 10,000 x g for 15 min at 4 °C. The obtained pellet containing the virus was resuspended in 10 mL PBS and applied to a sucrose gradient. The gradient used reached from 60-10% sucrose and ultracentrifugation took place at 175,000 x g for 17 h at 4 °C. Fractions of the sucrose gradient were taken and VP1 was detected on a Coomassie blot as well as infectious particles were detected by end-point titration. The fractions containing the virus were dialysed into 25 mM NaP using an Amicon® (Milipore) filter with a 100 kDa cut-off.

3.4.5 Analysis

3.4.5.1 Virus Quantification

3.4.5.1.1 Tissue culture infectious does$_{50}$

The tissue culture infectious dose 50 ($TCID_{50}$) was determined by an endpoint titration assay on BV-2 cells.

The endpoint titration assay was performed in a 96-well plate using 1-2x10^4 cells/well in DMEM5. Depending on the expected titre a 1:5 or 1:10 dilution series was done. For a 1:10 dilution the volume per well was 180 µL whereas for a 1:5 dilution the final volume was 160 µL per well. If a 1:5 dilution series is used titres up to 10^8 per mL can be determined and in a 1:10 dilution series titres up to 10^{11} can be determined. The cells for an end-point titration assay can be seeded 4-6 h in advance in the 96-well plate. After seeding the cells, the virus sample was applied to the first row and followed by a serial dilution. The assay was incubated for 3-5 days until a shift in medium colour was visible for the wells where no virus was present. The $TCID_{50}$ was scored based on cytopathic effect (CPE). If CPE was present in a well the medium kept its original pink colour. Whereas if no CPE was visible but cell growth was observed the medium colour changed to yellow caused by the pH indicator present in the medium.

Using the formula of Reed-Muench the $TCID_{50}$/mL was determined [208]

$$\frac{(\text{mortality at dilution next above 50\%}) - 50\%}{(\text{mortality at dilution next above 50\%}) - (\text{mortality next below 50\%})} \times \text{logarithm of dilution factor}$$

3.4.5.1.2 Plaque assay

A plaque assay is used to quantify the amount of infectious virus particles by scoring the plaque forming units (PFU). It is made use of the CPE shown by lytic viruses.

For the plaque assay different cell lines were used. The cells were seeded in a 6-well plate the day prior to the assay. For the plaque assay the cells need to be adherent and at a confluency of 80-90%. A serial dilution of the sample that needed to be titrated was prepared in a volume of 600 µL per dilution. The medium from the cells was aspirated, the serial dilution was added, and the cells were incubated for 1 h at 37 °C. After 1 h the virus dilution was aspirated, and the overlay was added. The overlay consisted of a 1:1 mix of 2.4% Avicel® and the appropriate medium (Table 17).Two mL per well were added. After

48 h the overlay was aspirated carefully to not detach the cells, the cells were washed twice with 1x PBS-T and stained with 1 mg/mL erythrosine B (diluted from 10 mg/mL stock solution in 1x PBS-T). The staining solution was left on the cells for about 10 min after which it was aspirated, and plaques were counted and the PFU/mL was determined.

Table 17 *Density of cells seeded for a plaque assay and the medium used.*

Cells	**Number of cells needed for 80-90% confluency**	**Medium used for plaque assay**
Huh7+mCD300lf	4-5x10^5	DMEM10 for plaque assays
Huh7.5+mCD300lf	4-5x10^5	
BV-2	0.5-1x10^6	
Raw264.7	1-2x10^6	
Lec2+mCD300lf	0.8-1x10^6	αMEM5
Pro5+mCD300lf	0.8-1x10^6	

3.4.6 Immunofluorescence assay

The immunofluorescence assay was performed on different cell lines to visualize the presence of a certain antigen. Either the immunofluorescence assay was a control to see if an infection or transduction worked or it was used to get an idea where the antigen is located.

Different cell lines and methods were used for the immunofluorescence assay since the optimal fixation and permeabilization varies for the different cell lines and antibodies used.

3.4.6.1 Paraformaldehyde fixation and N-Octylglycopyranoside permeabilization

The medium of the cells was removed and the cells were subsequently washed three times with 1x PBS. For the fixation of the cells 4% paraformaldehyde (PFA) (Affymetrix) in PBS was used. Per well of a 6-well plate 500 µL PBS was added. After an incubation of 10 min at RT the PFA was removed and the cells were washed 3 times with 1x PBS. The permeabilization was done by adding 500 µL 0.5% N-Octylglycopyranoside in PBS to the cells for 7 min at 4 °C. The cells were washed once with 1x PBS before staining them.

3.4.6.2 Methanol fixation and N-Octylglycopyranoside permeabilization

For the fixation of the cells using methanol (MeOH) (Roth) the medium of the cells was removed and the cells were washed three times with 1x PBS. The MeOH used was stored beforehand at 4 °C for at least one hour. 500 µL of the cold methanol was applied to a well of a 6-well plate. The incubation took place for 10 min on ice followed by a three time washing step with 1x PBS. For the permeabilization of the cells 0.5% N-Octylglycopyranoside (Roth) in PBS (w/) was used for 7 min on ice. Again, the cells were washed 3 times with 1x PBS followed by the staining of the cells.

3.4.6.3 Staining of the cells and visualization

For the fluorescence staining of the cells different antibodies (Table 18) were diluted in 1x PBS with 1% milk powder (Roth). The incubation steps took place for 1 h at 37 °C and for the secondary antibody

and the DAPI staining the plate was wrapped in aluminium foil to keep the exposure of the fluorophores to light low.

For the incubation with the antibodies a volume of 500 µL in a 6-well plate was used. After the incubation with the primary antibody the cells were washed three times with 1x PBS. The incubation with the secondary antibody and DAPI was done at the same time. After the incubation the cells were again washed three times with 1x PBS and stored in PBS for the visualization under the Axiovert 35 fluorescence microscope.

Table 18 *Antibody dilution used for immunofluorescence assays.*

Antibody	**Dilution**
α-FLAG	1:500
α-HA	1:500
TV-19	1:500
α-CD300lf	1:500
α-mouse Cy3	1:2000
α-rabbit Cy3	1:2000
DAPI	1:5000

3.4.6.4 Fluorescence assay using wheat germ agglutinin lectin

The cell line Lec2 originated from the cell line Pro5 and is deficient in sialic acid. To confirm the decrease of sialic acid on the cell surface of the Lec2 and Lec2+mCD300lf cells a stain using wheat germ agglutinin (WGA) lectin (Thermo Fisher Scientific) was used. The WGA lectin was directly conjugated with an Alexa Fluor® 488 fluorophore.

For the staining with WGA lectin the cells were seeded 24 h prior to the assay to allow them to attach to the surface of the dish. A 'live-stain' was performed and the cells were fixated directly after the stain.

The incubation took place in 1% BSA in 1x PBS (w/v). From the 1 mg/mL stock solution of WGA lectin a working solution in 1% BSA in PBS of 5 µg/mL was prepared. The cells were incubated for 10 min at RT with the WGA lectin. Afterwards the cells were washed three times with 1x PBS and fixed directly by applying 4% PFA in 1x PBS for 10 min at RT. The PFA was removed and the cells were again washed three times with 1x PBS, stored in PBS and visualized under the Axiovert 35 fluorescence microscope.

3.4.7 Analytical assays

3.4.7.1 pH assay

Since noroviruses infect in the gut and pass through some harsh conditions its stability at low pH is of importance. Thus, the pH assay is an assay to test the stability of in this case MNV-1 against low pH.

For the pH assay high titre MNV stocks purified by rate zonal centrifugation was used. For the low pH buffer, a 25 mM NaAc buffer was used whereas for neutral pH a 25 mM NaP buffer was used. The virus stock was diluted 1:100 in the buffer (MNV concentration $1x10^7$ $TCID_{50}$/mL). The incubation took place at 37 °C for 24 h while shaking vigorously. The titre was analysed by end-point titration on BV-2 cells directly following the incubation step.

3.4.7.2 Determination of growth kinetics

The growth kinetics of wt MNV-1 and different rec. MNV-1* was tested by a growth experiment. The experiment was carried out in a 6-weel plate. Different cell lines were seeded the day prior to infection to a confluency of 80-90%. The cells were infected with a defined MOI in DMEM5, after 1 h the virus containing medium was removed and replaced with fresh DMEM5 and samples were taken at different time points in order to determine the titre by end-point dilution assay. The samples were taken by lysing the cells at -80 °C and titrating the lysate.

3.4.7.4 Binding assay of MNV by plaque assay

A binding assay is a way to determine the amount of virus bound to the cells. Thus, only the input virus is measured that bound to the cells and no amplification of the virus should have taken place.

The binding assay was performed in plaque assay setting where the PFU/mL was determined in the end. As described in chapter 3.4.5.1 the cells were plated 1 day prior to the infection. The cells were then infected, and the virus was washed off. During the infection different glycans or GCDCA (Sigma-Aldrich) included. Then the plaque assay was performed by adding the overlay and staining the cells at 2 dpi. The determined titres of the control infection with the infections including glycans or GCDCA were compared showing a difference in binding in the presence or absence of glycans or GCDCA.

4. Results

4.1 Functional assays to investigate the stability of recombinant viruses to environmental factors

Different functional assays to test viral stability were established and improved. A focus of the functional assays was on glycans as well as bile acids and their role in infection. Furthermore, the stability of the virus at low pH was observed. The functional assays should help to examine the stability of the different recombinant viruses and how the present mutation influences the stability.

4.1.1 Glycans do not enhance MNV infection in cell culture

For HuNoV a role of HBGAs and especially fucosylated and sialylated glycans is known [91, 92, 209]. Furthermore, a role of sialic acid in MNV infection was described [210]. Here, we tested the role of different glycans in infection with MNV-1 and how they influence infection.

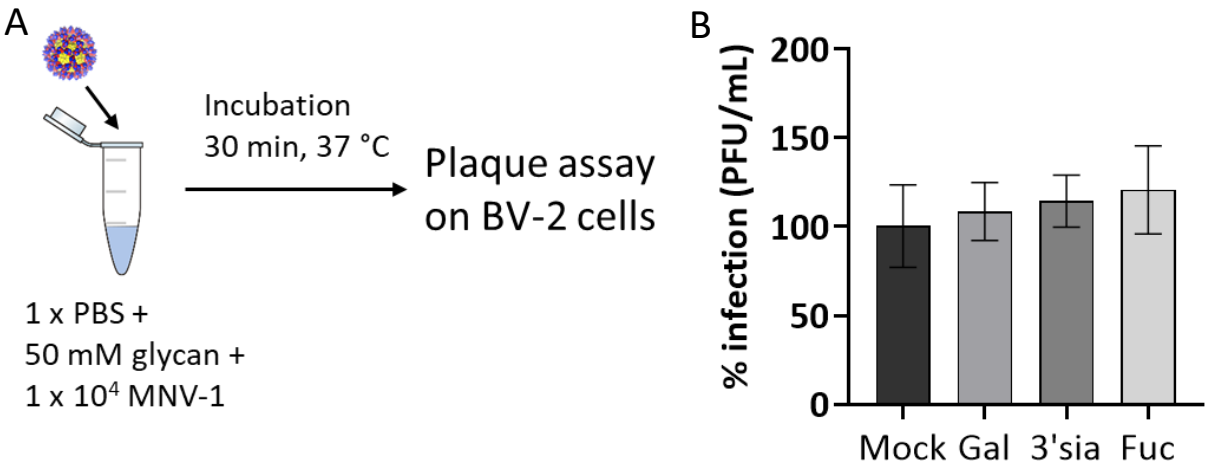

Figure 8 The influence of different glycans on viral infectivity. *(A) A schematic overview of the binding experiment performed to analyse putative glycan enhancement on MNV-1. (B) PFU/mL of the binding assay were calculated and normalised to the mock control. Adherent BV-2 cells were incubated with purified MNV-1 that was pre-treated with 50 mM of the different glycans. An Avicel® based plaque assay was performed and at 2 dpi the plaques were stained using erythrosin B. Gal=D-galactose, 3'sia= 3'sialyllactose, Fuc= L-fucose, N=3, SEM is depicted*

The binding of MNV-1 to BV-2 was investigated in the presence and absence of different glycans. Adherent BV-2 cells were incubated with MNV-1 that was either pre-treated with 1 x PBS (mock) or 50 mM glycans in 1 x PBS. After incubation with the virus a plaque assay was performed (Figure 8A) and the plaques were counted to determine the amount of virus that initially bound to the cells (Figure 8B). The plaques counted were normalised to the mock control. Galactose is known to be a non-binding glycan and was thus used as a control for the glycans. Neither for 3'sialyllactose nor for fucose an enhancing effect was found in the binding assay contrary to previous findings [211].

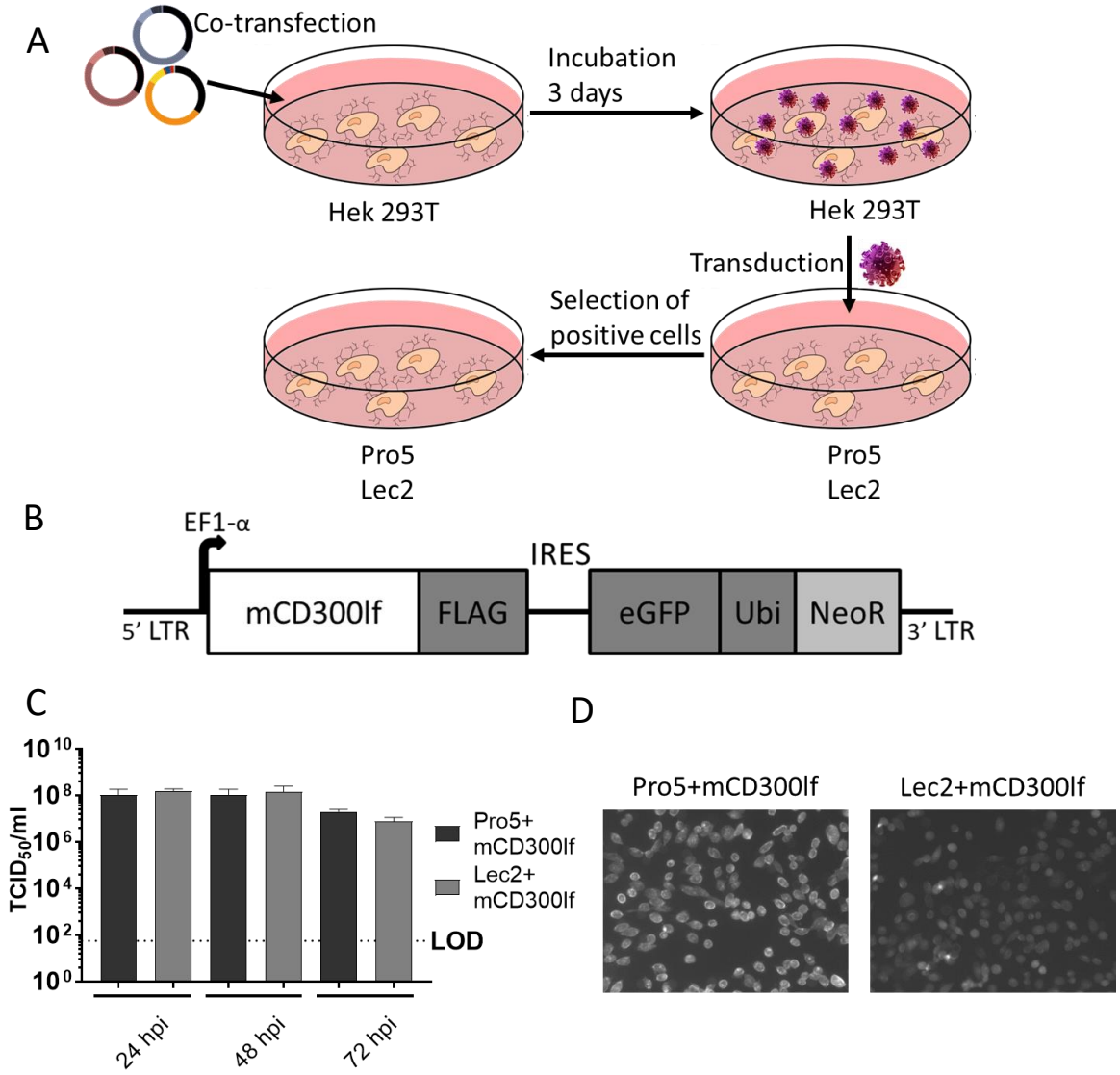

Figure 9 Sialic acid deficient cells support viral replication as well as sialic acid expressign cells. *(A) Flow chart explaining the generation of the stable cell lines starting with the generation of the lentivirus by co-transfection into Hek 293T cells, harvesting the virus after five days, using the obtained lentivirus for transduction and finally selection of the stable cell lines by antibiotic selection. (B) Schematic showing the mCD300lf-FLAG construct of the lentiviral packaging system flanked by the long terminal repeats (LTRs). The generated lentivirus is used to transduce Pro5 and Lec2 cell lines. Next to the mCD300lf-FLAG fusion an eGFP and neomycin resistance cassette is present controlled by an EMCV IRES. (C) The transduced Pro5+mCD300lf and Lec2+mCD300lf were tested for the presence of sialic acid on the cell surface by a stain with wheat-germ agglutinin lectin FITC conjugated. Fluorescent signal was observed under the fluorescence microscope of the fixed cells. (D) The stable cell lines were infected with MNV-1 at MOI 0.05 and at 24, 48, and 72 hpi lysate samples were taken and viral titres were determined by end-point titration on BV-2 cells. N=3; SEM is depicted*

To investigate the role of sialic acid during infection stable cell lines expressing the mCD300lf receptor were created by transduction (Chapter 3.4.3.4) (Figure 9A). To create the stable cell lines expressing mCD300lf, a lentiviral packaging system of the second generation was used to transduce Pro5 and Lec2 cells. First, the lentivirus was generated by transfection of Hek 293T cells with the gene of interest containing plasmid (pWPI_mcs GUN_mCD300lf) and two other plasmids carrying essential packaging genes (pCMV.gag/pol; pMD.G_vsv-g) (Figure 9A). The pWPI_mcs GUN_mCD300lf construct contains the genes for the mCD300lf receptor with a C-terminal FLAG fusion tag and for selection of the stable cell lines an eGFP and neomycin resistance cassette are present (Figure 9B).

The stable cell lines are based on the Pro5 and Lec2 cells which originate from the Chinese hamster ovarian epithelial cells. The Pro5 cells express sialic acid on the surface whereas the Lec2 cells have a significantly lower expression of sialic acid on the cell surface caused by a defective CMP-sialic acid transporter. The presence of sialic acid on the cell surface of the transduced cell lines was examined by a wheat-germ agglutinin lectin FITC conjugated stain that binds to sialic acid. The Pro5+mCD300lf showed a higher FITC signal compared to the Lec2+mCD300lf (Figure 9D). This shows that the amount of sialic acid present on the cell surface is higher in the Pro5+mCD300lf compared to the Lec2+mCD300lf.

To test the functionality of the Pro5+mCD300lf and Lec2+mCD300lf they were infected with MNV-1 and lysate samples were taken at 24-72 hpi. The titres obtained by end-point titration reached a maximum of 2 x 10^8 $TCID_{50}$/mL. No difference in obtained titres was observed between the Pro5+mCD300lf and Lec2+mCD300lf cells indicating that sialic acid has no crucial role in virus replication in this setting (Figure 9C).

Concluding from the functional assays established to observe influences of different glycans on MNV-1 infection it became obvious that 3'sialyllactose and fucose do not play a significant role in virus binding to BV-2 cells and that sialic acid deficient cells support MNV-1 replication equally well as the sialic acid expressing cells.

4.1.2 Bile acid enhances MNV-1 infection in select cell lines

The structure of the mCD300lf receptor in combination with the MNV P domain showed that bile acids interact with the P domain. This interaction was suggested to lead to an enhancement of MNV binding to the mCD300lf receptor [87]. Nelson et al. showed in their publication that GCDCA in contrast to TCA leads to an enhanced binding of MNV to mCD300lf. Here, the enhancing effect of GCDCA on different cell lines was investigated making use of the binding assay.

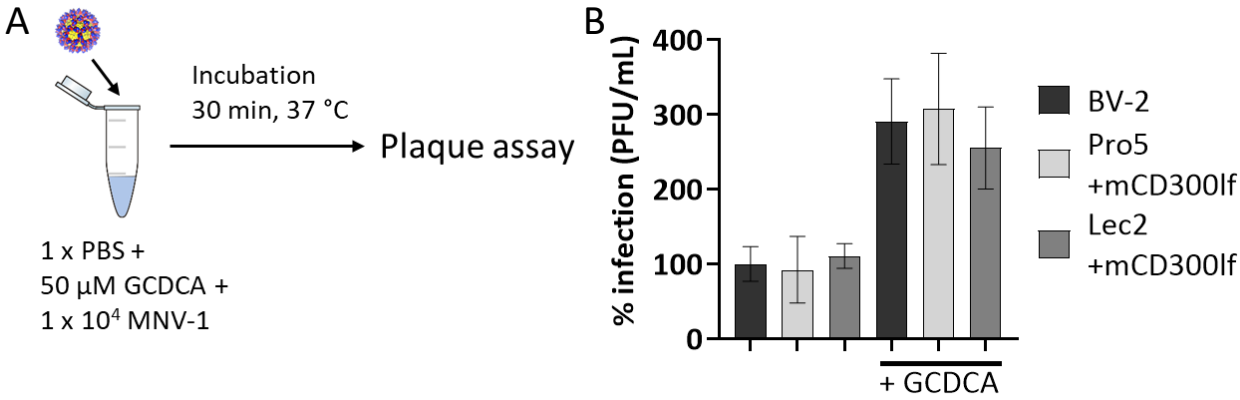

Figure 10 GCDCA enhances viral binding of MNV-1 to three different cell lines in a comparable fashion. *(A) A schematic of the set-up of the binding assay is shown. (B) The enhancing effect of GCDCA was tested on the binding to BV-2, Pro5+mCD300lf and Lec2+mCD300lf cells. MNV-1 was pre-incubated with 50 µM GCDCA for 30 min before it was incubated on the adherent cells. The infection was followed by a plaque assay which was stained at 2 dpi. PFU/mL were determined and normalised to the mock control. N=4, SEM is depicted*

For the binding assay the adherent BV-2 cells were incubated using purified MNV-1 that was mock pre-treated in 1x PBS or pre-treated with 50 µM GCDCA in 1x PBS (Figure 10A). Following the incubation, a plaque assay was performed, and viral titres were determined by staining the plaques after two days.

One experiment showing the enhancing effect of GCDCA was performed on BV-2 cells. The PFU/mL of the virus incubated with GCDCA was compared to the mock treated virus. The detected PFU/mL were normalized (Figure 10B) to the mock control. An enhancing effect of GCDCA was observed leading to a 3-fold increase in infectivity.

A similar experiment was performed on the Pro5+mCD300lf and Lec2+mCD300lf cells. Again, a purified MNV-1 stock was pre-treated with GCDCA and adherent cells were incubated with the pre-treated virus. A plaque assay was performed and at 2 dpi the PFU/mL were detected. The obtained titres were normalised to the mock control. In the Pro+mCD300lf and Lec2+mCD300lf a similar about 3-fold increase in viral titres was obtained when the virus was pre-treated with GCDCA. A small difference in enhancing effect between the Pro5+mCD300lf and Lec2+mCD300lf can be observed with a slightly lower enhancement in the Lec2+mCD300lf. Yet, a two-tailed T-test showed no significance between the enhancing effect of the two different cell lines.

Concluding, it can be said that GCDCA has an enhancing effect on viral infectivity when present during the incubation of the virus with the cells. This enhancing effect can be observed on BV-2 cells as well as Pro5+mCD300lf and Lec2+mCD300lf cells. This shows that sialic acid does not influence the binding to the mCD300lf receptor in the presence of GCDCA.

4.2 Stable expression of the mCD300lf receptor in select cell lines is detected and leads to gained susceptibility to MNV infection

The receptor mCD300lf was shown to be a *bona fide* receptor for MNV [45]. In addition, different cell lines including Hela [45] and Hek 293T [212] cells that are naturally persistent to MNV infection became susceptible to MNV infection upon expressing the mCD300lf receptor. Here, Huh7 and descendent cells were transduced to stably express the mCD300lf receptor. The stable cell lines were analysed for mCD300lf expression and compared to the naturally susceptible cell lines BV-2 and Raw 264.7 to determine whether replication efficiency of MNV was comparable in the different cell lines.

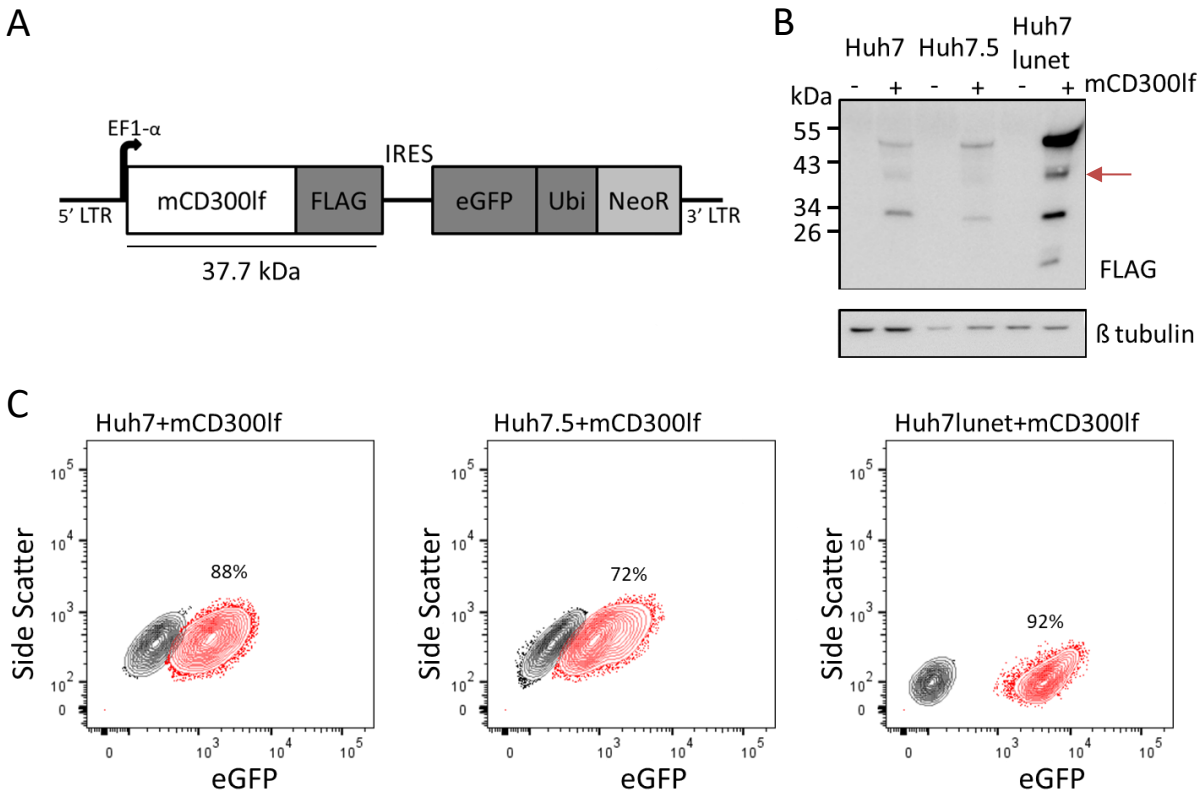

Figure 11 Analysis of Huh7 and descendent cell lines expressing the mCD300lf receptor. *(A) Schematic showing the mCD300lf-FLAG construct of the lentiviral packaging system flanked by the long terminal repeats (LTRs). The generated lentivirus is used to transduce Huh7 and descendent cell lines. Next to the mCD300lf-FLAG fusion an eGFP and neomycin resistance cassette is present controlled by an EMCV IRES. The protein size of the mCD300lf-FLAG fusion is indicated. (B) The mCD300lf receptor was detected in the transduced Huh7, Huh7.5 and Huh7lunet cells by Western blot using the C-terminal FLAG tag. The naïve parental cell lines not expressing the receptor were included as a control. The expected size of the mCD300lf-FLAG fusion was 37.7 kDa and the expected band is indicated with a red arrow. Beta Tubulin was used as loading control. (D) Using fluorescence-activated cell sorting (FACS) the percentage of eGFP positive cells in the cell population was enriched. The parental cell lines were used for comparison to determine the population of eGFP positive cells. In black the eGFP negative cells are shown and in red the eGFP positive cells.*

Stable cell lines expressing the mCD300lf receptor were obtained by lentiviral transduction. The same lentivirus previously described was used (Figure 9A). The Huh7, Huh7.5 and Huh7lunet cells were transduced with the lentivirus. The expression of the mCD300lf-FLAG fusion was shown by Western blot analysis of the transduced cells compared to the parental cell lines. As a loading control ß tubulin was detected (Figure 11B). The expected size of the mCD300lf-FLAG fusion is 37 kDa, yet 4 bands were detected with one (indicated with the red arrow) showed the expected size of about 37 kDa. Since the parental cell lines did not display any bands, all bands detect the FLAG fusion tag and thus the mCD300lf receptor.

Cells expressing mCD300lf were enriched by fluorescence-activated cell sorting (FACS) using the eGFP signal. For the Huh7+mCD300lf 88% positive cells were detected, for the Huh7.5+mCD300lf 72% and for the Huh7lunet+mCD300lf 92% (Figure 11C). In a later FACS analysis the cells were analysed for eGFP positive cells in order to determine the stability of the cell lines receptor negative cells were used as a comparison. Here, the stable cell lines were kept in culture for 14 – 18 passages. Comparing the eGFP positive cells after several passages (Huh7+mCD300lf 88.1%; Huh7.5+mCD300lf 65.2%; Huh7lunet+mCD300lf 92.4%). In conclusion cells are stably expressing the receptor over at least 18 passages, however, not all cells express the receptor.

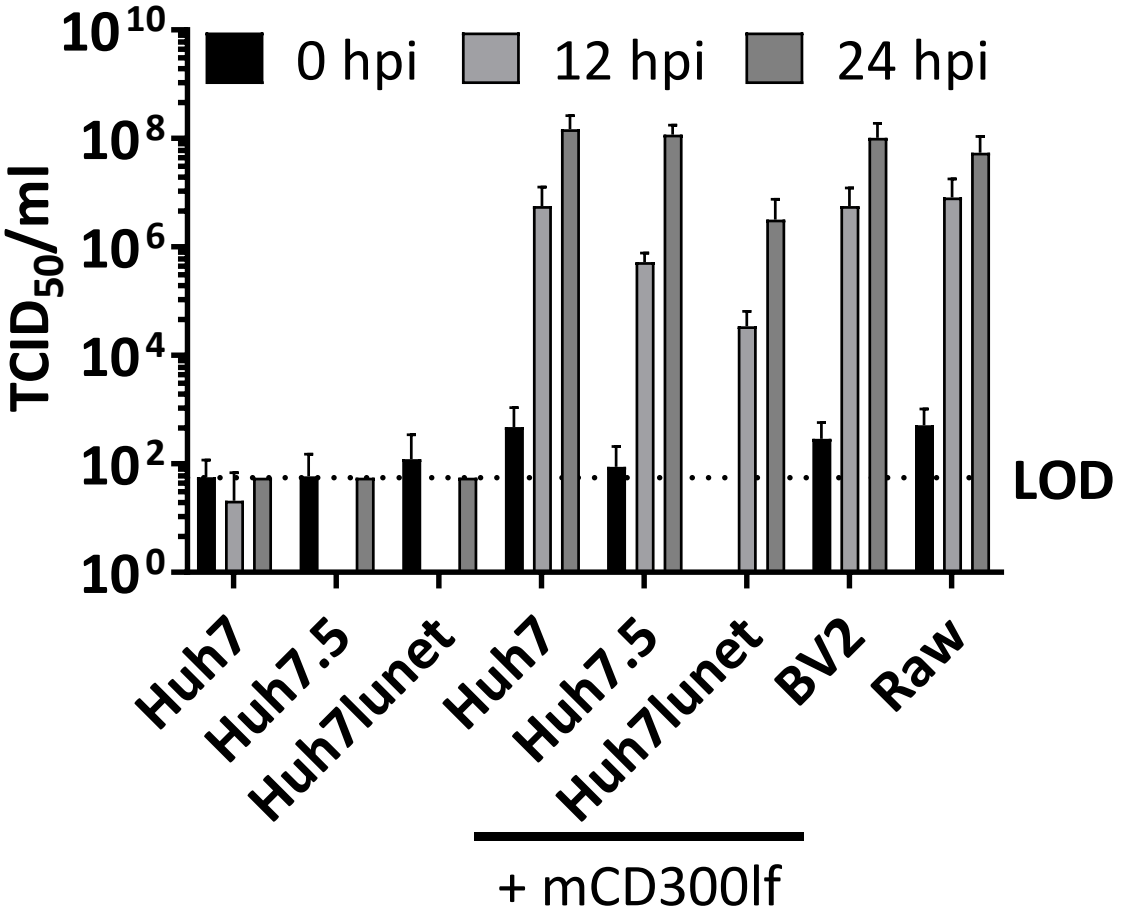

Figure 12 Infection of the transduced cell lines expressing mCD300lf leads to virus replication and plaque formation. *(A) Time course of the infection of parental and transduced Huh7 cell lines as well as naturally susceptible BV-2 and Raw cells. Cells were infected at MOI 0.05 with MNV-1 and the titre was determined by end-point titration on BV-2 cells. N=3; standard error of the mean (SEM) is depicted*

The susceptibility towards MNV infection of the transduced cell lines was investigated in comparison to the parental cell lines and naturally susceptible BV-2 and Raw 264.7 cells by infection (Figure 12). Huh7+mCD300lf and Huh7.5+mCD300lf reached similar viral titres at 24 hpi compared to naturally susceptible BV-2 or Raw 264.7 cells at about 1 x 10^8 $TCID_{50}$/mL whereas the Huh7lunet+mCD300lf cells only reached lower titres of up to 1 x 10^7 $TCID_{50}$/mL. This difference of 1 log_{10} in the Huh7lunet+mCD300lf was observed in three independent experiments at 12 hpi and 24 hpi. Later time points of the infection were not taken into consideration because MNV-1 is a cytopathic virus and the cells showed clear CPE at those time points.

In conclusion, the newly generated Huh7 and descendent cell lines express the MNV mCD300lf receptor leading to a gained susceptibility to MNV infection. Viral titres of the stable cell lines are comparable to those obtained by the naturally susceptible BV-2 and Raw 264.7 cell.

4.2.1 Stable mCD300lf-expressing cell lines support plaque formation

Plaque assays are a common tool used in research. The Huh7+mCD300lf, Huh7.5+mCD300lf and Huh7lunet+mCD300lf cells show CPE upon infection with MNV. In addition, naturally susceptible cell lines BV-2 and Raw 264.7 plaque assays are sensitive to cell numbers and medium conditions. We therefore asked the question whether our newly generated cell lines allow a more robust plaque assay.

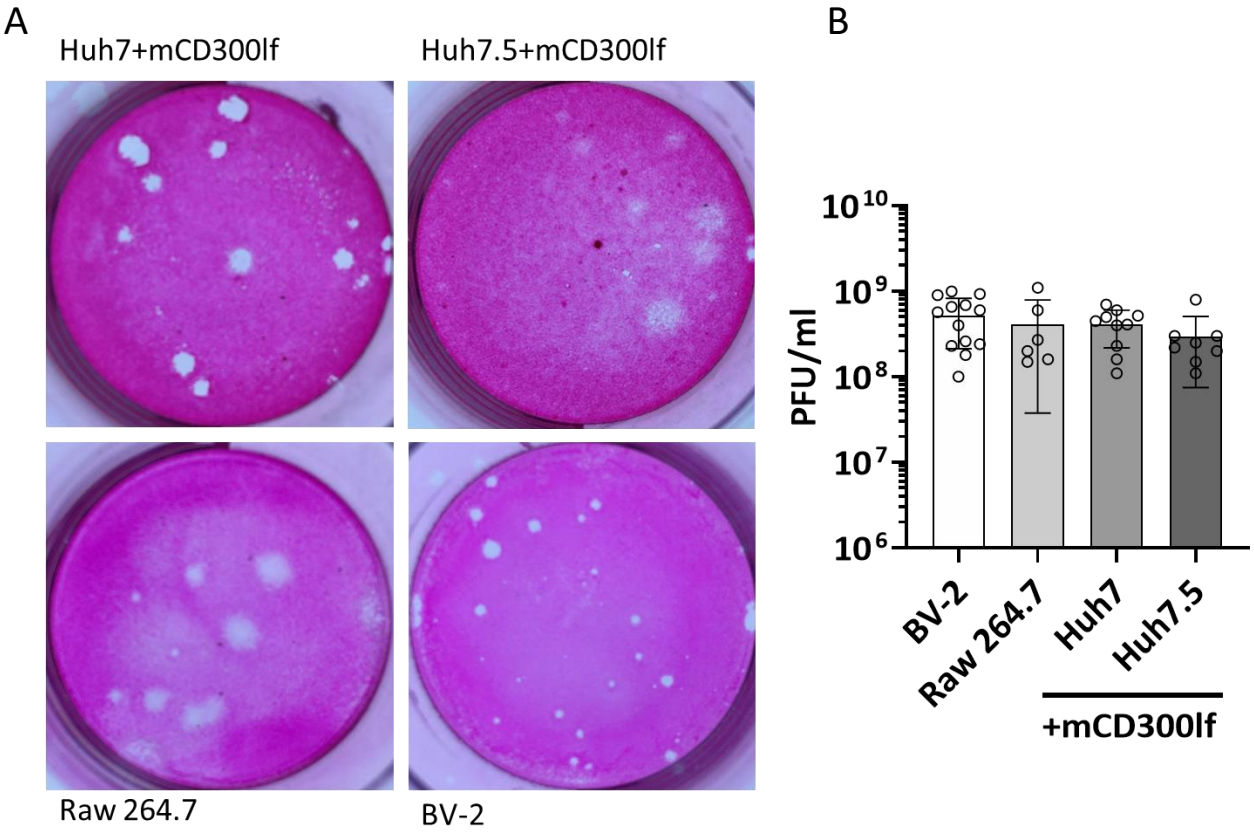

Figure 13 The Huh7 and Huh7.5 cell expressing mCD300lf support MNV-1 plaque formation. (A) The stable cell lines Huh7+mCD300lf and Huh7.5+mCD300lf show plaque formation when infected with MNV-1. The plaque formation was compared to the plaque assay established for BV-2 and Raw 264.7 cells. The plaque assay uses an Avicel®-based overlay and plaques are stained with erythrosine B. Huh7lunet+mCD300lf cells are not included since the cells detached during the experiment and thus no plaque formation could be observed. (B) The plaque formation of Huh7+mCD300lf, Huh7.5+mCD300lf and the naturally susceptible BV-2 and Raw 264.7 cells were quantified. At least three individual experiments were performed. Error bars display the standard deviation (SD) and at least three independent experiments in duplicate were performed. BV-2 N=6; Raw 264.7 N=3; Huh7+mCD300lf N=5, Huh7.5+mCD300lf N=4

Here we compare plaque formation of MNV-1 in naturally susceptible BV-2 and Raw 264.7 cells [213, 214] with our stable cell lines expressing the mCD300lf receptor. We further improved our plaque assay technique replacing the standard agarose with microcrystalline cellulose Avicel® (IMCD). The protocol was loosely based on a plaque assay protocol described for influenza viruses [215].

As shown in figure 13 the Huh7+mCD300lf and Huh7.5+mCD300lf show plaque formation and staining of the cells that made the plaques easy to detect. The Huh7lunet+mCD300lf (not shown) detached during the plaque assay incubation leading to non-interpretable results. Comparing the different plaques formed by the different cell lines showed that plaque size within one cell line varied which was observed in all four cell lines. Yet, comparison of the four different cell lines with one another led to comparable viral titres obtained in all four cell lines.

All in all, the Huh7+mCD300lf and Huh7.5+mCD300lf show plaque formation which is comparable to the plaques obtained by Raw 264.7 and BV-2 cells considering the titres. A difference in plaque size and morphology is found between the different cell lines. The Huh7lunet+mCD300lf cells do not work for the plaque assay since they are not adherent enough and detach during the different steps of the plaque assay.

4.3 mCD300lf-expressing clones of Huh7lunet support the DNA-based reverse genetics system

The DNA-based system of Ward et al. [176] is based on the transfection of the non-susceptible Hek 293T cells and passaging of the virus on susceptible cells like BV-2 or Raw 24.7. Here, the stable cell lines are analysed in a DNA-based system. The stable cell lines allow for efficient transfection and virus replication which are good requirements for a DNA-based reverse genetics system.

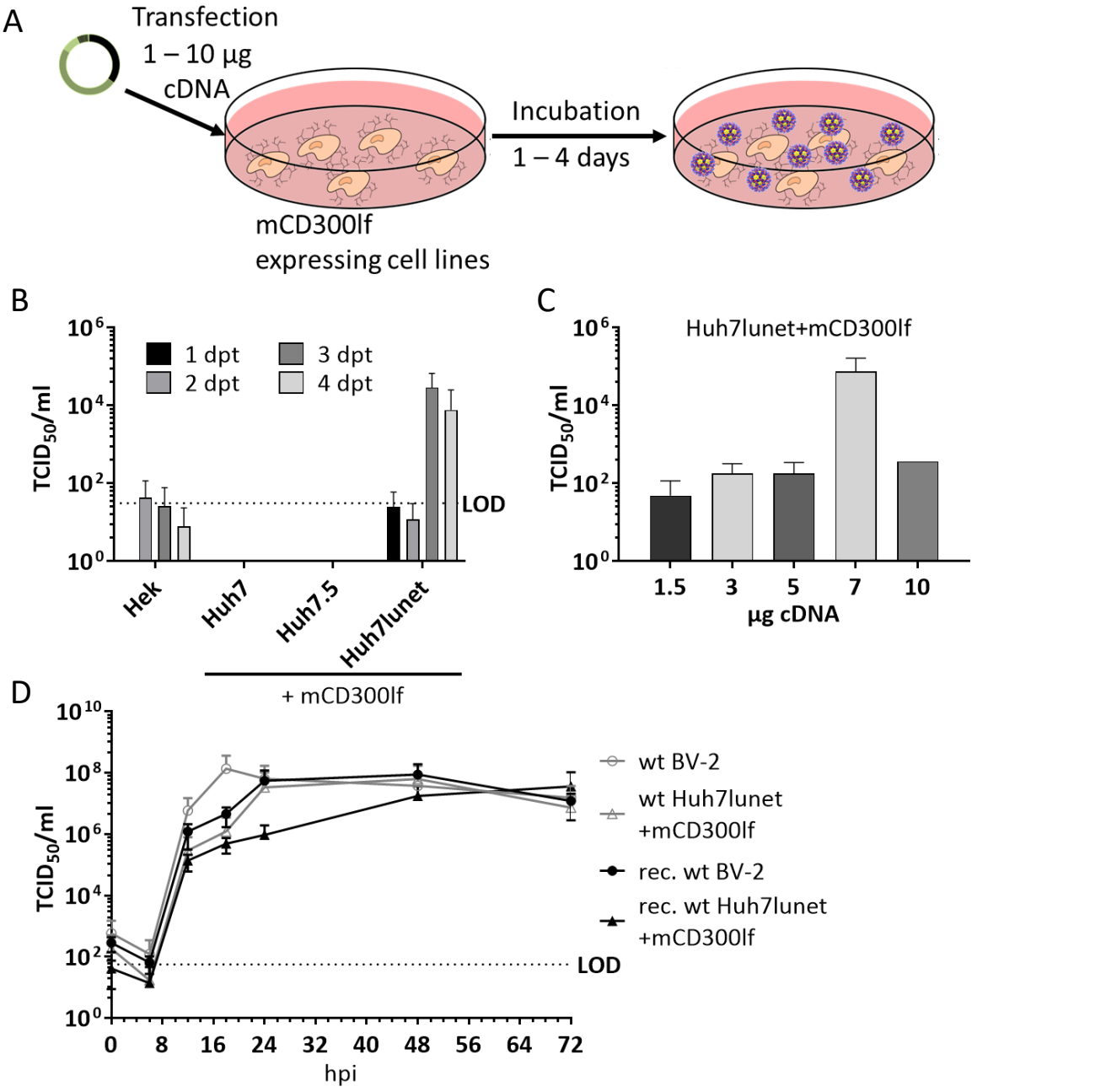

Figure 14 A DNA-based reverse genetics system was established on mCD300lf receptor expressing cells. *(A) Schematic overview of the experimental set-up used for the DNA-based reverse genetics system. The plasmid used for transfection contains a polII promoter and the full-length cDNA of MNV-1*. (B) The DNA-based system was tested on different reporter expressing cell lines descending from the Huh7 cells. The cells not expressing the reporter (not shown) were used as controls. N=3; SD is depicted (C) The amount of cDNA needed for the reverse genetics system to efficiently work was determined. Transfection was performed on Huh7lunet+mCD300lf cells and virus titres were determined by end-point titration at 3 dpt. N=3; SD is depicted (D) The recombinant MNV-1* was compared to MNV-1.CW3 in an exemplary detailed growth curve. The growth kinetics of both viruses were determined on the naturally susceptible BV-2 cells as well as on the stable cell line Huh7lunet+mCD300lf. N=3; SD is depicted*

The stable cell lines were transfected with pRevGen-MNV-1* #27 using PeiMAX (Figure 14A). As a comparison to the published DNA-based reverse genetics system the Hek 293T cells were included [176]. Transfection of the receptor expressing cell lines Huh7+mCD300lf, Huh7.5+mCD300lf and Huh7lunet+mCD300lf showed that Huh7lunet+mCD300lf are able to produce recombinant virus whereas the Huh7+mCD300lf and Huh7.5+mCD300lf did not show any detectable amounts of recombinant virus (Figure 14B). Also, the parental cell lines Huh7, Huh7.5 and Huh7lunet (not shown) did not produce detectable amounts of MNV. With viral titres of up to 1 x 10^5 $TCID_{50}$/mL following transfection of Huh7lunet+mCD300lf cells, the viral output is significantly higher compared to mCD300lf-deficient HEK 293T cells. Looking at 1-4 dpt as expected for Hek 293T cells the titres did not further increase whereas for the Huh7lunet+mCD300lf the titres increased significantly at 3-4 dpt. Hek 293T cells are limited to a single round of infection whereas Huh7lunet+mCD300lf are showing multiple rounds of infection which leads to the expected increase in titres.

To further examine the DNA-based system the Huh7lunet+mCD300lf cells were used to determine the amount of DNA needed to successfully rescue recombinant MNV-1*. In three independent experiments using different preparations of DNA the amounts varying between 1.5-10 µg DNA per well of a 6-weel plate were tested. A 1:3 (w/v) ratio (vector:transfection reagent) was used for the transfection. The cells were seeded the day prior at a density of 8 x 10^5 cells/well. It was shown that at 3 days post transfection (dpt) the maximum titres obtained from rescued MNV-1* is obtained by using 7 µg DNA per well. At 10 µg per well the titre drops again which is probably caused by the observed increase in cell death at early time points (Figure 14C).

The recombinant MNV-1* was passaged up to passage 3 (P3) on BV-2 cells and used for a comparison in growth kinetics including Huh7lunet+mCD300lf cells and the naturally susceptible BV-2 cells (Figure 14D). To compare it to wt virus a MNV-1 at P6 was used to infect both cell lines. As shown in the graph the recombinant MNV-1* (black) virus showed a delayed replication in the first 24 hpi compared to MNV-1 (light grey) but titres converged at 48-72 hpi. Furthermore, the Huh7lunet+mCD300lf cells also showed a slight delay in viral replication up to 24 hpi compared to the BV-2 cells. This counts for MNV-1* as well as MNV-1. Yet, the titres at 48-72 hpi were comparable.

Concluding from these results it can be said that the Huh7lunet+mCD300lf cells are supporting a DNA-based reverse genetics system whereas the Huh7+mCD300lf and Huh7.5+mCD300lf do not support the DNA-based reverse genetics system.

4.4 Select cells stably expressing the mCD300lf receptor support the RNA-based reverse genetics system

An RNA-based system for MNV-1* is published, which is based on the transfection of Raw 264.7 cells, which can be electroporated using the Neon transfection system (Thermo Fisher Scientific) [178]. The Neon transfection system is a unique electroporator that is not available in our group. Thus, a different set of cells is needed for the RNA-based system to be available to a broader range of research groups. For the Huh7, Huh7.5 and Huh7lunet cells it is known that they can be manipulated by transfection and electroporation and previous experiments showed that the mCD300lf expressing cells allow MNV infection. Thus, the stable cell lines were examined in an RNA-based reverse genetics system.

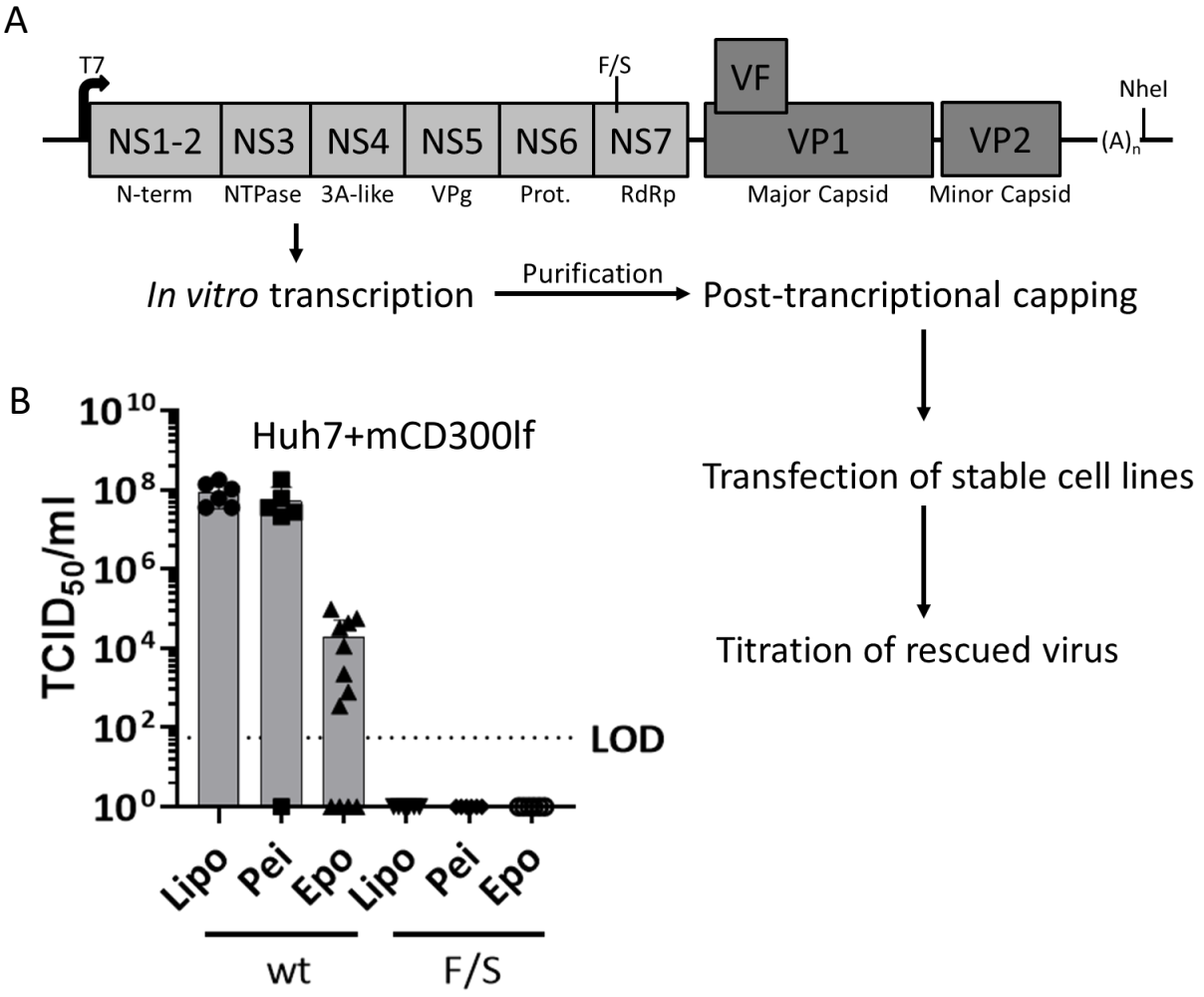

Figure 135 Experimental set-up and influence of the transfection method of the RNA-based reverse genetics system. *(A) Schematic overview of the RNA construct used to transfect the cells for the RNA-based reverse genetics system. At the 3'-end the site of the NheI cutting is indicated which is needed to linearize the DNA construct. The NS7 (RdRp) has F/S indicated which shows the location of a frameshift that is used as a control construct since it inactivates the RNA-dependent RNA polymerase (NS7). The following steps of in vitro-transcription, capping, purification steps and transfection of the cells is indicated. (B) Different methods of transfection and electroporation were compared for efficiency in the reverse genetics system. Lipofectamine2000 (Lipo) and PeiMAX (Pei) were the transfection reagents used and compared to electroporation (Epo). Viral titres were determined by end-point titration on BV-2 cells at 3 dpt. N=3, SEM is depicted*

It is known that different factors play a role in a system like the RNA-based reverse genetics system which includes the viability of the cells before and after manipulation, the quality of the genetic material, in this case the RNA and the incubation time.

To obtain a robust and reproducible RNA-based reverse genetics system different parameters including the way of cell manipulation, RNA preparation and incubation time were tested.

Two constructs for the RNA-based system were kindly provided by Ian Goodfellow (Cambridge, UK) [178] which are the pT7 MNV and pT7 MNV F/S (Figure 15A). Both contain a T7 promoter and the MNV-1* full length genome. The pT7 MNV F/S construct is a control construct which includes a frameshift (F/S) mutation in the viral RdRp making it replication deficient due to an early stop codon. For the experiment both DNA constructs were linearized with NheI, *in vitro* transcribed and post-transcriptionally capped.

Subsequently the post-transcriptionally capped RNA was used for the transfection of the stable cell line Huh7+mCD300lf to compare the influence of different transfection and electroporation methods on the RNA-based reverse genetics system (Figure 15). Differences were observed when comparing output viral titres following transfections with Lipofectamine2000 or PeiMAX to electroporation. Therefore, the optimal method to introduce RNA into the cells was initially determined. For Lipofectamine2000 and PeiMAX a 1:1 (v/v) ratio was used. Medium containing the transfection reagent was replaced after 3 h. To prepare the cells for the transfection and electroporation the cells were split the day prior. For the transfection they were seeded in 6-well plates to reach a confluency of 80-90% the following day. For electroporation, the cells were split the day prior and at the day of the electroporation the cells were trypsinized to obtain single cells and washed twice with 1 x PBS to remove any remaining FCS. To compare the transfection and electroporation the same post-transcriptionally capped RNA was used und the cells were plated in a 6-well dish and incubated at 37 °C, 5% CO_2. At 3 dpt the samples were lysed by freezing and the lysate samples were analysed for virus quantities by end-point titration. As shown in figure 15B transfection with either Lipofectamine2000 or PeiMAX led to high titres at about 1 x 10^8 $TCID_{50}$/mL whereas the titres obtained by electroporation of the cells were lower with a maximum of 1x10^5 $TCID_{50}$/mL. Furthermore, electroporation led to non-detectable titres in 33 % of the samples (4 out of 12). The F/S mutant did not lead to any detectable titres in any of the experiments.

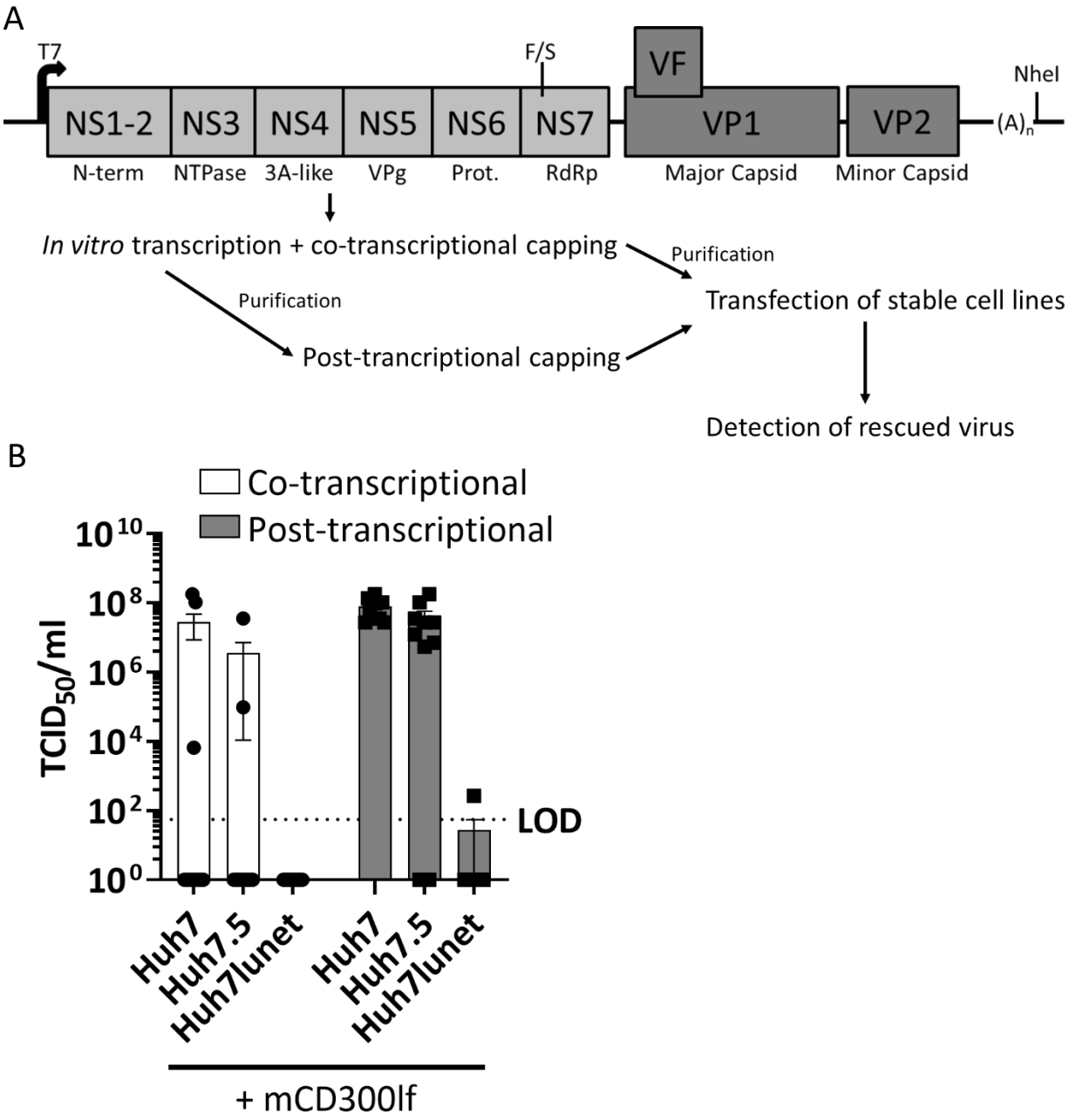

Figure 16 Capping method, transfection method and cell line affect reverse genetic system efficiency. *(A) Schematic overview of the in vitro transcription and two different capping mechanisms used. (B) Co-transcriptional and post-transcriptional capping kits were compared by the transfection of Huh7+mCD300lf Huh7.5+mCD300lf and Huh7lunet+mCD300lf cells with equal amounts of capped RNA. For the transfection PeiMAX was used. Viral titres were determined by end-point titration at 3 dpt. SEM is depicted, N=3 (B)*

As a second step different methods of capping the *in vitro* transcribed RNA were tested. A co-transcriptional capping kit was compared to a post-transcriptional capping kit. The steps of *in vitro* transcription and capping are different for the two methods (Figure 16A). The co-transcriptional capping kit is based on a m^7G cap analogue which is a methylated ribonucleotide that can be incorporated at the 5‘-end during *in vitro* transcription. The post-transcriptional capping is based on a *Vaccinia* virus capping enzyme (VCE) and incorporates the m^7G cap analogue after *in vitro* transcription at the 5‘-end of the RNA. The prepared RNA was used to transfect Huh7+mCD300lf, Huh7.5+mCD300lf and Huh7lunet+mCD300lf cells using PeiMAX to compare the functionality of the different capping

mechanisms and to discriminate whether there is a significant difference. The cells were seeded the day prior to transfection in a 6-well plate. For the transfection about 750 ng of capped RNA and 3 µL of PeiMAX were used. Lysate samples were collected at 3 dpt and analysed by end-point titration to determine viral titres. The results are shown in figure 16B. The post-transcriptionally capped RNA leads to a more stable virus production than the co-transcriptionally capped RNA in the Huh7+mCD300lf and Huh7.5+mCD300lf. But looking at the Huh7lunet+mCD300lf cells they do not lead to stable results with either of the two capping mechanisms. Furthermore, it was observed that amounts of *in vitro* transcribed RNA lower than 500 µg/per well of a 6-well plate led to a high uncertainty in viral titres obtained.

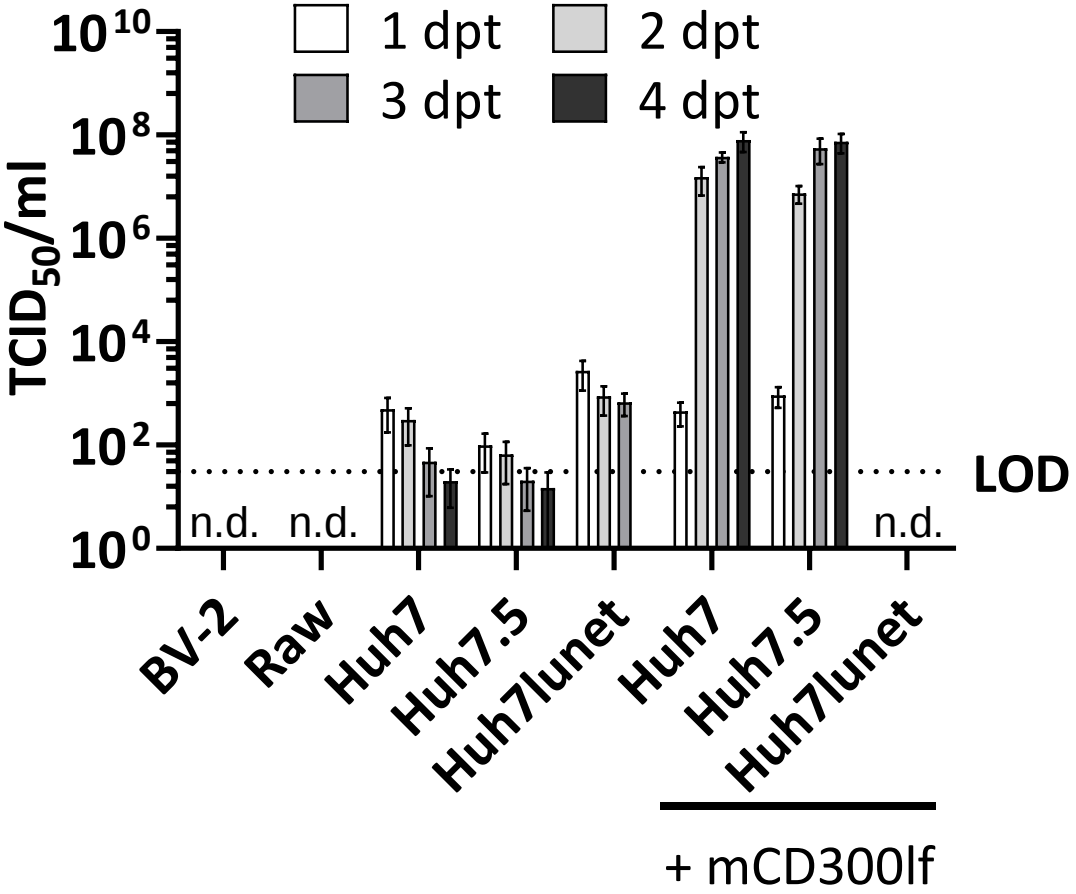

Figure 17 Transfection of the mCD300lf receptor expressing cells show a maximum viral titre at 3–4 dpt. *The Huh7+mCD300lf, Huh7.5+mCD300lf and Huh7lunet+mCD300lf cells were compared to the naturally susceptible BV-2 and Raw 264.7 cells in a transfection experiment. The experiment was performed 3 times with replicates and viral titres were determined at 1-4 dpt by end-point titration. A F/S mutant was included in the experiment (not shown) leading to non-detectable viral titres. N=3, SEM is depicted*

Another measure taken to analyse the production of recombinant MNV-1* was the determination of an optimal harvest time point. Thus, the three stable cell lines plus their parental non-susceptible cell lines were transfected using post-transcriptionally capped RNA and PeiMAX as a transfection reagent. In addition, the BV-2 and Raw 264.7 cells were transfected to compare them to the stable cell lines. Viral titres were determined by end-point titration at 1-4 dpt (Figure 17). As a control of the experiment

the F/S mutant was included. This F/S mutant did not lead to any detectable virus production (data not shown). As aimed for the Huh7+mCD300lf and Huh7.5+mCD300lf showed virus production with a maximum virus yield at 3-4 dpt with titres up to 2 x 10^8 $TCID_{50}$/mL. The Huh7lunet+mCD300lf did not lead to any detectable virus production and the parental cell lines Huh7, Huh7.5 and Huh7lunet produced only low titres of about 10^3 $TCID_{50}$/mL. The naturally susceptible BV-2 and Raw 264.7 cells did not produce detectable amounts of recombinant virus. It is known that BV-2 and Raw 264.7 cells are hard to manipulate by transfection [178]. Looking at the obtained results the Huh7+mCD300lf and Huh7.5+mCD300lf show an increase in viral titres at 2-3 dpt and remain stable at 4 dpt compared to their parental cell lines Huh7 and Huh7.5. This indicates that virus propagation occurs in the cells made susceptible to MNV infection by expression of the mCD300lf receptor.

All in all, the RNA-based reverse genetics system performs well in the Huh7+mCD300lf and Huh7.5+mCD300lf cells leading to titres comparable to titres obtained in an infection. The post-transcriptionally capped RNA combined with a transfection using either PeiMAX or lipofectamine2000 works most reliable.

4.5 Targeting the P domain by an alanine scan determines important binding sites

The MNV P domain is known to be important for the binding of glycans, antibodies and the mCD300lf receptor [35, 87, 88]. For HuNoV GII.4 a role of the canyon was described in HBGA binding [90] but the function of the loops remains to be determined. To get more insight into the role of the canyon and the loops in MNV infection they were targeted in an alanine scan where different regions of the loops and the canyon fucose binding regions of GII.4 were changed into alanine. Using reverse genetics, we tried to recover different recombinant viruses and test them in different functional assays.

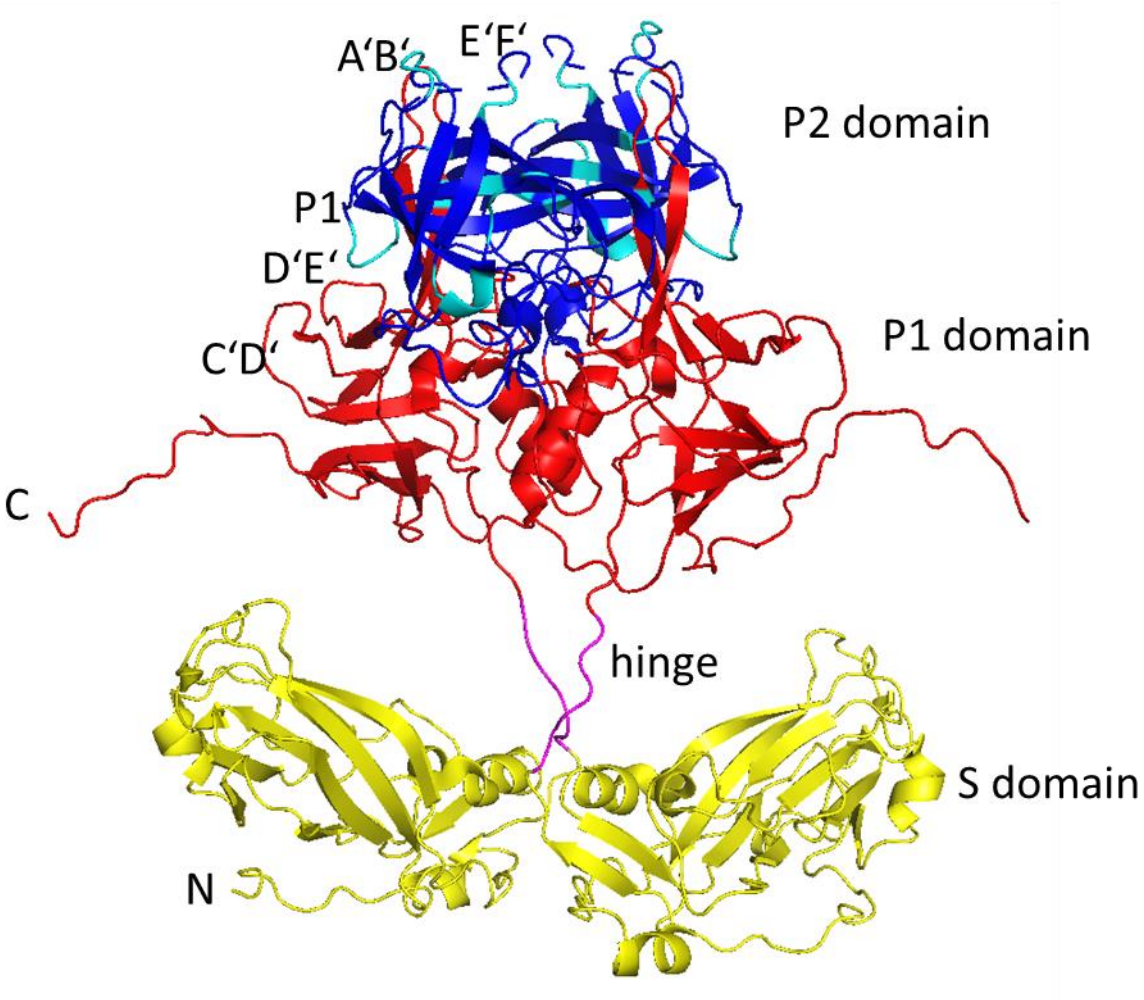

Figure 18 *MNV P dimer structure (PDB 6CRJ) with the different loops and canyon interfaces of the dimer that were targeted during the alanine scan assigned in cyan. The S domain is yellow, the P1 domain is red, the P2 domain is blue and the hinge is pink.*

Table 19 *All the desired recombinant viruses are listed including the location of mutation in the P domain, viral titres in a passage 3 (P3) viral stock and the mutations not leading to virus rescue. RBS: receptor binding site*

Mutation in P domain	**Function of site of mutagenesis**	**Location of mutation**	**$TCID_{50}$/mL of virus P3 stock**
P domain wt			1.28×10^7
SG299-300AA	Partial RBS	A'B' loop	5.56×10^6
SGT299-301AAA		A'B' loop	3.51×10^6
ETTK342-345AAA dT346-350	K345 Fab epitope [216]	C'D' loop	No rescue
ETTKT342-346AAAAA dT347-351		C'D' loop	No rescue
dL359-363 NDQ364-367AAA	Partial RBS	D'E' loop	No rescue
dL359-365 DQPYQG366-372AAAAAAA		D'E' loop	No rescue
VT378-379AA	mA.b A6.2 epitope [35]	E'F' loop	5.56×10^7
VT378-379AA dS383-388		E'F' loop	No rescue
TS379-383AA dL384-388	L386 antibody escape mutation [88]	E'F' loop	No rescue
T441A	Analog to HBGA binding site GII.4	P1 loop	2.58×10^6
E338A		Canyon	5.34×10^1
V352A		Canyon	4.90×10^2
R396A		Canyon	No rescue
R437A		Canyon	No rescue

For the alanine scan of the P domain different construct were obtained by site-directed mutagenesis. Since the RNA-based reverse genetics system was not yet established the background of the constructs is the pRevGen-MNV-1* plasmid used for the DNA-based reverse genetics system. Every construct was tried at least three times in a transfection experiment to obtain recombinant virus. For 6 out of the 14 desired mutations recombinant MNV-1* was rescued and succesfully passaged on BV-2 cells. The passage 3 (P3) viral titres were determined (Table 19). Four of the recombinant viruses have a mutation in one of the loops (two in A'B'-loop, one in E'F'-loop, one in P1 loop) and two of the rcombinant viruses have a mutation in the canyon interface which resembes the fucose binding site of HuNoV GII.4.

In the protein structure (Figure 18) the different sites of mutation are labeled in cyan. They are in the P1 domain in the different loops (annotated) and the canyon interface of the two P monomers.

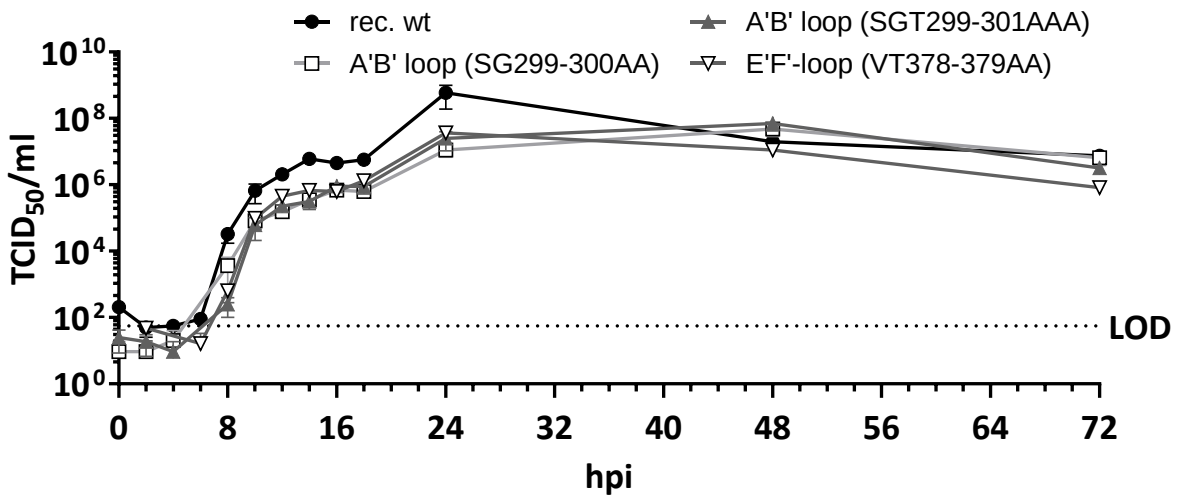

Figure 19 Exemplary growth kinetics of three recombinant MNV-1* compared to wt MNV-1*. *An exemplary growth kinetics of the wt recombinant virus MNV-1* is compared to three different mutant recombinant viruses in a growth curve spanning 72 h. Lysate samples were taken every 2 h for the first 18 h and then at 24, 48 and 72 hpi. N=3; SEM is depicted*

From the obtained recombinant viruses four were analysed in more detail in a growth curve where their growth kinetics was compared to the wt MNV-1* also obtained by the DNA-based reverse genetics system [197]. A P3 viral stock was incubated on BV-2 cells and lysate samples were taken every 2 h for the first 18 h and then at 24, 48, 72 hpi. The viral titres were determined by end-point titration and analysed for differences (Figure 19). Two of the recombinant viruses had a mutation in the A'B' loop and one in the E'F' loop. The recombinant viruses were sequence confirmed by preparing cDNA from the isolates' viral RNA. Sequencing showed the presence of the desired mutation in the P domain.

The detailed growth kinetics (Figure 19) showed that the viral titres of all three recombinant viruses were comparable to wt titres at 48-72 hpi yet a difference in growth kinetics was observed up to 24 hpi. The wt virus titre was up to 1 $\log_{10}$ higher than the different mutant viruses. A delay in growth of the mutant viruses was observed but final titres were comparable. The experiment was performed 3 times in independent setting showing comparable growth kinetics.

All in all, not all recombinant viruses aimed for were rescued by reverse genetics. Only six out of the 14 were successfully rescued of which three were analysed for their growth kinetics. Those three recombinant viruses showed a growth delay in the first 24 hpi compared to the wt recombinant virus but led to the same final titres at 72 hpi.

4.6 A novel reporter system detects norovirus replication based on eGFP re-localization

Different reporter constructs were kindly provided by Steeve Boulant (Heidelberg) which were designed that upon infection the viral protease can cleave the construct leading to a migration of an eGFP signal from either the mitochondrial or endoplasmic reticulum (ER) to the nucleus. A reporter cell line is a great tool to determine infected cells quickly and effectively. In comparison to immunofluorescence assays the detection of infected cells can be done in live cells and is not dependent on antibodies. Especially in the case of norovirus, antibodies are a bottleneck for successful immunofluorescence since not many are commercially available. Here, cell lines stably expressing the reporter constructs were analysed for the functionality of the reporter upon infection with MNV-1.

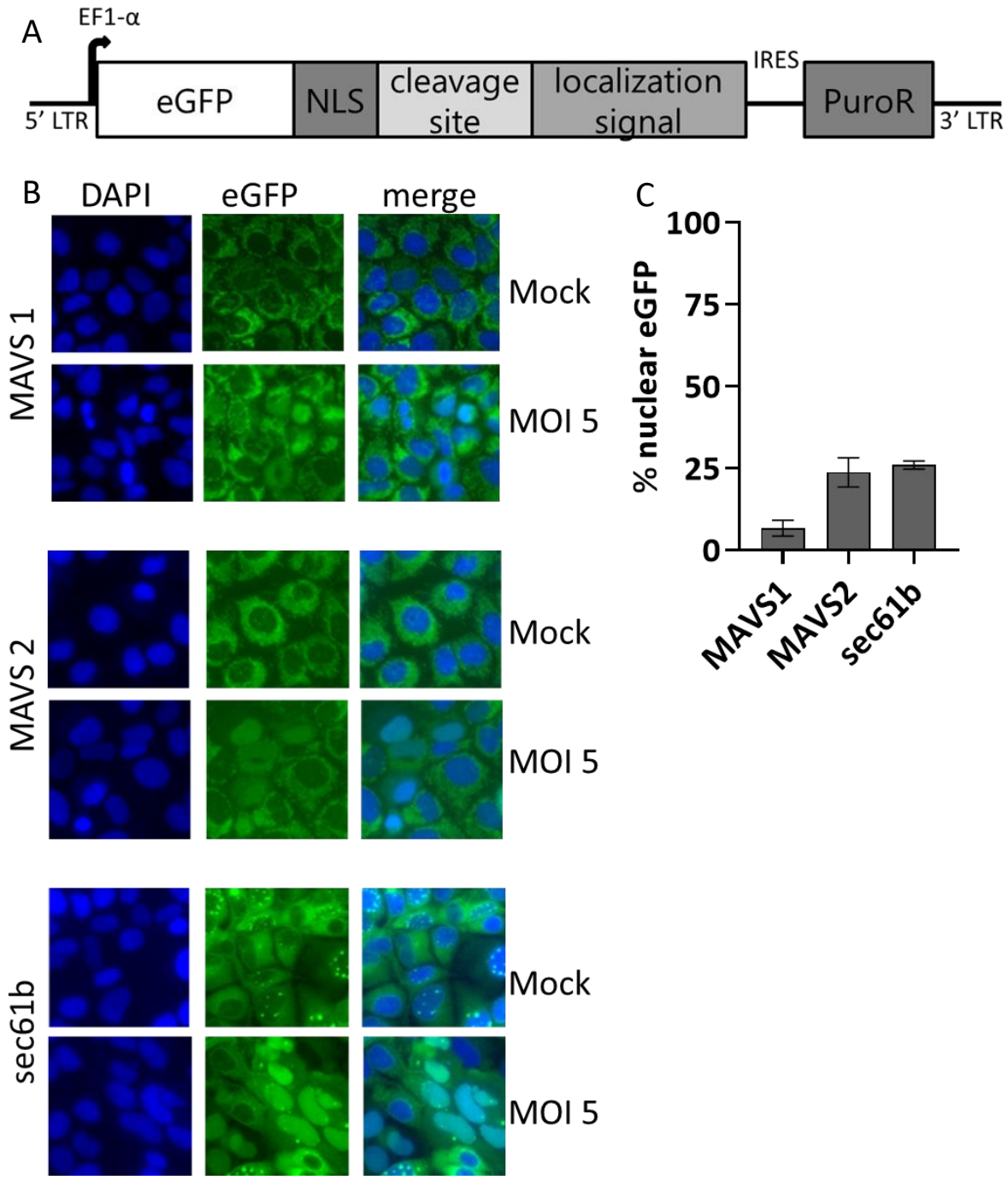

Figure 20 Reporter cell lines show a localization of eGFP to the nucleus upon infection with MNV-1. *(A) A schematic of the reporter construct is shown indicating the different elements included. It contains an eGFP with a nuclear localization signal (NLS) fused to it followed by a cleavage site and a localization marker. The cleavage site is a HuNoV cleavage site and cut by the 3C-like protease (NS6). For selection a puromycin resistance is present. (B) The stable reporter cell lines were infected with MNV-1 MOI 5 and compared to mock infected cells to show the re-localization of eGFP at 12 hpi. The nucleus was stained with DAPI. (C) The percentage of cells showing nuclear eGFP signal was quantified for the three different reporter cells. At least 100 cells of three individual pictures were counted. SEM is depicted*

Huh7+mCD300lf cells, which are robust and support MNV-1 replication as well as the RNA-based reverse genetics system were transduced with a lentivirus carrying a reporter construct (Figure 20A). The reporter construct contains an eGFP-nuclear localisation signal (NLS) fusion, a cleavage site and a localization marker as indicated. In addition, a puromycin resistance was present needed for selection of positive cells. The cleavage site is either the NS1/2-NS3 or NS3-NS4 cleavage site from HuNoV which is cleaved by the 3C-like protease encoded by NS6 [71]. The localization marker is either the mitochondrial antiviral signal (MAVS) or sec61b. Sec61b is a localization marker of the endoplasmic reticulum (ER). Three reporter constructs were tested which are either MAVS1 containing the NS1/2-NS3 cleavage site, MAVS2 containing the NS3-NS4 cleavage site or sec61b also containing the NS3-NS4 cleavage site. The plasmids (pWPI) containing the reporter were obtained from Steeve Boulant (Heidelberg) and used to obtain lentiviral particles by transfecting Hek 293T cells (Chapter 3.4.3.2) and 3.2.5.4). The lentivirus was used to transduce Huh7+mCD300lf cells which were selected using puromycin. Once selected the three different reporter cell lines (Huh7+mCD300lf+MAVS1, Huh7+mCD300lf+MAVS2, Huh7+mCD300lf+sec61b) were tested for their functionality by infection. The cells were infected with MNV-1 at MOI 5 and at 12 hpi the cells were fixed with 2% PFA for 20 min at RT. The nucleus was stained using DAPI. Pictures of the infected and mock-infected control cells were taken (Figure 20B). For the Huh7+mCD300lf+MAVS2 and the Huh7+mCD300lf+sec61b the re-localization of eGFP to the nucleus is clearly visible. For the Huh7+mCD300lf+MAVS1 the re-localization of eGFP to the nucleus is less obvious.

The amount of nuclear localization of eGFP in the three cell lines was detected by counting the cells. Three different sections of the cells were counted and the percentage of cells displaying nuclear eGFP localization was determined. As seen in figure 20C the Huh7+mCD300lf+MAVS2 and Huh7+mCD300lf+sec61b show comparable amounts of eGFP localization in the nucleus (about 25%) whereas the Huh7+mCD300lf+MAVS1 shows a lower percentage of nuclear eGFP localization (about 9%).

All three reporter constructs appear to work yet the efficiency varies between the reporter constructs which is most likely to be caused by the cleavage site. The NS3-4 cleavage site in the Huh7+mCD300lf+MAVS2 and Huh7+mCD300lf+sec61b led to comparable results in infection whereas the Huh7+mCD300lf+MAVS1 containing the NS1/2-NS3 cleavage site showed a lower percentage of nuclear eGFP localization. Furthermore, the intensity of the eGFP signal varied with the Huh7+mCD300lf+sec61b giving the strongest signal.

4.6 1 The reporter cells support the RNA-based reverse genetics system

The reporter system is based on the Huh7+mCD300lf cells which were shown to support the RNA-based reverse genetics system. Viral titres obtained reached 2 x 10^8 $TCID_{50}$/mL and were comparable to titres obtained during an infection with MNV-1. Taking this into consideration the reporter cell lines were tested whether they support the RNA-based reverse genetics system and would allow to observe the spread of the virus throughout the cells at 1-4 dpt.

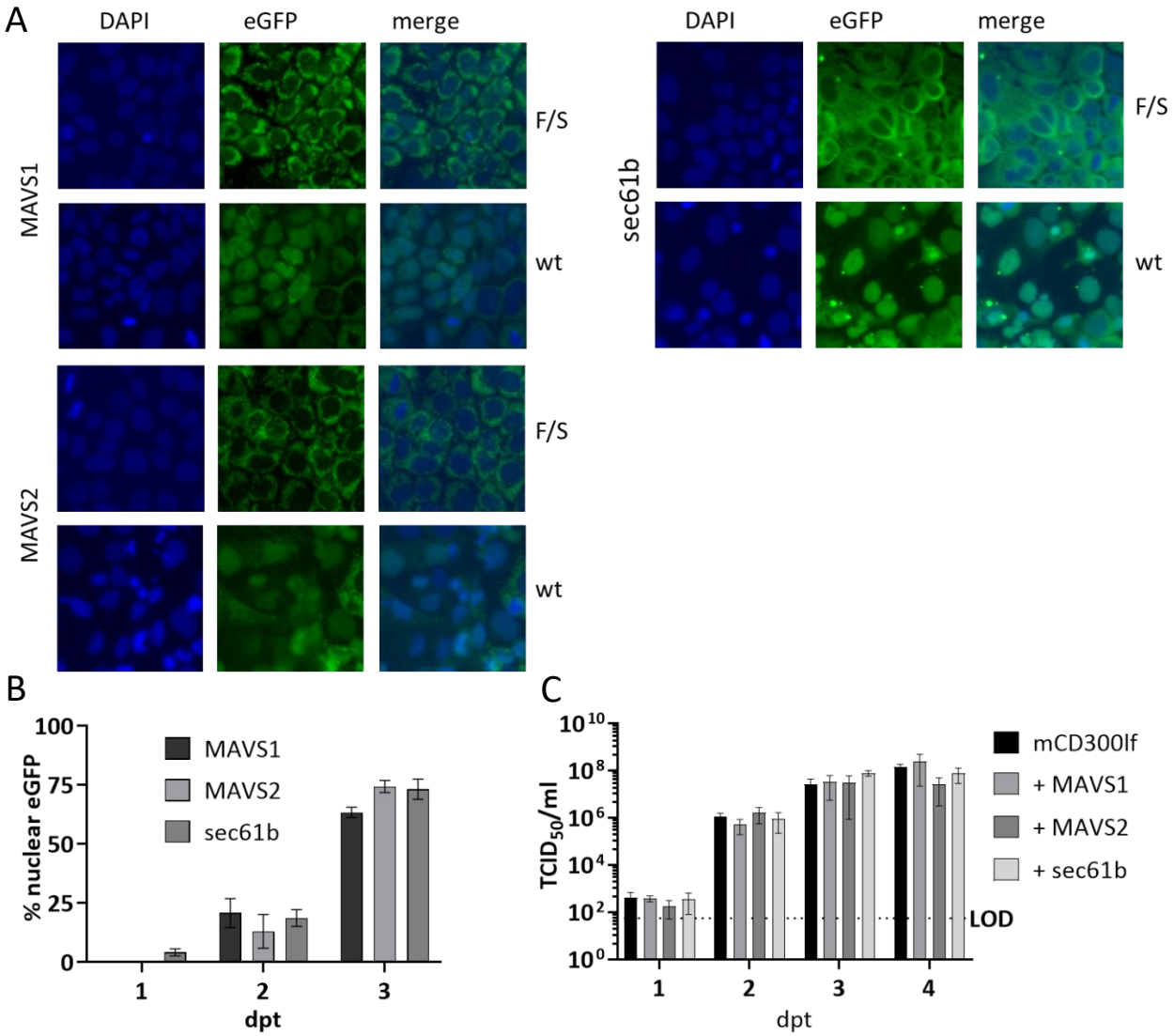

Figure 21 Three different reporter cell lines were transfected with in vitro transcribed RNA to show the progressing of the reverse genetics system in the cells. *(A) The different reporter cells were fixed at 3 dpt with 4% PFA and stained with DAPI. Fluorescent images were taken of the cells transfected either with wt RNA or the F/S mutant RNA. (B) For the three different reporter cell lines at 1-3 dpt the percentage of cells showing nuclear eGFP was determined. At least 3 different pictures from different experiments were counted. SEM is depicted (C) The virus titres of the transfected cells were determined at 1-4 dpt by end-point titration on BV-2 cells. The reporter cells were transfected with post-transcriptionally capped RNA using PeiMAX. The experiment was controlled by including the F/S mutant (data not shown). N=3, SEM is depicted*

To compare the three different reporter constructs they were all transfected with RNA for the reverse genetics system and at 1-4 dpt the cells were fixed and in addition, viral titres of the supernatant were determined by end-point titration.

The transfected cells show a shift in eGFP signal to the nucleus upon transfection (Figure 21A). The pictures shown are from 3 dpt. At 1-2 dpt the percentage of cells displaying an eGFP signal in the nucleus is not high making it difficult to detect. All three reporter cell lines show a shift of eGFP to the nucleus upon transfection and the cells were counted for eGFP signal in the nucleus (Figure 21B). At 1 dpt barely any cells with nuclear eGFP signal could be detected for all three cell lines whereas at 2 dpt for all three cell lines about 20% of cells showed a nuclear eGFP localization. At 3 dpt the percentage of cells with nuclear eGFP signal shifted up to 75% of the cells. At 4 dpt it was impossible to count the cells showing a nuclear eGFP localization due to CPE. The comparison of the viral titres obtained from the reporter cells compared to the parental cell line Huh7+mCD300lf shows that titres almost identical in the four different cell lines (Figure 21C). Titres of up to 10^8 $TCID_{50}$/mL were reached for the different cell lines indicating that the transduction with the reporter construct does not seem to have an influence on the capacity of the cells to produce recombinant virus.

As it turns out the reporter cells support the RNA-based reverse genetics system well and titres were comparable to the parental cell lines Huh7+mCD300lf. Comparing the different reporter constructs with each other it became obvious that the Huh7+mCD300lf+sec61b cells gave the most obvious signal. The intensity of the eGFP as well as the localization makes it most obvious. Following the reverse genetics system by counting the cells showing nuclear eGFP localization at 1-3 dpt showed that the number of cells initially replicating the viral RNA is quite low. Yet, due to the spread of the virus high viral titres can be achieved.

5. Discussion

5.1 Functional analysis of glycan and bile acid binding of MNV-1

Different functional assays were established to investigate the role of different glycans, bile acids and the *bona fide* receptor mCD300lf during infection with MNV-1. These functional assays are based on plaque assays where differences in binding can be observed. Select cell lines including BV-2 cells, Pro+mCD300lf and Lec2+mCD300lf cells were incubated with MNV-1 and different glycans including galactose, fucose and the human milk oligosaccharide 3'sialyllactose or the bile acid GCDCA. Virus binding to the cells was compared to the mock control.

5.1.1 Glycans show no enhancing effect on MNV-1

A role of fucosylated and sialylated glycans was described for the HuNoV GII.4 [92]. The P dimer of GII.4 interacts with 3'-sialyllactose as observed by saturation transfer difference nuclear magnetic resonance (STD NMR). Furthermore, the GII.4 P dimer appears to interact with fucose and B trisaccharide as shown by STD NMR and surface plasmon resonance (SPR). The interaction of MNV with sialylated and fucosylated glycans *in vitro* was examined by comparing effects of fucose and 3'sialyllactose to the non-binding glycan galactose and a mock control during infection. The binding assay showed no enhancing effects of fucose or 3'sialyllactose which is contradictory to previous results (Figure 8) [211]. Yet, the experimental set-up was different. The MNV-1 virus was pre-incubated with 50 mM glycans at 37 °C and here it was directly used in a plaque assay to determine binding whereas previously the samples were frozen and later analysed for viral titres by end-point titration. This measures infectivity whereas the plaque assay is more focused on the actual binding to the cells since the virus is removed from the cells after an incubation period. To further validate these results the most recent results obtained in a binding study by chemical shift perturbation (CSP) and saturation transfer difference (STD) nuclear magnetic resonance (NMR) need to be taken into consideration. Here, no binding of glycans to the MNV P dimer was observed [217]. This supports the findings of the binding assay that no enhancing effect of glycans on virus binding is observed and was previously potentially caused by an artificial freezing effect or was an artefact obtained by the detection method of viral titres that was used.

Another role of glycans during MNV infection was described for sialylated glycans [210] where a decreased infectivity of MNV-1 was shown after sialidase treatment of the cells which significantly decreases cell surface sialic acid moieties. For adenoviruses, the cell lines Pro5 and Lec2 were used to investigate the role of sialic acid during infection Pro5 are the parental cells and Lec2 are descendent cells with a significant decrease in sialic acid [192]. Stable cell lines expressing the receptor were obtained and infected with MNV-1 (Figure 9). No difference in viral titres was observed which is in line with the recent findings that sialic acid does not bind to the MNV P domain but contrary to the findings of cells treated with sialidase [210]. Yet, the two cell culture systems have significant differences. Taube et al. used the naturally susceptible Raw 264.7 and blocked sialic acid by sialic acid-binding lectins and observed a decreased infection in those cells compared to the mock treated cells. Furthermore, neuraminidase treatment of the cells supported the findings as this also led to a decrease

in infection of Raw 264.7 as well as BM-Mϕ cells. The influence of such treatments on the cells is unknown, yet the mCD300lf expressing Pro5 and Lec2 cells are also an artificial system. The cell lines are well characterised yet the influence of the lentiviral transduction and expression of mCD300lf is unknown. Interpretation of the results is thus difficult yet the absence of sialic acid binding in STD NMR and our results hint that sialic acid moieties are not necessary for infection.

5.1.2 Bile acids enhance MNV-1 binding

A role for the bile acid glycochenodeoxycholic acid (GCDCA) was described and binding of GCDCA was found for MNV-1 as well as the GII.4 HuNoV P domain [87, 217]. An enhancing effect of GCDCA on MNV infectivity was also described [87] and it was possible to reproduce the enhancing effect in a binding assay performed on BV-2 cells (Figure 10). The binding was 2-3 fold increased on BV-2 cells. Furthermore, the Pro5+mCD300lf and Lec2+mCD300lf were also tested in the binding assay and a similar enhancing effect was observed. The decreased amount of sialic acid on the surface of the Lec2+mCD300lf did not influence the binding of MNV in the presence of GCDCA. For GCDCA a crystal structure shows the binding to the MNV-1 P dimer at the P1/P2 interface. The binding of GCDCA did not lead to significant structural rearrangements yet for the soluble P domain a shift from the monomeric state to the dimeric state was found upon adding GCDCA [217]. Thus, GCDCA appears to influence dimer stability which might influence the mCD300lf binding. However, Nelson et al. mentions that the GCDCA binding site in MNV is different to the binding site found in HuNoV and they are unsure whether GCDCA is the co-factor that is found in serum or just one of the possible co-factors. So far, an enhancing effect of GCDCA on MNV-1 binding was observed which is independent on the cell line and the presence of cell surface sialic acid. However, it would be interesting to see whether GCDCA binding has an influence on other factors including glycans or neutralizing antibodies.

5.1.3 Can co-factors lead to conformational changes that influence receptor binding?

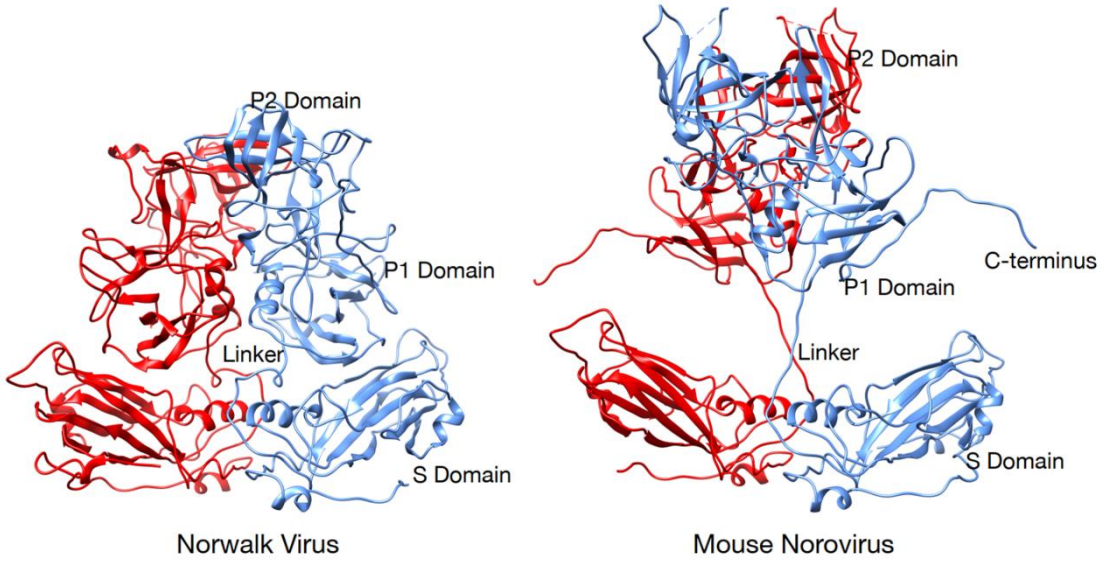

***Figure 22 The different shapes of the P domain and the virion are shown**. For Norwalk (GI.1) and MNV a compressed and expanded state is shown which is influenced by the flexibility of the linker found between the S domain and the P domain of VP1. Adapted from [218].*

The P domain is linked to the S domain via a flexible linker. This allows the P domain to change conformation leading to two sorts of particles being observed, the compressed particle where the P domain sits on top of the shell and the expanded particle where the P domain 'floats' above the shell domain. The flexibility of the P domain and the conformational change leads to different accessibilities of binding sites for antibodies and receptors and different orientations of the P dimers towards each other. For MNV and GII.10 cryo-EM structures of the expanded particle were observed whereas for GI.1 a condensed state was observed (Figure 22). Yet, it is thought that there are intermediate states and not only the compressed or expanded state. When comparing the compressed state to the expanded state the P dimer rotates by about 90° when expanded [218]. The interaction of the mCD300lf receptor with the P domain seems to favour the compressed particle [87]. In the expanded state due to the 90° rotation the space for the mCD300lf receptor to bind is smaller than in the compressed state. Thus, a higher saturation of the P domain with the receptor is expected in the compressed state. Whereas antibody binding sites for 5B18 Fab are partially hidden in the compressed state and thus for antibody binding the expanded state is more favourable [219]. Shown by these data it is not yet clear what exactly influences the change in conformation and what the role of the different states is. The linker appears to be conserved in the Caliciviruses which points towards such a transition between states in the different Caliciviruses.

For different glycans an influence on particle size was shown by electron microscopy (EM) [211]. It was shown that upon incubation of MNV-1 with either 3'sialylactose or B trisaccharide the particle size increased compared to the mock control. The binding of MNV-1 to mCD300lf appears to favour the compressed state of the particle which would support the findings observed in the glycan binding assay showing that glycans do not enhance the binding of MNV. However, an increased ratio of particles in the expanded form should inhibit viral infection if the compressed state is favoured for mCD300lf

binding. Yet, 3'sialylactose did not show a negative influence on virus binding. Furthermore, the antibody binding site of 5B18 is partially hidden in the compressed state which indicates that the compressed state might be a mechanisms of antibody escape. If glycans lead to an increase in particle size and thus an increase in particles present in the expanded state, the antibody binding of 5B18 should increase in the presence of glycans and binding should decrease.

However, which role GCDCA might play in the role of the floating P domain remains unclear. It is obvious that GCDCA acts as a co-factor in binding and its binding site is at the interface to the two P monomers in the dimer [87]. This could enhance P domain stability which is supported by the observation that the P domain in solution tends to form a dimer in the presence of GCDCA whereas without GCDCA the amount of P dimer present is lower [217]. With increasing stability of the P domain, the receptor binding might be increased through allosteric networks of the protein but how that might influence the conformation of the P domain between compressed and the expanded state remains unknown.

5.2 Stable expression of the mCD300lf receptor in select cell lines leads to gained susceptibility to MNV-1 infection

The mCD300lf receptor is the *bona fide* for murine norovirus [45, 212]. MCD300lf is a transmembrane receptor that was shown to render non-susceptible cell lines susceptible to MNV infection. Transduction with a lentiviral packaging system rendered different eukaryotic cell lines susceptible to MNV. This was tested in HeLa [45], Hek 293T, Cos7, CHO, CRFK, NIH 3T3 [212] as well as Huh7 [118] cells. All cell lines are naturally resistant to MNV infection but upon expression of the mCD300lf receptor they became susceptible to MNV infection. Infection of the mCD300lf-expressing cells with MNV showed that they support viral replication which was not observed in the parental cell lines not expressing mCD300lf. However, the obtained titres of the different cell lines varied. Comparison of the obtained titres is difficult since different strains of MNV were used in the different publications. The Huh7+mCD300lf cells [118] were the only cells infected with MNV-1CW.3 yet no titres were named only that they were comparable to titres obtained in the naturally susceptible Raw 264.7 cells. Thus, in different cell lines the mCD300lf receptor led to the cell lines being susceptible to MNV infection and thus creating cell lines that are easy to manipulate and support MNV replication.

Here, we established mCD300lf-expressing cell lines by transduction of Huh7 and descendent cells. A lentiviral packaging system of the second generation was used and the transduced cells were selected using antibiotic selection and FACS and analysed for mCD300lf expression and susceptibility to MNV infection (Figure 11).

The Huh7 cells are cells commonly used for HCV and DENV research with the related cell lines Huh7.5 and Huh7lunet cells. The Huh7.5 and Huh7lunet cells were cured from the HCV replicon leading to a deficiency in the cells immune system [190, 191]. A Rig-I deficiency was shown which is a pattern recognition receptor influencing the interferon-I (IFN-I) response of the cell [220]. In consideration of these information the Huh7 and descendent cells were chosen for the transduction with the mCD300lf receptor. Once transduced the three different cell lines (Huh7+mCD300lf, Huh7.5+mCD300lf and Huh7lunet+mCD300lf) were selected with G418 using the NeoR resistance marker of the lentiviral construct (Figure 15) and enriched by FACS using the eGFP signal introduced by the lentivirus. The selected cell lines were characterized by WB analysis using a FLAG antibody to detect the presence of the receptor. WB analysis showed signals unique for the mCD300lf-FLAG fusion protein. As a control the parental cell lines not expressing the receptor were applied to the WB. A band of ~37 kDa was expected yet up to 4 bands became visible. A WB of the HeLa cells expressing a mCD300lf-FLAG fusion was shown in the supplementary data of Orchard et al. [45] showing comparable bands. Smaller bands then the expected 37 kDa are probably due to degradation of the receptor yet bands with a size of around 55 kDa would not represent the size of a dimer. For human and murine CD300lf a complex formation is shown including complexes with *PI3K* and *Grb2* [221]. A possible complex could lead to the band observed with a higher molecular weight. However, the SDS-gel was run under denaturing conditions and adding 2 M urea to the application buffer did not lead to a shift in band size. This hints towards a covalently linked co-factor or possibly dimer.

Cells expressing mCD300lf were enriched by fluorescence-activated cell sorting (FACS) using the eGFP signal. For the Huh7+mCD300lf 88% positive cells were detected, for the Huh7.5+mCD300lf 72% and for the Huh7lunet+mCD300lf 92% (Figure 11D). In a later FACS analysis the cells were analysed for eGFP positive cells in order to determine the stability of the cell lines receptor negative cells were used as a comparison. Here, the stable cell lines were kept in culture for 14 – 18 passages. Comparing the

eGFP positive cells after several passages (Huh7+mCD300lf 88.1%; Huh7.5+mCD300lf 65.2%; Huh7lunet+mCD300lf 92.4%). In conclusion cells are stably expressing the receptor over at least 18 passages, however, not all cells express the receptor. Both FACS assays the initial enrichment and the second control FACS were only performed once. Thus, numbers obtained are only a snapshot of the actual stable cell lines and numbers could vary if the FACS would be repeated. However, the obtained percentages of eGFP positive cells indicate that the cell lines are fairly stable, and the receptor is still expressed.

Next, the susceptibility of the transduced cells was observed by infection and samples were taken at 0, 12, 24 hpi and compared to BV-2 and Raw 264.7 cells infected at the same time (Figure 12). As a control the parental cell lines Huh7, Huh7.5 and Huh7lunet were included which should not show viral replication. Huh7+mCD300lf and Huh7.5+mCD300lf showed viral titres compared to BV-2 and Raw 264.7 cells which supports the data already published for Huh7+mCD300lf [118]. Titres reached 2 x 10^8 $TCID_{50}$/mL. The Huh7lunet+mCD300lf showed a slightly lower titre with a maximum at 1 x 10^7 $TCID_{50}$/mL compared to the BV-2 and Raw 264.7 cells. The parental cell lines showed no viral replication and the titres observed are caused by the input virus.

For MNV it was shown that IFN can block replication [222] and reduced levels of Rig-I leads to a reduced IFN-I response. The cell lines Huh7.5 and Huh7lunet show deficiencies in Rig-I yet in the case of an infection with MNV-1 no influence of this deficiencies on viral titres was observed. One would expect that without the antiviral effect of the interferon response titres would increase yet no difference titre between Huh7+mCD300lf and Huh7.5+mCD300lf was observed and the Huh7lunet+mCD300lf even showed a one log_{10} decrease in titre. The Huh7lunet+mCD300lf cells did change upon transduction and became a less robust cell line. It must be kept in mind that the transduction created a cell pool, but it was only performed once. Thus, Huh7lunet cells that were to be transduced with a newly generated lentivirus containing the mCD300lf gene might behave differently.

The three different cell lines were also tested for their functionality in a plaque assay and compared to the BV-2 and Raw 264.7 cells (Figure 13). The Huh7+mCD300lf and Huh7.5+mCD300lf showed plaque formation and viral titres obtained were comparable to titres obtained on the naturally susceptible BV-2 and Raw 264.7 cells. This corelates to the results obtained by the infection experiments (Figure 13). However, the Huh7lunet+mCD300lf cells did not lead to detectable plaques which was caused by the cells detaching during the assay. The Huh7lunet are robust cells yet the expression of the mCD300lf receptor in such high amounts appears to influence the cells and decreases their capability to attach to a surface.

5.3 mCD300lf expressing cell lines support reverse genetics systems

1.13.6 The advantages and disadvantages of the different previously published reverse genetics systems

The described MNV reverse genetics systems differ in their experimental set-up, yet they all have disadvantages that can be detrimental [179]. The DNA-based, helper virus-based, and baculovirus-based systems all need cDNA as a nucleotide source. In all three cases the cell line used is a naturally non-susceptible cell line to MNV infection. Thus, only a single round of virus production is taking place. To obtain high titre stocks of the recombinant virus the supernatant containing the first round of recombinant MNV needs to be incubated with naturally susceptible cell lines like BV-2 or Raw 264.7 cells. In comparison, for the RNA-based system the Raw 264.7 cells are electroporated with *in vitro* transcribed and capped RNA which are naturally susceptible to MNV infection and thus allow multiple rounds of infection making it a uni-cellular system leading to high viral titres.

The resulting viral titres are only one experimental set back. The labour costs of the different systems range from low costs of the DNA-based system to high costs of the RNA-based system. The DNA-based system relies on the transfection of a plasmid into Hek 293T cells and a second incubation step on Raw 264.7 or BV-2 cells. Preparation time is thus limited. In the RNA-based system the preparation before electroporation is time consuming due to the preparation of the *in vitro* transcribed and capped RNA but once the cells are electroporated no more steps are necessary. The helper virus-based system needs a fowlpox-T7 virus that needs to be prepared and a second incubation step of the recombinant virus on susceptible cell lines is needed making it time consuming. The baculovirus-based system even needs three different cell lines. The Sf9 cells are needed to produce the recombinant baculovirus needed for transduction, then the HepG2 cells are needed for the transduction using the baculovirus and due to low viral titres obtained a susceptible cell line is needed to passage the recombinant virus containing supernatant to obtain high viral titres.

Taking these drawbacks into consideration the RNA-based system seems to be a good set-up to work with. Unfortunately, the electroporation of Raw 264.7 cells relies on an electroporation system that is not available in a wide range of research groups [178]. The electroporation system is unique and costly making the system less affordable.

The stable cell lines expressing the mCD300lf receptor are a promising tool for reverse genetics. For the parental cell lines Huh7, Huh7.5 and Huh7lunet it is known that they are easy to manipulate by transfection or electroporation and are quite robust cell lines. Another advantage is the gained susceptibility to MNV infection by expression of the mCD300lf receptor. For MNV different reverse genetics systems are published yet none is convenient and easy reproducible.

5.3.1 An improved DNA-based reverse genetics system

A DNA-system based on a polII promoter was published in 2007 that is based on a DNA-plasmid containing the whole genetic information of MNV-1* which contains a silent mutation leading to an EcoRV restriction site which allows to distinguish between virus isolates and recovered from a reverse

genetics system. This system needs the transfection of the non-susceptible Hek 293T cells leading to 10^3 PFU/mL virus production and virus replication is obtained on susceptible BV-2 or Raw 264.7 by incubation with the supernatant of the Hek 293T cells [176].

The three stable cell lines were tested whether they work for the DNA-based reverse genetics system compared to the Hek 293T cells and to the parental, non-susceptible cell lines. Titres were obtained for the Hek 293T and Huh7lunet+mCD300lf (up to 1 x 10^5 $TCID_{50}$/mL) but not for Huh7+mCD300lf or Huh7.5+mCD300lf (Figure 14). At least three different experiments were performed not leading to detectable viral titres. The reason why only the Huh7lunet+mCD300lf cells led to virus rescue and the other stable cell lines did not remains unclear.

Since the Huh7lunet+mCD300lf cells were the only cells supporting the DNA-based reverse genetics system the growth kinetics of the recombinant wt MNV-1* and the virus isolate MNV-1 were compared on the naturally susceptible BV-1 cells and the Huh7+mCD300lf cells. This exemplary and detailed comparison (Figure 14D) showed a delayed replication of the recombinant wt MNV-1* compared to MNV-1. The delay in replication is less significant in the BV-2 cells compared to the Huh7lunet+mCD00lf cells. BV-2 cells show a difference of 1.5 log_{10} at 18 hpi yet at 24 hpi no difference in viral titres can be observed. The Huh7+mCD300lf cells show a difference of 1.5 log_{10} at 24 hpi and the difference in viral titres between the recombinant MNV-1* and MNV-1 lasts until 48 hpi where titres are similar. Furthermore, the Huh7lunet+mCD300lf cells show a delayed replication compared to the BV-2 cells. This effect is observed for both, MNV-1 and MNV-1*. Comparable titres are only reached at 48 hpi. Titre differences at 18 hpi reach up to 2 log_{10}. The delay in replication observed in the Huh7lunet+mCD300lf cells could explain the titre difference observed in the infection of the different mCD300lf-expressing cell lines (Figure 14) since viral replication is only observed until 24 hpi yet viral titres appear to increase in the Huh7lunet+mCD300lf until 48 hpi. Here comparable titres to the naturally susceptible BV-2 cells are obtained.

5.3.2 An improved RNA-based reverse genetics system

An RNA-based reverse genetics system is described where Raw 264.7 cells are electroporated with *in vitro* transcribed RNA [178]. After testing the stable cell lines Huh7+mCD300lf, Huh7.5+mCD300lf and Huh7lunet+mCD300lf in the DNA-based reverse genetics system all three cell lines were tested in the RNA-based reverse genetics system and compared to the naturally susceptible Raw 264.7 and BV-2 cells. To establish the RNA-based reverse genetics system different measures were taken (Figure 15-17) which showed that in this setting post-transcriptionally capped RNA that is inserted into the cells via transfection with PeiMAX leads to a maximum yield of recombinant MNV-1* of 2 x 10^8 $TCID_{50}$/mL at 3 dpt in Huh7+mCD300lf and Huh7.5+mCD300lf cells. In comparison the Huh7lunet+mCD300lf cells did produce recombinant virus to a lesser extent and stability of the cells was not given leading to a significant amount of experiments failing to produce recombinant virus (around 85% of experiments failed). The Huh7lunet+mCD300lf are more sensitive to environmental circumstances. This decreased robustness might be a reason for the high percentage of failed experiments.

In a time, curve (Figure 17) the Huh7+mCD300lf, Huh7.5+mCD300lf and Huh7lunet+mCD300lf cells were compared to their parental cell lines as well as the naturally susceptible Raw 264.7 and BV-2 cells. Virus samples were taken at 1-4 dpt and viral titres were compared. At 3-4 dpt the Huh7+mCD300lf and Huh7.5+mCD300lf reached the maximum titre. It became obvious that the receptor expression

allowed for multiple rounds of infection due to the gained susceptibility of the cells [45, 118, 212]. The parental cells Huh7, Huh7.5 and Huh7lunet showed only a single round of virus production since titres dropped slightly over the 4 days post infection and did not increase. However, the BV-2 and Raw 264.7 cells did not show viral replication even though they are susceptible to MNV infection. The Raw 264.7 and BV-2 cells are difficult to manipulate by transfection which is probably the reason why no recombinant virus could be rescued.

The Huh7+mCD300lf and Huh7.5+mCD300lf cells showed comparable results in virus rescue. The decreased Rig-I and thus interferon response of the Huh7.5+mCD300lf cells appears to not influence the production of recombinant virus. Rig-I is known to target dsRNA and upon antiviral response Rig-I is localized to antiviral stress granules (avSGs) [223]. For different viruses it is known that membrane reorganization during viral replication is a mechanism to avert dsRNA degradation [224]. For MNV a membrane reorganization is shown yet the role of Rig-I and membrane reorganization has not been described [118].

However, the capping mechanism appears to have an influence on reproducibility of the RNA-based reverse genetics system. The co-transcriptional capping kit led to less reproducible results then the post-transcriptional capping kit. The co-transcriptional capping is based on the integration of the methylated ribonucleotide at the 5' end during *in vitro* transcription whereas the post-transcriptional capping is based on *Vaccinia* virus capping enzyme. According to manufacturer's guideline the post-transcriptional capping has 100% efficiency whereas co-transcriptional capping has only 80% efficiency (Cellscript). Capped RNA has an enhanced stability compared to uncapped RNA and furthermore uncapped RNA is recognized by the cells as foreign RNA leading to an immune response. Thus, avoiding uncapped RNA should lead to a lower extend of the immune response of the cells and thus higher viral titres. In addition, uncapped RNA is less stable due to degradation by host factors like Xrn1, an exoribonuclease targeting uncapped RNA [225].

Summing up the results obtained from the RNA-based reverse genetics system the Huh7+mCD300lf and Huh7.5+mCD300lf lead to comparable results when using post-transcriptionally capped RNA and transfect with either lipofectamine2000 or PeiMAX. These adjustments of the RNA-based reverse genetics system compared to the Raw 264.7 based reverse genetics system is better accessible and using PeiMAX for transfection the costs for the system are comparably low.

5.4 An alanine scan of the P domain hints towards important binding sites

Using the DNA-based reverse genetics system a panel of mutations in the P domain were designed (Table 19) and it was possible to rescue six recombinant viruses plus the recombinant wt virus. All desired mutations were tested at least five times to rescue the recombinant virus.

As shown in table 19 the P3 viral titres differ significantly already showing an attenuation of the E338A and V352A mutation which target the canyon on the P domain. Viral titres were as low as 5.34×10^1 and 4.90×10^2 $TCID_{50}$/mL with the wt reaching titres of 1.28×10^7 $TCID_{50}$/mL. Considering the low titres of those two recombinant viruses (E338A and V352A) one can say that the canyon of the P dimer is an important target, yet the low titres make it difficult to analyse the virus in cell culture assay. For HuNoV these sites at the canyon interface are known to be a HBGA binding site and were thus targeted by our alanine scan. For MNV-1 these sites at the canyon interface were not yet shown to be important for binding of glycans. However, the dimer interface is important for stability which could influence the fitness of the virus. Analysis of the P domain by biochemical approaches including NMR techniques, surface plasmon resonance (SPR) or crystallization could give more insight into the importance of these amino acids.

For three of the rescued recombinant viruses a first analytical assay was performed by observing the growth kinetics in a detailed growth curve and compare it to the recombinant wt virus (Figure 18). The recombinant viruses contain the mutations SG299-300AA and SGT299-301AAA both in the A'B'-loop and VT378-379AA in the E'F'-loop. The G300 is part of the mCD300lf receptor binding site being a H donor of one of the five hydrogen bonds formed in the receptor interaction. The E'F'-loop is the binding epitope of the monoclonal antibody A 2.6. The three different recombinant viruses showed a growth delay compared to the recombinant wt virus of about 1 $\log_{10}$. This difference is observed in the initial replication and lasts until 48 hpi where the titres of the recombinant viruses and the recombinant wt virus are comparable. The overall growth kinetics have a great similarity with previously published growth kinetics performed on BV-2 and Raw 264.7 cells [44, 213]. The recombinant viruses analysed have changes in the A'B'-loop and E'F'-loop. The G300 in the A'B'-loop is part of the mCD300lf receptor binding site whereas the E'F'-loop is the mAb A6.2 epitope. Mutations in both loops have a similar effect and lead to a maximum titre that is reached at 48 hpi and is comparable to wt. This indicates that the mutations are not detrimental. G300 appears to be one of the four H donors of the five hydrogen bonds that are formed in the receptor interaction [89]. It is highly conserved between the different MNV strains, yet the other receptor interaction sites appear to be enough for successful receptor binding and infection. Here, it would be interesting to mutate other receptor binding sites as well to determine which binding sites are important for receptor biding and which ones have a limited effect on receptor binding. Furthermore, a biding assay should show the difference in actual binding whereas here infection is measured. For the mutation of the E'F'-loop a binding assay especially including the mAb A6.2 should show whether the mutation plays a role in antibody detection. It would be expected that these mutations play a bigger role in the presence of antibodies and *in vivo* than it plays in a simple infection experiment.

All in all, a site directed mutagenesis of the P domain can give more insight into functional sites of the P domain. For the recombinant viruses, the previously described functional assays like the GCDCA enhancement assay or a binding assay on the different mCD300lf-expressing cell lines can be interesting. Furthermore, neutralizing effect of different antibodies can be tested in a binding assay.

For the desired mutations where no recombinant virus could be rescued the P domain can be bacterially synthesized and analysed. Here, assays include the formation of P dimers upon adding GCDCA, binding of glycans or the soluble mCD300lf exodomain. Furthermore, a tagged P dimer can be used for glycan arrays.

5.5 A novel reporter system indicates infected cells allowing live observation of viral spread

For MNV detection of infected cells either occurs via CPE or with the limited number of antibodies present. No recombinant MNV is available that carries a fluorescent signal helping to detect infected cells. Here different eGFP-based reporter constructs are validated and differences between the two cleavage sites used are examined.

For the design of the reporter constructs two cleavage sites of the HuNoV are tested being either the NS1/2-NS3 or the NS3-NS4 cleavage site (Figure 20A). The norovirus cleavage sites are well conserved being either Q-G/N or E-G/A [71, 226] thus it was expected that MNV can use the HuNoV cleavage sites as well. Next to the cleavage sites two localization marker were compared being either the mitochondrial antiviral signal (MAVS) or sec61b a localization marker of the ER. To test the different reporter systems the Huh7+mCD300lf cells were chosen as the parental cell line since they support MNV infection and the RNA-based reverse genetics system. Furthermore, the cell line is robust allowing different experiments including plaque assays and immunofluorescence assays. Unfortunately, due to the transduction with the mCD300lf containing lentivirus a weak background GFP signal was already present in the cells. For the reporter system this weak background signal is not of importance. However, for the selection process the background GFP signal is a problem since FACS based on an eGFP signal is impaired.

The first functional test of the reporter cells was an infection with MNV-1 where the cells were fixed at 12 hpi and the nucleus was stained with DAPI (Figure 20). Of the infected cells the percentage of cells displaying nuclear eGFP signal was determined and compared. This gave an insight into the difference between the different reporter construct next to the visual difference. At first glance the optical signal between the MAVS and sec61b differs in intensity as well as localization. The sec61b has a stronger signal compared to the MAVS. This makes it easier to detect nuclear eGFP signal in living cells. However, this is a personal preference and both the sec61b as well as the MAVS signal show nuclear localization. Looking at the different cleavage sites a more interesting difference was observed between the NS1/2-NS3 and the NS3-NS4 cleavage sites. The NS3-NS4 cleavage site in the Huh7+mCD300lf+MAVS2 and Huh7+mCD300lf+sec61b led to ~25% of cells showing nuclear eGFP signal whereas the signal of the Huh7+mCD300lf+MAVS1 cells containing the NS1/1-NS3 cleavage site was at ~9%. This hints that the NS1/2-NS3 HuNoV cleavage site is less functional for MNV than the NS3-NS4 cleavage site. Yet, this is not an analysis of the functionality of the cleavage sites, it only gives an indication.

Next, the cells were examined for their function in the RNA-based reverse genetics system (Figure 21). The reporter should allow to characterize the RNA-based reverse genetics system in more detail. Cells replicating the viral genome can be detected early on which indicates replication takes place which hopefully leads to the rescue of recombinant virus. Transfection with the *in vitro* transcribed and capped RNA showed that all three stable cell lines expressing the different reporter constructs support the reverse genetics system. The fluorescent pictures taken showed a clear localization of eGFP to the nucleus in all three reporter cell lines. Quantification of the eGFP localization at 1-3 dpt showed that nuclear eGFP signal was detected in all three different cell lines. Yet, as expected the signal in the Huh7+mCD300lf+MAVS1 cells was lower than in the other two cell lines. At 3 dpt the Huh7+mCD300lf+MAVS1 showed 63% of cells with nuclear eGFP whereas the Huh7+mCD300lf+MAVS2 and Huh7+mCD300lf+sec61b showed around 74% of nuclear eGFP signal.

This is in line with the results obtained from the quantification of the infected cells. However, the viral titres obtained for 1-4- dpt were comparable to the titres detected in the parental cell line Huh7+mCD300lf (up to 2 x 10^8 $TCID_{50}$/mL). Thus, the expression of the reporter system does not influence the support of the RNA-based reverse genetics system. Having established a reporter system in cell lines made susceptible to MNV infection allows for further investigation of virus replication as well as effects on receptor biding. Being able to control replication during a reverse genetics approach to rescue recombinant viruses can give insight into the influence of the mutation. When the virus cannot be rescued it is of importance to see whether it is replication deficient or unable to package the virus. This could hint towards an influence of the mutation on the replication cycle. Another useful setting of the reporter system would be during binding and enhancement/inhibition assays. Normally to observe the influence of binding and an interruption or enhancement the viral titre is of importance. This can be detected either by plaque assay or end-point titration. Here, the influence can be detected live and be observed over time. Furthermore, it is still possible to detect viral titres by end-point titration and compare them with the observations made using the fluorescent signals.

5.6 Influences of the gained knowledge on the development of a HuNoV reverse genetics system

Studying HuNoV is still defined by the cell culture systems not allowing efficient viral replication and being quite elaborate. Murine noroviruses are a great model to study HuNoVs. Here, we were able to observe a few details that can be a bottleneck in the development of a HuNoV reverse genetics system. For the HuNoV GII.3 U201 a plasmid based reverse genetics system is published [180]. Yet, obtained quantities of recombinant virus are low. For the zebrafish and enteroid system it is known that enough infectious particles must be present to overcome bottlenecks and get virus replication [32, 103]. Thus, an efficient reverse genetics system for HuNoVs is desirable. Using the RNA-based reverse genetics system in the reporter cells we could show that initial virus production is low and high viral titres are obtained only through replication in the cell lines. At 1 dpt only a few cells of the Huh7+mCD300lf+sec61b show detectable translocation of eGFP to the nucleus indicating viral replication. Thus, without the spreading of the virus no high titres will be obtained which supports the urge for an efficient and reproducible cell culture system that is universally available.

6. Conclusion

The here presented thesis focussed initially on a mutagenesis study of MNV to determine important glycan binding sites. For norovirus a role of sialylated and fucosylated glycans was published [92]. More recently [45] the *bona fide* MNV receptor mCD300lf was published which shifted the focus of this thesis to tools to study host-virus interaction of MNV. The receptor binding sites of MNV are known and were also targeted in the mutagenesis study of the MNV P domain. Since it became known that the mCD300lf receptor renders cell lines susceptible to MNV infection this led to the idea to obtain novel cell lines and test these for improved reverse genetics systems for MNV. An improved DNA-based system supported by the Huh7lunet+mCD300lf cells was established as well as an improved and more affordable RNA-based system making use of the Huh7+mCD300lf and Huh7.5+mCD300lf cells.

Using the improved DNA-based reverse genetics system the first recombinant MNV-1* were rescued and analysis was started. A detailed growth kinetics showed an influence of the mutations in the A'B'- and E'F'-loop on viral replication. The A'B'-loop is part of the RBS and the E'F'-loop is an antibody binding site. Only a minor effect of the mutations on viral replication were observed and final vial titres at 48 and 72 hpi reached the height as the wt MNV-1*. Yet, for further analysis of these recombinant viruses and the other rescued recombinant viruses (Table 19) time was too short.

Another tool that was established and characterized was a reporter system for norovirus infection. Here, the detection of MNV by the reporter system was tested yet it should in theory also work for HuNoVs. Based on an eGFP signal that is re-located to the nucleus viral replication in the cell can be detected. Huh7+mCD300lf cells were transduced with different lentiviruses containing either of the three reporter systems. Characterization of the reporter expressing Huh7+mCD300lf cells showed that the two reporter systems containing the HuNoV NS1/2-NS3 cleavage site show a higher cleavage rate and thus a higher re-localization of eGFP to the nucleus. These reporter cells also support the RNA-based reverse genetics system giving more insight into the spread of the virus during the reverse genetics approach. This can help to detect whether viral replication takes place and if no virus can be rescued it can give a first hint to where the problem is, either in viral replication or packaging.

All in all, different tools were established and improved that help to investigate host-virus interaction of MNV and hopefully this will eventually lead to systems becoming available for HuNoV.

7. Outlook:

The aim of this PhD thesis was initially to test the host virus interaction considering glycan interaction as well as receptor binding. Unfortunately, not all aims were reached including the alanine scan of the P domain including the analysis of the recombinant viruses. Different assays were established to analyse the recombinant viruses. According to latest results [217] glycans are not a binding factor and are thus less of interest. However, binding of GCDCA should be examined for the recombinant viruses. Especially the ones where the receptor binding epitope is involved since it is thought to be a co-factor during receptor binding. Furthermore, binding assays should include neutralizing antibodies and how the different mutations interfere with the neutralizing effect. Here, the different cell lines should be used, including the naturally susceptible BV-2 and Raw 264.7 cells as well as the reporter cells to track infection live.

Since not all desired recombinant viruses could be rescued using the at the time available DNA-based reverse genetics system it should be considered to use the RNA-based reverse genetics system. The template plasmid for the RNA-based reverse genetics system differs from the DNA-based reverse genetics system and thus the desired mutations need to be inserted into the template plasmid of the RNA-based reverse genetics system. With the higher titres that are typically achieved in the RNA-based reverse genetics system it is hopefully possible to rescue more of the recombinant viruses. However, if the rescue of the recombinant viruses is not possible one might consider changing the mutation. Some mutations contain multiple changes to alanine as well as multiple deletions. Decreasing the sice of the mutation might lead to the rescue of the recombinant virus and the influence of this mutation can be examined.

The reporter cells are a great tool to analyse different inhibitors as well as co-factors in infection. The infection can be analysed by the observation of the cells as well as determination of the viral titres by end-point titration. Yet, another analytical assay that should be established is a Western Blot using an α-GFP antibody. Upon cleavage of the reporter construct the eGFP loses its localization marker leading to a size shift that can be observed on a WB. Quantification of the band intensity should thus give insight into the infection process. Combined with viral titres and the visualization of the eGFP fluorescent signal a quantification of infection should be possible.

8. Acknowledgements

The lentivirus system was a generous gift from Prof. Didier Trono (University of Geneva, Switzerland), who provided the packaging vector (pCMVΔR8.91) and the vector expressing VSV-G (pMD.G) and Prof. Thomas Pietschmann (Twincore, Hannover, Germany), who provided the pWPI msc GUN vector.

I am grateful to Niklas Arnberg (Umeå University, Sweden) who kindly provided the Pro5 and Lec2 cell lines including some basic instructions and helpful answers.

For the reporter constructs the plasmids were kindly provided by Steeve Boulant (Heidelberg University, Germany).

Furthermore, I want to thank my doctoral adviser Prof. Dr Stefan Taube for the chance to write my doctoral thesis in his group and his support. Also, his help during growth experiments and inconvenient time points where presence in the laboratory was necessary.

Des Weiteren möchte ich den anderen Mitgliedern und ehemaligen Mitgliedern der AG Taube danken. Henrik, der mir gerade am Anfang geduldig alle meine Fragen beantwortet hat und stets mit Rat zur Seite stand. Außerdem Katja, die mich tatkräftig unterstützt hat und dabei stets ihr Bestes gegeben hat.

Auch den unterschiedlichen Bachelor und Masterstudenten danke ich für ihre Arbeit und der Unterstützung meiner Projekte.

Ein großes Dankeschön gilt auch der AG Tautz. Ihre Hilfe in den Seminaren schätze ich sehr. Außerdem haben mich insbesondere Danilo Dubrau und Barbara Bruhn bei der Generierung der stabilen Zelllinien mittels lentiviraler Transduktion unterstützt.

9. References:

1. Green, K., R. Chanock, and A. Kapikian, *Human Caliciviruses, Fields VIROLOGY volume 1 fourth edition, pp841-874*. 2001, Lippincott, Williams & Wilkins, USA.
2. Prasad, B.V., M.E. Hardy, T. Dokland, J. Bella, M.G. Rossmann, and M.K. Estes, *X-ray crystallographic structure of the Norwalk virus capsid.* Science, 1999. **286**(5438): p. 287-290.
3. Schaffer, F.L., H.L. Bachrach, F. Brown, J.H. Gillespie, N. Burroughs, S.H. Madin, R. Madeley, C. Povey, F. Scott, and A.W. Smith, *Caliciviridae.* Intervirology, 1980. **14**(1): p. 1-6.
4. Farkas, T., K. Sestak, C. Wei, and X. Jiang, *Characterization of a rhesus monkey calicivirus representing a new genus of Caliciviridae.* Journal of virology, 2008. **82**(11): p. 5408-5416.
5. L'Homme, Y., R. Sansregret, É. Plante-Fortier, A.-M. Lamontagne, M. Ouardani, G. Lacroix, and C. Simard, *Genomic characterization of swine caliciviruses representing a new genus of Caliciviridae.* Virus genes, 2009. **39**(1): p. 66-75.
6. Chen, R., J.D. Neill, and B.V. Venkataram Prasad, *Crystallization and preliminary crystallographic analysis of San Miguel sea lion virus: An animal calicivirus.* Journal of Structural Biology, 2003. **141**(2): p. 143-148.
7. Wolf, S., J. Reetz, and P. Otto, *Genetic characterization of a novel calicivirus from a chicken.* Archives of virology, 2011. **156**(7): p. 1143-1150.
8. Day, J.M., L.L. Ballard, M.V. Duke, B.E. Scheffler, and L. Zsak, *Metagenomic analysis of the turkey gut RNA virus community.* Virology journal, 2010. **7**(1): p. 313.
9. Mor, S.K., N.B. Phelps, T.F.F. Ng, K. Subramaniam, A. Primus, A.G. Armien, R. McCann, C. Puzach, T.B. Waltzek, and S.M. Goyal, *Genomic characterization of a novel calicivirus, FHMCV-2012, from baitfish in the USA.* Archives of virology, 2017. **162**(12): p. 3619-3627.
10. Mikalsen, A.B., P. Nilsen, M. Frøystad-Saugen, K. Lindmo, T.M. Eliassen, M. Rode, and Ø. Evensen, *Characterization of a novel calicivirus causing systemic infection in Atlantic salmon (Salmo salar L.): proposal for a new genus of Caliciviridae.* PloS one, 2014. **9**(9).
11. Lopman, B.A., *Global burden of norovirus and prospects for vaccine development.* 2015.
12. Prevention, C.f.D.C.a. *Norovirus Worldwide*. Available from: https://www.cdc.gov/norovirus/trends-outbreaks/worldwide.html.
13. KAPLAN, J.E., G.W. GARY, R.C. BARON, N. SINGH, L.B. SCHONBERGER, R. FELDMAN, and H.B. GREENBERG, *Epidemiology of Norwalk gastroenteritis and the role of Norwalk virus in outbreaks of acute nonbacterial gastroenteritis.* Annals of Internal Medicine, 1982. **96**(6_part_1): p. 756-761.
14. Turcios, R.M., M.-A. Widdowson, A.C. Sulka, P.S. Mead, and R.I. Glass, *Reevaluation of epidemiological criteria for identifying outbreaks of acute gastroenteritis due to norovirus: United States, 1998–2000.* Clinical Infectious Diseases, 2006. **42**(7): p. 964-969.
15. Devasia, T., B. Lopman, J. Leon, and A. Handel, *Association of host, agent and environment characteristics and the duration of incubation and symptomatic periods of norovirus gastroenteritis.* Epidemiology & Infection, 2015. **143**(11): p. 2308-2314.
16. Roth, A.N. and S.M. Karst, *Norovirus mechanisms of immune antagonism.* Current opinion in virology, 2016. **16**: p. 24-30.
17. Atmar, R.L., A.R. Opekun, M.A. Gilger, M.K. Estes, S.E. Crawford, F.H. Neill, and D.Y. Graham, *Norwalk virus shedding after experimental human infection.* Emerging infectious diseases, 2008. **14**(10): p. 1553.
18. Atmar, R.L., A.R. Opekun, M.A. Gilger, M.K. Estes, S.E. Crawford, F.H. Neill, S. Ramani, H. Hill, J. Ferreira, and D.Y. Graham, *Determination of the 50% human infectious dose for Norwalk virus.* The Journal of infectious diseases, 2014. **209**(7): p. 1016-1022.
19. Institut, R.K., *Infektionsepidemiologisches Jahrbuch 2018*. 2019. p. 191-195.
20. Ahmed, S.M., B.A. Lopman, and K. Levy, *A systematic review and meta-analysis of the global seasonality of norovirus.* PloS one, 2013. **8**(10): p. e75922-e75922.

21. Lopman, B.A., A.J. Hall, A.T. Curns, and U.D. Parashar, *Increasing rates of gastroenteritis hospital discharges in US adults and the contribution of norovirus, 1996–2007.* Clinical infectious diseases, 2011. **52**(4): p. 466-474.
22. Lopman, B.A., M.H. Reacher, I.B. Vipond, J. Sarangi, and D.W. Brown, *Clinical manifestation of norovirus gastroenteritis in health care settings.* Clinical Infectious Diseases, 2004. **39**(3): p. 318-324.
23. Wikswo, M.E., J. Cortes, A.J. Hall, G. Vaughan, C. Howard, N. Gregoricus, and E.H. Cramer, *Disease transmission and passenger behaviors during a high morbidity Norovirus outbreak on a cruise ship, January 2009.* Clinical infectious diseases, 2011. **52**(9): p. 1116-1122.
24. Reimann, H.A., A.H. Price, and J.H. Hodges, *The cause of epidemic diarrhea, nausea and vomiting.(Viral dysentery?).* Proceedings of the Society for Experimental Biology and Medicine, 1945. **59**(1): p. 8-9.
25. Dolin, R., N.R. Blacklow, H. DuPont, S. Formal, R.F. Buscho, J.A. Kasel, R.P. Chames, R. Hornick, and R.M. Chanock, *Transmission of acute infectious nonbacterial gastroenteritis to volunteers by oral administration of stool filtrates.* The Journal of infectious diseases, 1971. **123**(3): p. 307-312.
26. Dolin, R., N.R. Blacklow, H. DuPont, R.F. Buscho, R.G. Wyatt, J.A. Kasel, R. Hornick, and R.M. Chanock, *Biological properties of Norwalk agent of acute infectious nonbacterial gastroenteritis.* Proceedings of the Society for Experimental Biology and Medicine, 1972. **140**(2): p. 578-583.
27. Kapikian, A.Z., R.G. Wyatt, R. Dolin, T.S. Thornhill, A.R. Kalica, and R.M. Chanock, *Visualization by immune electron microscopy of a 27-nm particle associated with acute infectious nonbacterial gastroenteritis.* Journal of virology, 1972. **10**(5): p. 1075-1081.
28. Noel, J.S., T. Ando, J.P. Leite, K.Y. Green, K.E. Dingle, M.K. Estes, Y. Seto, S.S. Monroe, and R.I. Glass, *Correlation of patient immune responses with genetically characterized small round-structured viruses involved in outbreaks of nonbacterial acute gastroenteritis in the United States, 1990 to 1995.* Journal of medical virology, 1997. **53**(4): p. 372-383.
29. Pringle, C., *Virus taxonomy at the XIth international congress of virology, Sydney, Australia, 1999.* Archives of virology, 1999. **144**(10): p. 2065-2070.
30. Karst, S.M., C.E. Wobus, M. Lay, J. Davidson, and H.W. Virgin, *STAT1-dependent innate immunity to a Norwalk-like virus.* Science, 2003. **299**(5612): p. 1575-1578.
31. Bartnicki, E., J.B. Cunha, A.O. Kolawole, and C.E. Wobus, *Recent advances in understanding noroviruses.* F1000Research, 2017. **6**.
32. Van Dycke, J., A. Ny, N. Conceição-Neto, J. Maes, M. Hosmillo, A. Cuvry, I. Goodfellow, T.C. Nogueira, E. Verbeken, and J. Matthijnssens, *A robust human norovirus replication model in zebrafish larvae.* PLoS pathogens, 2019. **15**(9).
33. Ettayebi, K., S.E. Crawford, K. Murakami, J.R. Broughman, U. Karandikar, V.R. Tenge, F.H. Neill, S.E. Blutt, X.-L. Zeng, L. Qu, B. Kou, A.R. Opekun, D. Burrin, D.Y. Graham, S. Ramani, R.L. Atmar, and M.K. Estes, *Replication of human noroviruses in stem cell-derived human enteroids.* Science (New York, N.Y.), 2016. **353**(6306): p. 1387-1393.
34. Jones, M.K., M. Watanabe, S. Zhu, C.L. Graves, L.R. Keyes, K.R. Grau, M.B. Gonzalez-Hernandez, N.M. Iovine, C.E. Wobus, and J. Vinjé, *Enteric bacteria promote human and mouse norovirus infection of B cells.* Science, 2014. **346**(6210): p. 755-759.
35. Taube, S., J.R. Rubin, U. Katpally, T.J. Smith, A. Kendall, J.A. Stuckey, and C.E. Wobus, *High-resolution x-ray structure and functional analysis of the murine norovirus 1 capsid protein protruding domain.* Journal of virology, 2010. **84**(11): p. 5695-5705.
36. Karst, S.M. and C.E. Wobus, *A working model of how noroviruses infect the intestine.* PLoS pathogens, 2015. **11**(2).
37. Jiang, X., M. Wang, D.Y. Graham, and M.K. Estes, *Expression, self-assembly, and antigenicity of the Norwalk virus capsid protein.* Journal of virology, 1992. **66**(11): p. 6527-6532.

38. Cao, S., Z. Lou, M. Tan, Y. Chen, Y. Liu, Z. Zhang, X.C. Zhang, X. Jiang, X. Li, and Z. Rao, *Structural basis for the recognition of blood group trisaccharides by norovirus.* Journal of virology, 2007. **81**(11): p. 5949-5957.
39. Bu, W., A. Mamedova, M. Tan, M. Xia, X. Jiang, and R.S. Hegde, *Structural Basis for the Receptor Binding Specificity of Norwalk Virus.* Journal of Virology, 2008. **82**(11): p. 5340-5347.
40. Lindesmith, L.C., E.F. Donaldson, A.D. LoBue, J.L. Cannon, D.-P. Zheng, J. Vinje, and R.S. Baric, *Mechanisms of GII. 4 norovirus persistence in human populations.* PLoS medicine, 2008. **5**(2).
41. Huang, P., T. Farkas, W. Zhong, M. Tan, S. Thornton, A.L. Morrow, and X. Jiang, *Norovirus and histo-blood group antigens: demonstration of a wide spectrum of strain specificities and classification of two major binding groups among multiple binding patterns.* Journal of virology, 2005. **79**(11): p. 6714-6722.
42. Grau, K.R., A.N. Roth, S. Zhu, A. Hernandez, N. Colliou, B.B. DiVita, D.T. Philip, C. Riffe, B. Giasson, S.M. Wallet, M. Mohamadzadeh, and S.M. Karst, *The major targets of acute norovirus infection are immune cells in the gut-associated lymphoid tissue.* Nature Microbiology, 2017. **2**(12): p. 1586-1591.
43. Wilen, C.B., S. Lee, L.L. Hsieh, R.C. Orchard, C. Desai, B.L. Hykes, M.R. McAllaster, D.R. Balce, T. Feehley, and J.R. Brestoff, *Tropism for tuft cells determines immune promotion of norovirus pathogenesis.* Science, 2018. **360**(6385): p. 204-208.
44. Wobus, C.E., S.M. Karst, L.B. Thackray, K.-O. Chang, S.V. Sosnovtsev, G. Belliot, A. Krug, J.M. Mackenzie, K.Y. Green, and H.W. Virgin IV, *Replication of Norovirus in cell culture reveals a tropism for dendritic cells and macrophages.* PLoS biology, 2004. **2**(12).
45. Orchard, R.C., C.B. Wilen, J.G. Doench, M.T. Baldridge, B.T. McCune, Y.-C.J. Lee, S. Lee, S.M. Pruett-Miller, C.A. Nelson, and D.H. Fremont, *Discovery of a proteinaceous cellular receptor for a norovirus.* Science, 2016. **353**(6302): p. 933-936.
46. Thackray, L.B., C.E. Wobus, K.A. Chachu, B. Liu, E.R. Alegre, K.S. Henderson, S.T. Kelley, and H.W. Virgin, *Murine noroviruses comprising a single genogroup exhibit biological diversity despite limited sequence divergence.* Journal of virology, 2007. **81**(19): p. 10460-10473.
47. Farkas, T., B. Fey, G. Keller, V. Martella, and L. Egyed, *Molecular detection of murine noroviruses in laboratory and wild mice.* Veterinary microbiology, 2012. **160**(3-4): p. 463-467.
48. Gonzalez-Hernandez, M.B., T. Liu, H.C. Payne, J.E. Stencel-Baerenwald, M. Ikizler, H. Yagita, T.S. Dermody, I.R. Williams, and C.E. Wobus, *Efficient norovirus and reovirus replication in the mouse intestine requires microfold (M) cells.* Journal of virology, 2014. **88**(12): p. 6934-6943.
49. Baldridge, M.T., H. Turula, and C.E. Wobus, *Norovirus Regulation by Host and Microbe.* Trends in Molecular Medicine, 2016. **22**(12): p. 1047-1059.
50. Lee, S. and M.T. Baldridge, *Interferon-Lambda: A Potent Regulator of Intestinal Viral Infections.* Frontiers in Immunology, 2017. **8**(749).
51. Nice, T.J., M.T. Baldridge, B.T. McCune, J.M. Norman, H.M. Lazear, M. Artyomov, M.S. Diamond, and H.W. Virgin, *Interferon-λ cures persistent murine norovirus infection in the absence of adaptive immunity.* Science, 2015. **347**(6219): p. 269-273.
52. Nice, T.J., D.W. Strong, B.T. McCune, C.S. Pohl, and H.W. Virgin, *A Single-Amino-Acid Change in Murine Norovirus NS1/2 Is Sufficient for Colonic Tropism and Persistence.* Journal of Virology, 2013. **87**(1): p. 327-334.
53. Thomas, H., *Tuft cells revealed as norovirus target.* Nature Reviews Gastroenterology & Hepatology, 2018. **15**(7): p. 390-390.
54. Wobus, C.E., *The dual tropism of noroviruses.* Journal of virology, 2018. **92**(16): p. e01010-17.
55. Ando, T., J. Noel, and R. Fankhauser, *Genetic classification of "Norwalk-like viruses".* The Journal of infectious diseases, 2000. **181**(Supplement_2): p. S336-S348.
56. Green, S.M., P.R. Lambden, E. Owen Caul, C.R. Ashley, and I.N. Clarke, *Capsid diversity in small round-structured viruses: molecular characterization of an antigenically distinct human enteric calicivirus.* Virus Research, 1995. **37**(3): p. 271-283.

57. Vinje, J. and M.P. Koopmans, *Molecular detection and epidemiology of small round-structured viruses in outbreaks of gastroenteritis in the Netherlands.* Journal of Infectious Diseases, 1996. **174**(3): p. 610-615.
58. Vinje, J., J. Green, D. Lewis, C. Gallimore, D. Brown, and M. Koopmans, *Genetic polymorphism across regions of the three open reading frames of "Norwalk-like viruses".* Archives of virology, 2000. **145**(2): p. 223-241.
59. Zheng, D.-P., T. Ando, R.L. Fankhauser, R.S. Beard, R.I. Glass, and S.S. Monroe, *Norovirus classification and proposed strain nomenclature.* Virology, 2006. **346**(2): p. 312-323.
60. Kroneman, A., E. Vega, H. Vennema, J. Vinjé, P.A. White, G. Hansman, K. Green, V. Martella, K. Katayama, and M. Koopmans, *Proposal for a unified norovirus nomenclature and genotyping.* Archives of virology, 2013. **158**(10): p. 2059-2068.
61. Chhabra, P., M. de Graaf, G.I. Parra, M.C.-W. Chan, K. Green, V. Martella, Q. Wang, P.A. White, K. Katayama, and H. Vennema, *Updated classification of norovirus genogroups and genotypes.* Journal of General Virology, 2019. **100**(10): p. 1393-1406.
62. Ford-Siltz, L.A., L. Mullis, Y.M. Sanad, K. Tohma, C.J. Lepore, M. Azevedo, and G.I. Parra, *Genomics analyses of giv and gvi noroviruses reveal the distinct clustering of human and animal viruses.* Viruses, 2019. **11**(3): p. 204.
63. Bull, R.A. and P.A. White, *Mechanisms of GII. 4 norovirus evolution.* Trends in microbiology, 2011. **19**(5): p. 233-240.
64. Lim, K.L., J. Hewitt, A. Sitabkhan, J.-S. Eden, J. Lun, A. Levy, J. Merif, D. Smith, W.D. Rawlinson, and P.A. White, *A multi-site study of norovirus molecular epidemiology in Australia and New Zealand, 2013-2014.* PLoS One, 2016. **11**(4).
65. Mans, J., T. Murray, S. Nadan, R. Netshikweta, N. Page, and M. Taylor, *Norovirus diversity in children with gastroenteritis in South Africa from 2009 to 2013: GII. 4 variants and recombinant strains predominate.* Epidemiology & Infection, 2016. **144**(5): p. 907-916.
66. Green, K., *Caliciviridae: the noroviruses, p 582–608.* Fields virology, 2013. **1**.
67. Vinje, J., *Advances in laboratory methods for detection and typing of norovirus.* J Clin Microbiol, 2015. **53**(2): p. 373-81.
68. Karst, S.M., C.E. Wobus, I.G. Goodfellow, K.Y. Green, and H.W. Virgin, *Advances in norovirus biology.* Cell host & microbe, 2014. **15**(6): p. 668-680.
69. Herbert, T., I. Brierley, and T. Brown, *Identification of a protein linked to the genomic and subgenomic mRNAs of feline calicivirus and its role in translation.* Journal of General Virology, 1997. **78**(5): p. 1033-1040.
70. Seah, E.L., J.A. Marshall, and P.J. Wright, *Open Reading Frame 1 of the Norwalk-Like Virus Camberwell: Completion of Sequence and Expression in Mammalian Cells.* Journal of Virology, 1999. **73**(12): p. 10531-10535.
71. Sosnovtsev, S.V., G. Belliot, K.-O. Chang, V.G. Prikhodko, L.B. Thackray, C.E. Wobus, S.M. Karst, H.W. Virgin, and K.Y. Green, *Cleavage map and proteolytic processing of the murine norovirus nonstructural polyprotein in infected cells.* Journal of virology, 2006. **80**(16): p. 7816-7831.
72. Lee, S., H. Liu, C.B. Wilen, Z.E. Sychev, C. Desai, B.L. Hykes Jr, R.C. Orchard, B.T. McCune, K.-W. Kim, and T.J. Nice, *A secreted viral nonstructural protein determines intestinal norovirus pathogenesis.* Cell host & microbe, 2019. **25**(6): p. 845-857. e5.
73. Hyde, J.L., L.K. Gillespie, and J.M. Mackenzie, *Mouse norovirus 1 utilizes the cytoskeleton network to establish localization of the replication complex proximal to the microtubule organizing center.* Journal of virology, 2012. **86**(8): p. 4110-4122.
74. Hyde, J.L. and J.M. Mackenzie, *Subcellular localization of the MNV-1 ORF1 proteins and their potential roles in the formation of the MNV-1 replication complex.* Virology, 2010. **406**(1): p. 138-148.
75. Hyde, J.L., S.V. Sosnovtsev, K.Y. Green, C. Wobus, H.W. Virgin, and J.M. Mackenzie, *Mouse norovirus replication is associated with virus-induced vesicle clusters originating from*

membranes derived from the secretory pathway. Journal of virology, 2009. **83**(19): p. 9709-9719.
76. Cotton, B.T., J.L. Hyde, S.T. Sarvestani, S.V. Sosnovtsev, K.Y. Green, P.A. White, and J.M. Mackenzie, *The norovirus NS3 protein is a dynamic lipid-and microtubule-associated protein involved in viral RNA replication.* Journal of virology, 2017. **91**(3): p. e02138-16.
77. Li, T.-F., M. Hosmillo, H. Schwanke, T. Shu, Z. Wang, L. Yin, S. Curry, I.G. Goodfellow, and X. Zhou, *Human norovirus NS3 has RNA helicase and chaperoning activities.* Journal of virology, 2018. **92**(5): p. e01606-17.
78. Subba-Reddy, C.V., I. Goodfellow, and C.C. Kao, *VPg-Primed RNA Synthesis by Norovirus RNA-Dependent RNA Polymerases Using a Novel Cell-based Assay.* Journal of virology, 2011: p. JVI. 06191-11.
79. Davies, C., C.M. Brown, D. Westphal, J.M. Ward, and V.K. Ward, *Murine norovirus replication induces G0/G1 cell cycle arrest in asynchronously growing cells.* Journal of virology, 2015. **89**(11): p. 6057-6066.
80. Sosnovtseva, S.A., S.V. Sosnovtsev, and K.Y. Green, *Mapping of the feline calicivirus proteinase responsible for autocatalytic processing of the nonstructural polyprotein and identification of a stable proteinase-polymerase precursor protein.* Journal of virology, 1999. **73**(8): p. 6626-6633.
81. Oehmig, A., M. Büttner, F. Weiland, W. Werz, K. Bergemann, and E. Pfaff, *Identification of a calicivirus isolate of unknown origin.* Journal of General Virology, 2003. **84**(10): p. 2837-2845.
82. Hardy, M.E., *Norovirus protein structure and function.* FEMS microbiology letters, 2005. **253**(1): p. 1-8.
83. Alam, I., J.-H. Lee, K.J. Cho, K.R. Han, J.M. Yang, M.S. Chung, and K.H. Kim, *Crystal structures of murine norovirus-1 RNA-dependent RNA polymerase in complex with 2-thiouridine or ribavirin.* Virology, 2012. **426**(2): p. 143-151.
84. Högbom, M., K. Jäger, I. Robel, T. Unge, and J. Rohayem, *The active form of the norovirus RNA-dependent RNA polymerase is a homodimer with cooperative activity.* Journal of General Virology, 2009. **90**(2): p. 281-291.
85. Ng, K.K.-S., N. Pendás-Franco, J. Rojo, J.A. Boga, À. Machín, J.M.M. Alonso, and F. Parra, *Crystal structure of norwalk virus polymerase reveals the carboxyl terminus in the active site cleft.* Journal of Biological Chemistry, 2004. **279**(16): p. 16638-16645.
86. Zamyatkin, D.F., F. Parra, J.M.M. Alonso, D.A. Harki, B.R. Peterson, P. Grochulski, and K.K.-S. Ng, *Structural insights into mechanisms of catalysis and inhibition in Norwalk virus polymerase.* Journal of Biological Chemistry, 2008. **283**(12): p. 7705-7712.
87. Nelson, C.A., C.B. Wilen, Y.-N. Dai, R.C. Orchard, A.S. Kim, R.A. Stegeman, L.L. Hsieh, T.J. Smith, H.W. Virgin, and D.H. Fremont, *Structural basis for murine norovirus engagement of bile acids and the CD300lf receptor.* Proceedings of the National Academy of Sciences, 2018. **115**(39): p. E9201-E9210.
88. Lochridge, V.P. and M.E. Hardy, *A Single-Amino-Acid Substitution in the P2 Domain of VP1 of Murine Norovirus Is Sufficient for Escape from Antibody Neutralization.* Journal of Virology, 2007. **81**(22): p. 12316-12322.
89. Kilic, T., A. Koromyslova, V. Malak, and G.S. Hansman, *Atomic structure of the murine norovirus protruding domain and soluble CD300lf receptor complex.* Journal of virology, 2018. **92**(11): p. e00413-18.
90. Chen, Y., M. Tan, M. Xia, N. Hao, X.C. Zhang, P. Huang, X. Jiang, X. Li, and Z. Rao, *Crystallography of a Lewis-binding norovirus, elucidation of strain-specificity to the polymorphic human histo-blood group antigens.* PLoS pathogens, 2011. **7**(7): p. e1002152-e1002152.
91. Shanker, S., J.-M. Choi, B. Sankaran, R.L. Atmar, M.K. Estes, and B.V.V. Prasad, *Structural Analysis of Histo-Blood Group Antigen Binding Specificity in a Norovirus GII.4 Epidemic Variant: Implications for Epochal Evolution.* Journal of Virology, 2011. **85**(17): p. 8635-8645.

92. Wegener, H., A. Mallagaray, T. Schone, T. Peters, J. Lockhauserbaumer, H. Yan, C. Uetrecht, G.S. Hansman, and S. Taube, *Human norovirus GII.4(MI001) P dimer binds fucosylated and sialylated carbohydrates.* Glycobiology, 2017. **27**(11): p. 1027-1037.
93. Wirblich, C., H.-J. Thiel, and G. Meyers, *Genetic map of the calicivirus rabbit hemorrhagic disease virus as deduced from in vitro translation studies.* Journal of virology, 1996. **70**(11): p. 7974-7983.
94. Sosnovtsev, S.V. and K.Y. Green, *Identification and genomic mapping of the ORF3 and VPg proteins in feline calicivirus virions.* Virology, 2000. **277**(1): p. 193-203.
95. Sosnovtsev, S.V., G. Belliot, K.-O. Chang, O. Onwudiwe, and K.Y. Green, *Feline calicivirus VP2 is essential for the production of infectious virions.* Journal of virology, 2005. **79**(7): p. 4012-4024.
96. Meyers, G., *Translation of the minor capsid protein of a calicivirus is initiated by a novel termination-dependent reinitiation mechanism.* J Biol Chem, 2003. **278**(36): p. 34051-60.
97. Napthine, S., R.A. Lever, M.L. Powell, R.J. Jackson, T.D.K. Brown, and I. Brierley, *Expression of the VP2 Protein of Murine Norovirus by a Translation Termination-Reinitiation Strategy.* PLOS ONE, 2009. **4**(12): p. e8390.
98. McFadden, N., D. Bailey, G. Carrara, A. Benson, Y. Chaudhry, A. Shortland, J. Heeney, F. Yarovinsky, P. Simmonds, and A. Macdonald, *Norovirus regulation of the innate immune response and apoptosis occurs via the product of the alternative open reading frame 4.* PLoS pathogens, 2011. **7**(12).
99. Cuellar, J.L., F. Meinhoevel, M. Hoehne, and E. Donath, *Size and mechanical stability of norovirus capsids depend on pH: a nanoindentation study.* Journal of General Virology, 2010. **91**(10): p. 2449-2456.
100. Nicollier-Jamot, B., V. Pico, P. Pothier, and E. Kohli, *Molecular Cloning, Expression, Self-Assembly, Antigenicity, and Seroepidemiology of a Genogroup II Norovirus Isolated in France.* Journal of Clinical Microbiology, 2003. **41**(8): p. 3901-3904.
101. Devant, J., G. Hofhaus, and G.S. Hansman, *Novel Structural Features of Human Norovirus Capsid.* bioRxiv, 2019: p. 528240.
102. Pogan, R., J. Dülfer, and C. Uetrecht, *Norovirus assembly and stability.* Current Opinion in Virology, 2018. **31**: p. 59-65.
103. Estes, M.K., K. Ettayebi, V.R. Tenge, K. Murakami, U. Karandikar, S.-C. Lin, B.V. Ayyar, N.W. Cortes-Penfield, K. Haga, and F.H. Neill, *Human Norovirus Cultivation in Nontransformed Stem Cell-Derived Human Intestinal Enteroid Cultures: Success and Challenges.* Viruses, 2019. **11**(7): p. 638.
104. Blutt, S.E., S.E. Crawford, S. Ramani, W.Y. Zou, and M.K. Estes, *Engineered human gastrointestinal cultures to study the microbiome and infectious diseases.* Cellular and molecular gastroenterology and hepatology, 2018. **5**(3): p. 241-251.
105. Van Beek, J., K. Ambert-Balay, N. Botteldoorn, J. Eden, J. Fonager, J. Hewitt, N. Iritani, A. Kroneman, H. Vennema, and J. Vinje, *Indications for worldwide increased norovirus activity associated with emergence of a new variant of genotype II. 4, late 2012.* Eurosurveillance, 2013. **18**(1): p. 20345.
106. Eden, J.-S., J. Hewitt, K.L. Lim, M.F. Boni, J. Merif, G. Greening, R.M. Ratcliff, E.C. Holmes, M.M. Tanaka, and W.D. Rawlinson, *The emergence and evolution of the novel epidemic norovirus GII. 4 variant Sydney 2012.* Virology, 2014. **450**: p. 106-113.
107. Eden, J.-S., M.M. Tanaka, M.F. Boni, W.D. Rawlinson, and P.A. White, *Recombination within the pandemic norovirus GII. 4 lineage.* Journal of virology, 2013. **87**(11): p. 6270-6282.
108. Cheetham, S., M. Souza, T. Meulia, S. Grimes, M.G. Han, and L.J. Saif, *Pathogenesis of a genogroup II human norovirus in gnotobiotic pigs.* Journal of virology, 2006. **80**(21): p. 10372-10381.
109. Lou, F., M. Ye, Y. Ma, X. Li, E. DiCaprio, H. Chen, S. Krakowka, J. Hughes, D. Kingsley, and J. Li, *A gnotobiotic pig model for determining human norovirus inactivation by high-pressure processing.* Appl. Environ. Microbiol., 2015. **81**(19): p. 6679-6687.

110. Miura, T., D. Sano, A. Suenaga, T. Yoshimura, M. Fuzawa, T. Nakagomi, O. Nakagomi, and S. Okabe, *Histo-blood group antigen-like substances of human enteric bacteria as specific adsorbents for human noroviruses.* Journal of virology, 2013. **87**(17): p. 9441-9451.
111. Lei, S., H. Samuel, E. Twitchell, T. Bui, A. Ramesh, K. Wen, M. Weiss, G. Li, X. Yang, and X. Jiang, *Enterobacter cloacae inhibits human norovirus infectivity in gnotobiotic pigs.* Scientific reports, 2016. **6**: p. 25017.
112. Taube, S., A.O. Kolawole, M. Höhne, J.E. Wilkinson, S.A. Handley, J.W. Perry, L.B. Thackray, R. Akkina, and C.E. Wobus, *A mouse model for human norovirus.* MBio, 2013. **4**(4).
113. Kolawole, A.O., J. Rocha-Pereira, M.D. Elftman, J. Neyts, and C.E. Wobus, *Inhibition of human norovirus by a viral polymerase inhibitor in the B cell culture system and in the mouse model.* Antiviral research, 2016. **132**: p. 46-49.
114. Goody, M.F., C. Sullivan, and C.H. Kim, *Studying the immune response to human viral infections using zebrafish.* Developmental & Comparative Immunology, 2014. **46**(1): p. 84-95.
115. Wobus, C.E., L.B. Thackray, and H.W. Virgin, *Murine norovirus: a model system to study norovirus biology and pathogenesis.* Journal of virology, 2006. **80**(11): p. 5104-5112.
116. Asanaka, M., R.L. Atmar, V. Ruvolo, S.E. Crawford, F.H. Neill, and M.K. Estes, *Replication and packaging of Norwalk virus RNA in cultured mammalian cells.* Proceedings of the National Academy of Sciences, 2005. **102**(29): p. 10327-10332.
117. Katayama, K., G. Hansman, T. Oka, S. Ogawa, and N. Takeda, *Investigation of norovirus replication in a human cell line.* Archives of virology, 2006. **151**(7): p. 1291-1308.
118. Doerflinger, S.Y., M. Cortese, I. Romero-Brey, Z. Menne, T. Tubiana, C. Schenk, P.A. White, R. Bartenschlager, S. Bressanelli, and G.S. Hansman, *Membrane alterations induced by nonstructural proteins of human norovirus.* PLoS pathogens, 2017. **13**(10): p. e1006705.
119. Stancevic, B. and R. Kolesnick, *Ceramide-rich platforms in transmembrane signaling.* FEBS letters, 2010. **584**(9): p. 1728-1740.
120. Montes, L.R., M.B. Ruiz-Argüello, F.M. Goñi, and A. Alonso, *Membrane restructuring via ceramide results in enhanced solute efflux.* Journal of Biological Chemistry, 2002. **277**(14): p. 11788-11794.
121. Orchard, R.C., C.B. Wilen, and H.W. Virgin, *Sphingolipid biosynthesis induces a conformational change in the murine norovirus receptor and facilitates viral infection.* Nature microbiology, 2018. **3**(10): p. 1109-1114.
122. Perry, J.W. and C.E. Wobus, *Endocytosis of murine norovirus 1 into murine macrophages is dependent on dynamin II and cholesterol.* Journal of virology, 2010. **84**(12): p. 6163-6176.
123. Gerondopoulos, A., T. Jackson, P. Monaghan, N. Doyle, and L.O. Roberts, *Murine norovirus-1 cell entry is mediated through a non-clathrin-, non-caveolae-, dynamin-and cholesterol-dependent pathway.* Journal of General Virology, 2010. **91**(6): p. 1428-1438.
124. Perry, J.W., S. Taube, and C.E. Wobus, *Murine norovirus-1 entry into permissive macrophages and dendritic cells is pH-independent.* Virus research, 2009. **143**(1): p. 125-129.
125. Chung, L., D. Bailey, E.N. Leen, E.P. Emmott, Y. Chaudhry, L.O. Roberts, S. Curry, N. Locker, and I.G. Goodfellow, *Norovirus translation requires an interaction between the C terminus of the genome-linked viral protein VPg and eukaryotic translation initiation factor 4G.* Journal of Biological Chemistry, 2014. **289**(31): p. 21738-21750.
126. Belliot, G., S.V. Sosnovtsev, K.-O. Chang, V. Babu, U. Uche, J.J. Arnold, C.E. Cameron, and K.Y. Green, *Norovirus proteinase-polymerase and polymerase are both active forms of RNA-dependent RNA polymerase.* Journal of virology, 2005. **79**(4): p. 2393-2403.
127. Lee, J.-H., B.S. Park, I. Alam, K.R. Han, S.B. Biering, S.J. Kim, J. Choi, J.H. Seok, M.S. Chung, H.M. Kim, S. Hwang, and K.H. Kim, *Insight Into the Interaction Between RNA Polymerase and VPg for Murine Norovirus Replication.* Frontiers in Microbiology, 2018. **9**(1466).
128. Yunus, M.A., X. Lin, D. Bailey, I. Karakasiliotis, Y. Chaudhry, S. Vashist, G. Zhang, L. Thorne, C.C. Kao, and I. Goodfellow, *The murine norovirus core subgenomic RNA promoter consists of a stable stem-loop that can direct accurate initiation of RNA synthesis.* Journal of virology, 2015. **89**(2): p. 1218-1229.

129. Bertolotti-Ciarlet, A., L.J. White, R. Chen, B.V.V. Prasad, and M.K. Estes, *Structural requirements for the assembly of Norwalk virus-like particles.* Journal of virology, 2002. **76**(8): p. 4044-4055.
130. Kaiser, W.J., Y. Chaudhry, S.V. Sosnovtsev, and I.G. Goodfellow, *Analysis of protein–protein interactions in the feline calicivirus replication complex.* Journal of General Virology, 2006. **87**(2): p. 363-368.
131. Bok, K., V.G. Prikhodko, K.Y. Green, and S.V. Sosnovtsev, *Apoptosis in murine norovirus-infected RAW264. 7 cells is associated with downregulation of survivin.* Journal of virology, 2009. **83**(8): p. 3647-3656.
132. Thorne, L.G. and I.G. Goodfellow, *Norovirus gene expression and replication.* Journal of General Virology, 2014. **95**(2): p. 278-291.
133. Borrego, F., *The CD300 molecules: an emerging family of regulators of the immune system.* Blood, The Journal of the American Society of Hematology, 2013. **121**(11): p. 1951-1960.
134. Marionneau, S., N. Ruvoën, B. Le Moullac-Vaidye, M. Clement, A. Cailleau-Thomas, G. Ruiz-Palacois, P. Huang, X. Jiang, and J. Le Pendu, *Norwalk virus binds to histo-blood group antigens present on gastroduodenal epithelial cells of secretor individuals.* Gastroenterology, 2002. **122**(7): p. 1967-77.
135. Harrington, P.R., L. Lindesmith, B. Yount, C.L. Moe, and R.S. Baric, *Binding of Norwalk virus-like particles to ABH histo-blood group antigens is blocked by antisera from infected human volunteers or experimentally vaccinated mice.* Journal of virology, 2002. **76**(23): p. 12335-12343.
136. Harrington, P.R., J. Vinjé, C.L. Moe, and R.S. Baric, *Norovirus capture with histo-blood group antigens reveals novel virus-ligand interactions.* Journal of virology, 2004. **78**(6): p. 3035-3045.
137. Marionneau, S., A. Cailleau-Thomas, J. Rocher, B. Le Moullac-Vaidye, N. Ruvoën, M. Clément, and J. Le Pendu, *ABH and Lewis histo-blood group antigens, a model for the meaning of oligosaccharide diversity in the face of a changing world.* Biochimie, 2001. **83**(7): p. 565-573.
138. Donaldson, E.F., L.C. Lindesmith, A.D. Lobue, and R.S. Baric, *Norovirus pathogenesis: mechanisms of persistence and immune evasion in human populations.* Immunological reviews, 2008. **225**(1): p. 190-211.
139. Pickard, J.M. and A.V. Chervonsky, *Intestinal fucose as a mediator of host–microbe symbiosis.* The Journal of Immunology, 2015. **194**(12): p. 5588-5593.
140. Tan, M., P. Huang, J. Meller, W. Zhong, T. Farkas, and X. Jiang, *Mutations within the P2 domain of norovirus capsid affect binding to human histo-blood group antigens: evidence for a binding pocket.* Journal of virology, 2003. **77**(23): p. 12562-12571.
141. Rockx, B.H., H. Vennema, C.J. Hoebe, E. Duizer, and M.P. Koopmans, *Association of histo–blood group antigens and susceptibility to norovirus infections.* The Journal of infectious diseases, 2005. **191**(5): p. 749-754.
142. Kubota, T., A. Kumagai, H. Ito, S. Furukawa, Y. Someya, N. Takeda, K. Ishii, T. Wakita, H. Narimatsu, and H. Shirato, *Structural Basis for the Recognition of Lewis Antigens by Genogroup I Norovirus.* Journal of Virology, 2012. **86**(20): p. 11138-11150.
143. Tan, M. and X. Jiang, *The p domain of norovirus capsid protein forms a subviral particle that binds to histo-blood group antigen receptors.* Journal of virology, 2005. **79**(22): p. 14017-14030.
144. Tan, M. and X. Jiang, *Norovirus-host interaction: multi-selections by human histo-blood group antigens.* Trends in microbiology, 2011. **19**(8): p. 382-388.
145. Lindesmith, L., C. Moe, S. Marionneau, N. Ruvoen, X. Jiang, L. Lindblad, P. Stewart, J. LePendu, and R. Baric, *Human susceptibility and resistance to Norwalk virus infection.* Nature medicine, 2003. **9**(5): p. 548-553.
146. Hutson, A.M., R.L. Atmar, D.Y. Graham, and M.K. Estes, *Norwalk virus infection and disease is associated with ABO histo-blood group type.* The Journal of infectious diseases, 2002. **185**(9): p. 1335-1337.

147. Tan, M., M. Xia, Y. Chen, W. Bu, R.S. Hegde, J. Meller, X. Li, and X. Jiang, *Conservation of carbohydrate binding interfaces—evidence of human HBGA selection in norovirus evolution.* PloS one, 2009. **4**(4).
148. Barbé, L., B. Le Moullac-Vaidye, K. Echasserieau, K. Bernardeau, T. Carton, N. Bovin, J. Nordgren, L. Svensson, N. Ruvoën-Clouet, and J. Le Pendu, *Histo-blood group antigen-binding specificities of human rotaviruses are associated with gastroenteritis but not with in vitro infection.* Scientific reports, 2018. **8**(1): p. 1-14.
149. Barnes, S., P. Burhol, R. Zander, G. Haggstrom, R. Settine, and B. Hirschowitz, *Enzymatic sulfation of glycochenodeoxycholic acid by tissue fractions from adult hamsters.* Journal of lipid research, 1979. **20**(8): p. 952-959.
150. Lefebvre, P., B. Cariou, F. Lien, F. Kuipers, and B. Staels, *Role of Bile Acids and Bile Acid Receptors in Metabolic Regulation.* Physiological Reviews, 2009. **89**(1): p. 147-191.
151. Tailford, L.E., E.H. Crost, D. Kavanaugh, and N. Juge, *Mucin glycan foraging in the human gut microbiome.* Frontiers in Genetics, 2015. **6**(81).
152. Johansson, M.E.V. and G.C. Hansson, *Keeping Bacteria at a Distance.* Science, 2011. **334**(6053): p. 182-183.
153. Johansson, M.E.V., M. Phillipson, J. Petersson, A. Velcich, L. Holm, and G.C. Hansson, *The inner of the two Muc2 mucin-dependent mucus layers in colon is devoid of bacteria.* Proceedings of the National Academy of Sciences, 2008. **105**(39): p. 15064-15069.
154. Corfield, A., *Eukaryotic protein glycosylation: a primer for histochemists and cell biologists.* Histochemistry and Cell Biology, 2017. **147**(2): p. 119-147.
155. Moran, A.P., A. Gupta, and L. Joshi, *Sweet-talk: role of host glycosylation in bacterial pathogenesis of the gastrointestinal tract.* Gut, 2011. **60**(10): p. 1412-1425.
156. S J Gendler, a. and A.P. Spicer, *Epithelial Mucin Genes.* Annual Review of Physiology, 1995. **57**(1): p. 607-634.
157. Bergstrom, K.S.B. and L. Xia, *Mucin-type O-glycans and their roles in intestinal homeostasis.* Glycobiology, 2013. **23**(9): p. 1026-1037.
158. Jonckheere, N. and I. Van Seuningen, *The membrane-bound mucins: From cell signalling to transcriptional regulation and expression in epithelial cancers.* Biochimie, 2010. **92**(1): p. 1-11.
159. Moncada, D.M., S.J. Kammanadiminti, and K. Chadee, *Mucin and Toll-like receptors in host defense against intestinal parasites.* Trends in parasitology, 2003. **19**(7): p. 305-311.
160. Brockhausen, I., T. Dowler, and H. Paulsen, *Site directed processing: Role of amino acid sequences and glycosylation of acceptor glycopeptides in the assembly of extended mucin type O-glycan core 2.* Biochimica et Biophysica Acta (BBA) - General Subjects, 2009. **1790**(10): p. 1244-1257.
161. Li, D., A. Breiman, J. le Pendu, and M. Uyttendaele, *Binding to histo-blood group antigen-expressing bacteria protects human norovirus from acute heat stress.* Frontiers in Microbiology, 2015. **6**(659).
162. Almagro-Moreno, S. and E.F. Boyd, *Bacterial catabolism of nonulosonic (sialic) acid and fitness in the gut.* Gut Microbes, 2010. **1**(1): p. 45-50.
163. Baldridge, M.T., T.J. Nice, B.T. McCune, C.C. Yokoyama, A. Kambal, M. Wheadon, M.S. Diamond, Y. Ivanova, M. Artyomov, and H.W. Virgin, *Commensal microbes and interferon-λ determine persistence of enteric murine norovirus infection.* Science, 2015. **347**(6219): p. 266-269.
164. Chen, Z., S.V. Sosnovtsev, K. Bok, G.I. Parra, M. Makiya, L. Agulto, K.Y. Green, and R.H. Purcell, *Development of Norwalk Virus-Specific Monoclonal Antibodies with Therapeutic Potential for the Treatment of Norwalk Virus Gastroenteritis.* Journal of Virology, 2013. **87**(17): p. 9547-9557.
165. Nelson, A.M., S.T. Walk, S. Taube, M. Taniuchi, E.R. Houpt, C.E. Wobus, and V.B. Young, *Disruption of the Human Gut Microbiota following Norovirus Infection.* PLOS ONE, 2012. **7**(10): p. e48224.

166. Hickman, D., M.K. Jones, S. Zhu, E. Kirkpatrick, D.A. Ostrov, X. Wang, M. Ukhanova, Y. Sun, V. Mai, M. Salemi, and S.M. Karst, *The Effect of Malnutrition on Norovirus Infection.* mBio, 2014. **5**(2): p. e01032-13.
167. Nelson, A.M., M.D. Elftman, A.K. Pinto, M. Baldridge, P. Hooper, J. Kuczynski, J.F. Petrosino, V.B. Young, and C.E. Wobus, *Murine norovirus infection does not cause major disruptions in the murine intestinal microbiota.* Microbiome, 2013. **1**(1): p. 7.
168. Taube, S., A. Kurth, and E. Schreier, *Generation of recombinant norovirus-like particles (VLP) in the human endothelial kidney cell line 293T.* Archives of virology, 2005. **150**(7): p. 1425-1431.
169. Chang, K.-O., S.V. Sosnovtsev, G. Belliot, A.D. King, and K.Y. Green, *Stable expression of a Norwalk virus RNA replicon in a human hepatoma cell line.* Virology, 2006. **353**(2): p. 463-473.
170. Fraser, D., H.R. Mahler, A.L. Shug, and C.A. Thomas, *THE INFECTION OF SUB-CELLULAR ESCHERICHIA COLI, STRAIN B, WITH A DNA PREPARATION FROM T2 BACTERIOPHAGE.* Proceedings of the National Academy of Sciences of the United States of America, 1957. **43**(11): p. 939-947.
171. Taniguchi, T., M. Palmieri, and C. Weissmann, *Qβ DNA-containing hybrid plasmids giving rise to Qβ phage formation in the bacterial host.* Nature, 1978. **274**(5668): p. 223-228.
172. Racaniello, V. and D. Baltimore, *Cloned poliovirus complementary DNA is infectious in mammalian cells.* Science, 1981. **214**(4523): p. 916-919.
173. Boyer, J.-C. and A.-L. Haenni, *Infectious Transcripts and cDNA Clones of RNA Viruses.* Virology, 1994. **198**(2): p. 415-426.
174. Schnell, M.J., T. Mebatsion, and K.K. Conzelmann, *Infectious rabies viruses from cloned cDNA.* The EMBO Journal, 1994. **13**(18): p. 4195-4203.
175. Sosnovtsev, S. and K.Y. Green, *RNA Transcripts Derived from a Cloned Full-Length Copy of the Feline Calicivirus Genome Do Not Require VpG for Infectivity.* Virology, 1995. **210**(2): p. 383-390.
176. Ward, V.K., C.J. McCormick, I.N. Clarke, O. Salim, C.E. Wobus, L.B. Thackray, H.W. Virgin, and P.R. Lambden, *Recovery of infectious murine norovirus using pol II-driven expression of full-length cDNA.* Proceedings of the National Academy of Sciences, 2007. **104**(26): p. 11050-11055.
177. Arias, A., L. Ureña, L. Thorne, M.A. Yunus, and I. Goodfellow, *Reverse genetics mediated recovery of infectious murine norovirus.* Journal of visualized experiments: JoVE, 2012(64).
178. Yunus, M.A., L.M.W. Chung, Y. Chaudhry, D. Bailey, and I. Goodfellow, *Development of an optimized RNA-based murine norovirus reverse genetics system.* Journal of Virological Methods, 2010. **169**(1): p. 112-118.
179. Goodfellow, I. and S. Taube, *Chapter 3.2 - Calicivirus Replication and Reverse Genetics*, in *Viral Gastroenteritis*, L. Svensson, et al., Editors. 2016, Academic Press: Boston. p. 355-378.
180. Katayama, K., K. Murakami, T.M. Sharp, S. Guix, T. Oka, R. Takai-Todaka, A. Nakanishi, S.E. Crawford, R.L. Atmar, and M.K. Estes, *Plasmid-based human norovirus reverse genetics system produces reporter-tagged progeny virus containing infectious genomic RNA.* Proceedings of the National Academy of Sciences, 2014. **111**(38): p. E4043-E4052.
181. Chaudhry, Y., M.A. Skinner, and I.G. Goodfellow, *Recovery of genetically defined murine norovirus in tissue culture by using a fowlpox virus expressing T7 RNA polymerase.* The Journal of general virology, 2007. **88**(Pt 8): p. 2091-2100.
182. Iro, M., J. Witteveldt, A.G. Angus, I. Woerz, A. Kaul, R. Bartenschlager, and A.H. Patel, *A reporter cell line for rapid and sensitive evaluation of hepatitis C virus infectivity and replication.* Antiviral research, 2009. **83**(2): p. 148-155.
183. Nelson, P.T., L.A. Soma, and E. Lavi, *Microglia in diseases of the central nervous system.* Annals of Medicine, 2002. **34**(7): p. 491-500.

184. Bocchini, V., R. Mazzolla, R. Barluzzi, E. Blasi, P. Sick, and H. Kettenmann, *An immortalized cell line expresses properties of activated microglial cells.* Journal of Neuroscience Research, 1992. **31**(4): p. 616-621.
185. Henn, A., S. Lund, M. Hedtjarn, A. Schrattenholz, P. Porzgen, and M. Leist, *The suitability of BV2 cells as alternative model system for primary microglia cultures or for animal experiments examining brain inflammation.* ALTEX, 2009. **26**(2): p. 83-94.
186. Raschke, W.C., S. Baird, P. Ralph, and I. Nakoinz, *Functional macrophage cell lines transformed by abelson leukemia virus.* Cell, 1978. **15**(1): p. 261-267.
187. ATCC, L.S. *Hek 293T cells*. Available from: https://www.lgcstandards-atcc.org/Products/All/CRL-3216.aspx?geo_country=de#.
188. Nakabayashi, H., K. Taketa, K. Miyano, T. Yamane, and J. Sato, *Growth of Human Hepatoma Cell Lines with Differentiated Functions in Chemically Defined Medium.* Cancer Research, 1982. **42**(9): p. 3858-3863.
189. Koutsoudakis, G., E. Herrmann, S. Kallis, R. Bartenschlager, and T. Pietschmann, *The Level of CD81 Cell Surface Expression Is a Key Determinant for Productive Entry of Hepatitis C Virus into Host Cells.* Journal of Virology, 2007. **81**(2): p. 588-598.
190. Blight, K.J., J.A. McKeating, and C.M. Rice, *Highly permissive cell lines for subgenomic and genomic hepatitis C virus RNA replication.* Journal of virology, 2002. **76**(24): p. 13001-13014.
191. Sumpter, R., Jr., Y.-M. Loo, E. Foy, K. Li, M. Yoneyama, T. Fujita, S.M. Lemon, and M. Gale, Jr., *Regulating intracellular antiviral defense and permissiveness to hepatitis C virus RNA replication through a cellular RNA helicase, RIG-I.* Journal of virology, 2005. **79**(5): p. 2689-2699.
192. Arnberg, N., K. Edlund, A.H. Kidd, and G. Wadell, *Adenovirus Type 37 Uses Sialic Acid as a Cellular Receptor.* Journal of Virology, 2000. **74**(1): p. 42-48.
193. Eckhardt, M., B. Gotza, and R. Gerardy-Schahn, *Mutants of the CMP-sialic acid transporter causing the Lec2 phenotype.* Journal of Biological Chemistry, 1998. **273**(32): p. 20189-20195.
194. Hanahan, D., *Studies on transformation of Escherichia coli with plasmids.* Journal of molecular biology, 1983. **166**(4): p. 557-580.
195. Bimboim, H. and J. Doly, *A rapid alkaline extraction procedure for screening recombinant plasmid DNA.* Nucleic acids research, 1979. **7**(6): p. 1513-1523.
196. Liu, H. and J.H. Naismith, *An efficient one-step site-directed deletion, insertion, single and multiple-site plasmid mutagenesis protocol.* BMC biotechnology, 2008. **8**(1): p. 91.
197. Mulugova, M., *Generation and Characterization of Recombinant Murine Noroviruses*, in *Virology and Cell Biology*. 2018, University of Lübeck.
198. Northwestern, O.; Available from: http://biotools.nubic.northwestern.edu/OligoCAlc.html.
199. Biozym. *ScriptCap m7G*. Available from: https://www.biozym.com/DesktopModules/WebShop/shopdisplayproducts.aspx?productid=8104&id=231.
200. Promega. *Ribo m7G cap analog*. Available from: https://www.promega.de/en/products/rna-analysis/in-vitro-transcription/ribo-m7g-cap-analog/?catNum=P1711.
201. Lohmann, V., F. Körner, J.-O. Koch, U. Herian, L. Theilmann, and R. Bartenschlager, *Replication of subgenomic hepatitis C virus RNAs in a hepatoma cell line.* Science, 1999. **285**(5424): p. 110-113.
202. Stanley, P., V. Caillibot, and L. Siminovitch, *Selection and characterization of eight phenotypically distinct lines of lectin-resistant Chinese hamster ovary cells.* Cell, 1975. **6**(2): p. 121-128.
203. Deutscher, S.L., N. Nuwayhid, P. Stanley, E.I.B. Briles, and C.B. Hirschberg, *Translocation across Golgi vesicle membranes: a CHO glycosylation mutant deficient in CMP-sialic acid transport.* Cell, 1984. **39**(2): p. 295-299.
204. Boussif, O., F. Lezoualc'h, M.A. Zanta, M.D. Mergny, D. Scherman, B. Demeneix, and J.-P. Behr, *A versatile vector for gene and oligonucleotide transfer into cells in culture and in vivo:*

polyethylenimine. Proceedings of the National Academy of Sciences, 1995. **92**(16): p. 7297-7301.
205. Naldini, L., U. Blömer, P. Gallay, D. Ory, R. Mulligan, F.H. Gage, I.M. Verma, and D. Trono, *In vivo gene delivery and stable transduction of nondividing cells by a lentiviral vector.* Science, 1996. **272**(5259): p. 263-267.
206. Salmon, P. and D. Trono, *Lentiviral Vectors for the Gene Therapy of Lympho-Hematological Disorders*, in *Lentiviral Vectors*, D. Trono, Editor. 2002, Springer Berlin Heidelberg: Berlin, Heidelberg. p. 211-227.
207. Sakuma, T., Michael A. Barry, and Y. Ikeda, *Lentiviral vectors: basic to translational.* Biochemical Journal, 2012. **443**(3): p. 603-618.
208. Reed, L.J. and H. Muench, *A simple method of estimating fifty per cent endpoints.* American journal of epidemiology, 1938. **27**(3): p. 493-497.
209. Tan, M., M. Jin, H. Xie, Z. Duan, X. Jiang, and Z. Fang, *Outbreak studies of a GII-3 and a GII-4 norovirus revealed an association between HBGA phenotypes and viral infection.* Journal of Medical Virology, 2008. **80**(7): p. 1296-1301.
210. Taube, S., J.W. Perry, K. Yetming, S.P. Patel, H. Auble, L. Shu, H.F. Nawar, C.H. Lee, T.D. Connell, and J.A. Shayman, *Ganglioside-linked terminal sialic acid moieties on murine macrophages function as attachment receptors for murine noroviruses.* Journal of virology, 2009. **83**(9): p. 4092-4101.
211. Wegener, L.H., *Die Rolle der Kohlenhydrate in der Bindung und Infektion von Noroviren*, in *Institute of Virology and Cell Biology*. 2019, University of Lübeck: Lübeck. p. 218.
212. Haga, K., A. Fujimoto, R. Takai-Todaka, M. Miki, Y.H. Doan, K. Murakami, M. Yokoyama, K. Murata, A. Nakanishi, and K. Katayama, *Functional receptor molecules CD300lf and CD300ld within the CD300 family enable murine noroviruses to infect cells.* Proceedings of the National Academy of Sciences, 2016. **113**(41): p. E6248-E6255.
213. Cox, C., S. Cao, and Y. Lu, *Enhanced detection and study of murine norovirus-1 using a more efficient microglial cell line.* Virology journal, 2009. **6**: p. 196-196.
214. Gonzalez-Hernandez, M.B., J.B. Cunha, and C.E. Wobus, *Plaque assay for murine norovirus.* JoVE (Journal of Visualized Experiments), 2012(66): p. e4297.
215. Matrosovich, M., T. Matrosovich, W. Garten, and H.-D. Klenk, *New low-viscosity overlay medium for viral plaque assays.* Virology journal, 2006. **3**(1): p. 63.
216. Katpally, U., C.E. Wobus, K. Dryden, H.W. Virgin, and T.J. Smith, *Structure of Antibody-Neutralized Murine Norovirus and Unexpected Differences from Viruslike Particles.* Journal of Virology, 2008. **82**(5): p. 2079-2088.
217. Robert Creutznacher, G.W., Thorben Maass, Patrick Ogrissek, Clara Feldmann, Thomas Peters, and Alvaro Mallagaray, *Chemical shift perturbation NMR experiments shed new light on glycan recognition by human and murine Norovirus capsid proteins* I.o.C.a.M. University of Lübeck, Editor. 2020.
218. Smith, H.Q. and T.J. Smith, *The dynamic capsid structures of the noroviruses.* Viruses, 2019. **11**(3): p. 235.
219. Hansman, G.S., S. Shahzad-ul-Hussan, J.S. McLellan, G.-Y. Chuang, I. Georgiev, T. Shimoike, K. Katayama, C.A. Bewley, and P.D. Kwong, *Structural basis for norovirus inhibition and fucose mimicry by citrate.* Journal of virology, 2012. **86**(1): p. 284-292.
220. Mi, Z., J. Fu, Y. Xiong, and H. Tang, *SUMOylation of RIG-I positively regulates the type I interferon signaling.* Protein & cell, 2010. **1**(3): p. 275-283.
221. Vitallé, J., I. Terrén, A. Orrantia, O. Zenarruzabeitia, and F. Borrego, *CD300 receptor family in viral infections.* European journal of immunology, 2019. **49**(3): p. 364-374.
222. Changotra, H., Y. Jia, T.N. Moore, G. Liu, S.M. Kahan, S.V. Sosnovtsev, and S.M. Karst, *Type I and Type II Interferons Inhibit the Translation of Murine Norovirus Proteins.* Journal of Virology, 2009. **83**(11): p. 5683-5692.

223. Kim, S.S.-Y., L. Sze, and K.-P. Lam, *The stress granule protein G3BP1 binds viral dsRNA and RIG-I to enhance interferon-β response.* Journal of Biological Chemistry, 2019. **294**(16): p. 6430-6438.
224. Romero-Brey, I., A. Merz, A. Chiramel, J.-Y. Lee, P. Chlanda, U. Haselman, R. Santarella-Mellwig, A. Habermann, S. Hoppe, and S. Kallis, *Three-dimensional architecture and biogenesis of membrane structures associated with hepatitis C virus replication.* PLoS pathogens, 2012. **8**(12).
225. Gaglia, M.M., S. Covarrubias, W. Wong, and B.A. Glaunsinger, *A common strategy for host RNA degradation by divergent viruses.* Journal of virology, 2012. **86**(17): p. 9527-9530.
226. May, J., B. Korba, A. Medvedev, and P. Viswanathan, *Enzyme kinetics of the human norovirus protease control virus polyprotein processing order.* Virology, 2013. **444**(1): p. 218-224.